UNIVERSITY OF CALIFORNIA
Santa Barbara

# Long-Wavelength Vertical-Cavity Semiconductor Optical Amplifiers

A Dissertation submitted in partial satisfaction of the
requirements for the degree Doctor of Philosophy
in Electrical and Computer Engineering

by

E. Staffan Björlin

Committee in charge:

Professor John E. Bowers, Chair
Professor Daniel J. Blumenthal
Professor Larry A. Coldren
Professor Evelyn L. Hu

December 2002

The dissertation of E. Staffan Björlin is approved.

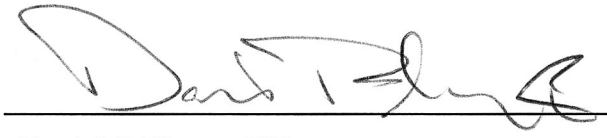

Daniel J. Blumenthal

Larry A. Coldren

Evelyn L. Hu

John E. Bowers, Chair

December 2002

Long-Wavelength Vertical-Cavity Semiconductor Optical Amplifiers

*This dissertation is dedicated to*

*Alexis Black*

**Acknowledgements**

My decision to pursue a Ph.D. at UCSB, the success of the VCSOA project, and my general well-being over the past three years were helped by a number of people. First of all, I would like to thank Alexis Black for convincing me to stay in the U.S., for her help, support, and encouragement during my first year at UCSB, and, in general, for being the most important person in my life over the past three years. I would like to thank my family back home in Sweden for giving me the freedom to undertake any career and education I wanted to, and for not complaining too much when I left Sweden. I also need to thank all my relatively new friends here in California for making my life here very enjoyable.

My advisor Professor John Bowers has of course played an invaluable role in my education here. His expertise, enthusiasm, and energy have been a tremendous source of inspiration. He has given me a great deal of freedom on this project, which I greatly appreciate. In addition to being a great advisor, he has been a good friend; the annual Bowers' group snowboarding trips were some of the highlights of my time at UCSB. I would also like to thank the rest of my committee, Professors Dan Blumenthal, Larry Coldren, and Evelyn Hu.

A project like this can obviously not be done by one person alone. I would like to acknowledge the following people, who in one way or another have contributed to the VCSOA project at UCSB: Patrick Abraham, Alexis Black, Yi-Jen Chiu, Anders Dahl, Sangyoun Gee, Jon Geske, Kian-Giap Gan, Chris Harder, Adrian Keating, Stefan Mohrdiek, Donato Pasquariello, Joachim Piprek, Masa Rao, and Bertrand Riou.

## Curriculum Vitæ

E. Staffan Björlin

### Personal

| | |
|---|---|
| Born | September 3, 1971<br>Nynäshamn, Sweden |

### Education

| | |
|---|---|
| 1993-2000 | M.S. in Engineering Physics<br>Royal Institute of Technology<br>Stockholm, Sweden |
| 2000-2002 | Ph.D. in Electrical and Computer Engineering<br>University of California, Santa Barbara, CA |

### Awards

Best Student Paper, 14th International Conference on Indium Phosphide and Related Materials (IPRM '02), May 2002, Stockholm, Sweden.

Optical Society of America/New Focus Student Award 2002

### Publications

*First author journal papers*

E. S. Björlin, J. Geske, and J. E. Bowers, "Optically preamplified receiver at 10 Gbit/s using vertical-cavity SOA," *Electronic Letters*, vol. 37, no. 24, pp. 1474-1475, November 2001.

E. S. Björlin and J. E. Bowers, "Noise Figure of Vertical-Cavity Semiconductor Optical Amplifiers," *IEEE Journal of Quantum Electronics*, vol. 38, no. 1, pp. 61-66, January 2002.

E. Staffan Björlin, Joachim Piprek, Sangyoun Gee, Yi-Jen Chiu, John E. Bowers, Anders Dahl, Patrick Abraham, "1.3μm vertical-cavity amplifying switch," *OSA Trends in Optics and Photonics*, vol. 60, "Optical Amplifiers and Their Applications," pp. 154-160, 2001.

E. S. Björlin, A. Dahl, J. Piprek, P. Abraham, Y.-J. Chiu, and J. E. Bowers, "Vertical-Cavity Amplifying Modulator at 1.3 μm," *IEEE Photonics Technology Letters*, vol. 13, no. 12, pp. 1271-1273, December 2001.

E. S. Björlin, B. Riou, P. Abraham, J. Piprek, Y.-J. Chiu, K. A. Black, A. Keating, and J. E. Bowers, "Long Wavelength Vertical-Cavity Semiconductor Optical Amplifiers," *IEEE Journal of Quantum Electronics*, vol. 37, no. 2, pp. 274-281, February 2001.

E. S. Björlin, B. Riou, A. Keating, P. Abraham, Y-J Chiu, J. Piprek, and J. E. Bowers, "1.3-μm Vertical-Cavity Amplifier," *IEEE Photonics Technology Letters*, vol. 12, no. 8, pp. 951-953, August 2000.

*First author presentations*

E. Staffan Björlin, "Long Wavelength Vertical-Cavity Semiconductor Optical Amplifiers," presented at SPIE ITcom02, August 2002, Boston, MA. (invited)

E. Staffan Björlin, Patrick Abraham, Yi-Jen Chiu, Joachim Piprek, Donato Pasquariello, John E. Bowers, "High Gain, High Efficiency Vertical-Cavity Semiconductor Optical Amplifiers," *Conference Proceedings of 14th International Conference on Indium Phosphide and Related Materials (IPRM '02)*, pp. 307-310, May 2002, Stockholm, Sweden.

E. S. Björlin, J. Geske, J. E. Bowers, "10Gb/s optically preamplified receiver using a vertical-cavity amplifying optical filter," *Technical Digest of 27th Optical Fiber Communication Conference (OFC '02)*, pp. 153-155, March 2002, Anaheim, CA.

E. Staffan Björlin, Joachim Piprek, John E. Bowers, "Noise in Vertical-Cavity Semiconductor Optical Amplifiers," *Conference Proceedings of LEOS 14th annual meeting*, pp. 542-543, November 2001, San Diego, CA.

E. Staffan Björlin, Joachim Piprek, Yi-Jen Chiu, John E. Bowers, Anders Dahl, Patrick Abraham, Chris Harder, "1.3μm vertical-cavity amplifying switch," *Technical Digest of 12th Optical Amplifiers and their Applications OSA Topical Meeting and Exhibit*, paper OtuE11, July 2001, Stresa, Italy.

E. S. Björlin, B. Riou, P. Abraham, J. Piprek, Y-J Chiu, K. A. Black, and J. E. Bowers, "Vertical-Cavity Semiconductor Optical Amplifiers," *Conference Proceedings of LEOS 13th annual meeting*, pp. 573-574, November 2000, Puerto Rico. (invited)

*Co-authored articles and presentations:*

K. A. Black, E. S. Björlin, J. Piprek, E. L. Hu, and J. E. Bowers, "Small Signal Frequency Response of Long Wavelength Vertical Cavity Lasers," *IEEE Photonics Technology Letters*, vol. 13, no. 10, pp. 1049-1051, October 2001.

J. Piprek, E. S. Björlin, and J. E. Bowers, "Optical gain-bandwidth product of vertical-cavity laser amplifiers," *Electronic Letters*, vol. 37, no. 5, pp. 298-299, March 2001.

A. Karim, E. S. Bjorlin, J. Piprek, and J. E. Bowers, "Long Wavelength Vertical Cavity Lasers and Amplifiers," *IEEE Journal of Selected Topics in Quantum Electronics*, vol. 6, no. 6, pp. 1244-1253, November/December 2001. (invited)

J. Piprek, S. Björlin, and J. E. Bowers, "Modeling and optimization of Vertical-Cavity Semiconductor Laser Amplifiers," *SPIE Proceedings 4283-15: Physics and Simulation of Optoelectronic Devices IX, Photonics West*, January 2001.

J. Piprek, S. Björlin, and J. E. Bowers, "Design and Analysis of Vertical-Cavity Semiconductor Optical Amplifiers," *IEEE Journal of Quantum Electronics*, vol. 37, no. 1, pp. 127-134, January 2001.

J. Piprek, S. Björlin, B. Riou, P. Abraham, Y-J Chiu, and J. E. Bowers, "Performance Optimization of 1.3um Vertical-Cavity Semiconductor Optical Amplifiers," *Proceedings of European Conference on Optical Communication (ECOC '00)*, vol. 2, pp. 61-62, September 2000, Munich, Germany.

A. Karim, K. A. Black, E. S. Bjorlin, P. Abraham, Y.-J. Chiu, J. Piprek, and J. E. Bowers, "Long Wavelength Vertical Cavity Lasers and Amplifiers," *Proceedings of 5th Optoelectronics and Communications Conference*, July 2000, Chiba, Japan. (invited)

B. Riou, S. Björlin, A. Keating, A. Black, J. Piprek, P. Abraham, and J. Bowers, "1.3 μm Vertical Cavity Amplifier," *Technical Digest of 25th Optical Fiber Communication Conference (OFC '00)*, March 2000, Baltimore, MD.

**Abstract**

Long-Wavelength Vertical-Cavity Semiconductor Optical Amplifiers

by

E. Staffan Björlin

There is currently significant interest in technologies that can provide compact, low-cost optical amplifiers for metro and access networks. Vertical-cavity semiconductor optical amplifiers (VCSOAs) are a new class of devices that show promising characteristics for these applications. VCSOAs have a number of advantages over in-plane SOAs, such as high coupling efficiency to optical fiber (facilitating a low noise figure), polarization independent gain, and low power consumption due to a small active volume. The typically narrow gain bandwidth of VCSOAs makes these devices function as amplifying filters. In addition, the vertical cavity design allows for on-wafer testing and fabrication of two-dimensional arrays.

This thesis presents two generations of long-wavelength VCSOAs and a broad theoretical VCSOA model, and investigates potential VCSOA applications. The theoretical model is based on the Fabry-Perot equations for a cavity with gain, and rate equations for the carrier density and photon density. It includes an analysis of how the mirror reflectivities affect all VCSOA properties—gain, gain bandwidth, saturation, and noise figure. Two generations of optically pumped long-wavelength VCSOAs were designed, fabricated, and analyzed. Both generations were optimized for reflection mode operation and fabricated by InP-GaAs wafer bonding. The first generation was a fairly simple planar structure where the lateral dimensions of the active region were defined by the optical pump beam. The objectives of these devices were to investigate basic VCSOA properties and to validate the theoretical model. The goals of the

second generation VCSOAs were to improve the efficiency and reach higher gain than what was achieved with Generation 1. The difference in the designs was the carrier confining structure in Generation 2. This resulted in significantly decreased carrier loss, and produced a threefold efficiency improvement. The results of the second generation VCSOAs are, in summary: 17 dB fiber-to-fiber gain, 6.1 dB noise figure, and –5 dBm saturated output power. Two applications, switching/modulation and optical preamplification of high-speed receivers, were investigated. Optical preamplification at 10 Gb/s was demonstrated. Using a VCSOA operated at 11 dB of gain, the sensitivity of a PIN receiver was improved by 7 dB resulting in a receiver sensitivity of –26.2 dBm.

# Contents

# Chapter 1

# Introduction

Data and telecommunication traffic are currently growing at an unprecedented rate. The only available technology that can meet the massive demand for bandwidth is lightwave transmission over optical fiber. Fiber-optics have been used for many years for long distance transmissions and today the fiber-optic networks are expanding into the homes. A natural limitation to the possible transmission distance is the attenuation of the signal power in the fiber, as well as losses associated with connectors and passive components. Using modern, low-loss fiber, the signal can travel about 60 to 100 km before the attenuation makes it too weak for error free detection. The solution to this problem used to be repeaters, which are bulky, expensive devices that detect and regenerate the signal. Besides being bulky and expensive, the optical to electrical to optical (OEO) conversion limits the bit rate to that of the electronics, making upgrades problematic. In the late eighties the Erbium doped fiber amplifier (EDFA) revolutionized fiber optics by offering amplification of the lightwave signal without transferring the signal to the electrical domain. The use of optical amplifiers made the fiber-optic networks more versatile and new

links could be added at a lower cost. EDFAs are now widely deployed in long-haul networks and have recently been introduced into metropolitan area networks.

During the telecommunication boom of the past decade, two important research areas have been to increase the capacity of long-haul links and to expand the fiber-optic networks closer to the end-user. Development within both areas has been strongly dependent on improvements made in optical amplifier technology. Upgrades to higher bit rates and the introduction of wavelength division multiplexing (WDM) in the long-haul would not have been possible without EDFAs. The expansion into metropolitan areas and ultimately towards fiber-to-the-home (FTTH) has made the component size, power consumption, and, mainly, component cost increasingly important parameters. This has spawned a huge interest in alternative amplifier technologies that are less expensive and more compact than EDFAs. Examples of compact, low-cost amplifiers include Erbium doped waveguide amplifiers (EDWAs) and semiconductor optical amplifiers (SOAs).

The massive interest in vertical-cavity surface emitting lasers (VCSELs) has lead to the idea of an SOA based on VCSEL technology—a vertical-cavity semiconductor optical amplifier (VCOSA). These devices show some very interesting characteristics stemming from the unique physics of the Fabry-Perot cavity. They also offer a number of advantages over in-plane SOAs. The feed-back constricts the gain bandwidth to the linewidth of the Fabry-Perot mode, which essentially limits the operation to amplification of a single signal. The narrow bandwidth also filters out out-of-band noise, making VCSOAs ideal as preamplifiers in receiver modules. The vertical cavity is circular symmetric around the axis perpendicular to the two mirrors and naturally supports a circular optical mode. This yields high coupling efficiency to optical fiber, which is beneficial for achieving a low noise figure. The perpendicular travel of

the optical mode through the material layers ensures that the optical field is always parallel to the quantum wells (QWs). This, together with the circular symmetric waveguide, makes it easier to achieve polarization independent gain as compared to the in-plane geometry. VCSOAs are also smaller and less power-consuming than in-plane SOAs. Furthermore, the vertical-cavity structure enables fabrication of two-dimensional (2D) arrays as well as testing the devices on-wafer, which lowers the manufacturing cost.

This thesis investigates the properties of VCSOAs and explores some of the possible applications for these devices. Two generations of long-wavelength VCSOAs are designed, fabricated, and analyzed. The feasibility of using VCSOAs for modulation applications and in optically preamplified high-speed receivers is examined.

## 1.1 Amplifier needs

Optical amplifiers are used for a wide variety of applications in fiber optic communication systems. The three most basic functions are booster amplifiers, in-line amplifiers, and preamplifiers. These functionalities are shown in the schematic of a communication link shown in Figure 1.1.

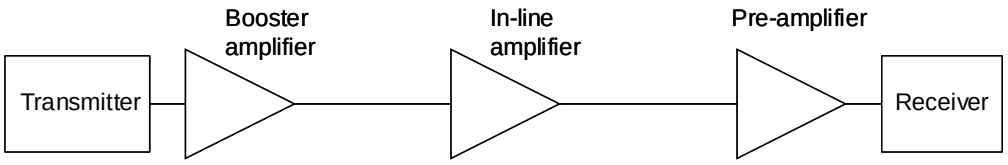


*Figure 1.1. Communication link showing basic applications of optical amplifiers.*

The booster, or post amplifier, is used immediately after the transmitter in order to boost the signal power before the signal enters the fiber. This is desired for example when external modulation is used and there is substantial loss through the modulator. It is also useful if the signal is divided, *e.g.* for broadcasting of information. The requirements for booster amplifiers are high gain and high saturation output power. Wide gain bandwidth is required if the transmitter is tunable; for a fixed wavelength source there is no constraint on the bandwidth (as long as it is wide enough to pass the modulated signal). Depending on technology, the booster amplifier can be integrated with the transmitter. In this case the polarization of the input signal is known and the amplifier does not have to be polarization independent.

In-line amplifiers are inserted in the link periodically in order to keep the signal power at a receivable level. If the signal power is too low, it is impossible to recover the information; if it is too high nonlinear effects in the fiber can distort the signal. The requirements on in-line amplifiers are high gain, high saturation power, polarization independent gain, and low noise figure. Because of the widespread use of WDM, in-line amplifiers usually have to support a large number of signals. For this reason, wide bandwidth is needed and cross talk between channels must be avoided. EDFAs are ideal for this application. However, the gain spectrum of EDFAs is limited to about 1530 to 1620 nm. This covers the conventional WDM band (C-band—about 1530 to 1560 nm) and the long WDM band (L-band—about 1560 to 1620 nm) in the 3$^{rd}$ telecommunication window. The 2$^{nd}$ transmission window around 1.3 μm is still used in many communication systems and there are efforts to expand the 3$^{rd}$ windows down toward 1480 nm, thereby utilizing a bigger part of the low-loss window of the fiber. (The wavelength region from 1480 nm to 1530 nm is referred to as the S-band—the short WDM band.) These wavelength regions cannot be covered by EDFAs. Extensive work has been done to develop fiber

amplifiers for these wavelength regions. Research has also been done on the feasibility of using Raman amplification instead of, or in combination with, EDFAs. Raman amplification can be used in any wavelength region. The main advantage of Raman or Raman/EDFA hybrid amplifiers is the noise performance. These technologies are mainly attractive for long-haul links. (Most installed fiber has these two low-loss windows separated by an absorption peak at 1.4 μm. Recent advances in fiber technology have eliminated this peak and there is now fiber available with a low-loss window stretching all the way from about 1250 nm to over 1600 nm. This clearly opens up new possibilities for expansion of the WDM wavelength spectrum. As this new fiber is not yet widely deployed however, most amplifier research is done with the properties of the conventional fiber in mind).

A preamplifier boosts the power level of the signal right before the receiver. This is a good method to increase the sensitivity of the receiver without compromising its high-speed performance. The signal power reaching a preamplifier is typically low so the saturation power is not an important parameter. There are no requirements for wide bandwidth if the channels are demultiplexed before preamplification. However, in some applications all channels or a band of channels are preamplified before demultiplexing and in these cases a wide gain bandwidth is obviously needed. The most important issues are high polarization independent gain and good noise performance.

In addition to these three basic functions there are a number of other applications for optical amplifiers. There are many situations in WDM systems where only one or a few channels need to be amplified. One example is when losses through passive components have to be compensated, another is channel power equalization. In these cases wide bandwidth and high gain might not be needed, but compactness, low power consumption and low cost are desired

properties. This is an area where SOAs and EDWAs are expected to find many applications.

Most amplifier technologies have been developed with a specific application in mind but in some cases the properties of the amplifier suggest an unexpected application. SOAs were studied in the early eighties with the objective of using them as in-line amplifiers in long-haul systems. As we know now, the EDFA turned out to be far superior for this task. However, the fast gain dynamics of SOAs have lead to the idea of using them for various optical processing tasks. Two examples of applications that have attracted a lot of interest recently are switching [1,2] and wavelength conversion [3]. For switching applications the signal is divided and fed through a matrix of SOAs. An amplifier that is turned off naturally absorbs the signal. By turning a combination of amplifiers on, a path through the grid opens up that routs the signal to the desired output port. Switches based on SOAs can be extremely fast with gating times on the order of nanoseconds, something that is needed in future all-optical packet-switched systems. The amplifier gain compensates for coupling loss through the switch.

Wavelength conversion is expected to be an extremely important functionality in future WDM networks. The main application for wavelength converters will be to make all-optical cross connects non-blocking for all wavelengths. Wavelength conversion can be performed in optical amplifiers by utilizing either cross gain modulation (XGM) or cross phase modulation (XPM) to transfer information from a modulated signal to a continuous signal at the desired output wavelength. SOAs are one of the most promising candidates to perform this task because of their fast gain dynamics and possibility of on-chip integration.

## 1.2 Amplification technologies

Amplification through stimulated emission at optical frequencies was first proposed and theoretically analyzed by A. L. Schawlow and C. H. Townes in 1958 [4]. Experimental results of coherent optical amplification were presented in the early sixties using HeNe lasers, Ruby lasers, as well as semiconductor lasers. During this time, experiments were also carried out on stimulated emission in rare-earth doped glass fibers, experiments that much later lead to the EDFA in 1987. Optical amplification through stimulated Raman scattering—a nonlinear effect in silica fiber—was first studied in the early seventies. Raman amplification is today highly interesting for long-haul applications.

This section gives an introduction to the different amplifier technologies used in communication networks today: SOAs, EDFAs, EDWAs, and Raman amplification. It is, however, not a complete listing of all possible technologies that can amplify light coherently, nor is it a complete description of the physics behind the amplification technologies; in-depth descriptions of these technologies can be found in the references. The section is concluded by a table comparing the performance of the different approaches.

*Semiconductor optical amplifiers (SOA)*

In 1963, only one year after the demonstration of the first semiconductor laser, Coupland *et al.* demonstrated amplification of an injected signal in a GaAs laser diode [5]. Since then, semiconductor optical amplifiers (SOAs), also referred to as semiconductor laser amplifiers, have been extensively studied [6 and references therein]. During the seventies and early eighties SOAs were considered the most promising candidate for in-line amplification in optical fiber communication systems. This presumption changed drastically in the late eighties when the EDFA was introduced. However, the properties of SOAs and

EDFAs are drastically different, and there are numerous applications where SOAs are better suited. SOAs can be grouped into two fundamentally different categories: Fabry-Perot amplifiers (FPA), which use feedback to enhance the gain of the active region, and traveling wave amplifiers (TWA) where the facets are antireflection coated to suppress feedback. Whereas the oscillations in FPAs only allows amplification within the Fabry-Perot modes, the entire gain spectrum of the active material can be utilized in TWAs. As much as 300 nm gain-bandwidth have been obtained using a nonidentical-multiple-quantum-well active region [7]. The main advantages of SOAs are small size, low power consumption, and low manufacturing cost. Semiconductor technology also enables amplification at virtually any desired wavelength as well as on-chip integration with other semiconductor devices. SOAs and drive circuitry can be integrated on the same chip, or SOAs can be integrated with other optical components in photonic integrated circuits [8]. Disadvantages of conventional in-plane devices include polarization dependent gain (PDG) and poor coupling efficiency to optical fiber, the latter resulting in a high noise figure. Specially designed active regions that minimize PDG have been developed [9]. Mode converters are used for improved coupling efficiency [10]. These modifications, however, make the devices more complex and increase the manufacturing cost. SOAs have very fast gain dynamics which makes them respond to changes in drive current or signal power very fast. This results in cross-talk if two or more signals are amplified simultaneously and has obstructed the use of SOAs in WDM systems. On the other hand, it has opened up a wide range of new interesting applications, such as switching and wavelength conversion.

SOAs have recently experienced something of a revival, thanks to the increased need for low-cost components. The devices that have generated the most interest, however, are not traditional SOAs but gain-clamped SOAs [11]. Gain clamping is achieved by having a lasing mode share the same gain medium

as the amplifier. The lasing action clamps the gain at a constant value and fluctuations in signal power are absorbed by the lasing mode instead of transferred to other signals. Cross-talk is thereby greatly reduced and these amplifiers can be used for WDM applications. Commercially available SOAs offer about 25 dB of gain over 40 nm bandwidth and a saturation output power of about +10 dBm. The noise figure is typically rather high, 7 to 9 dB, and the PDG is about 0.5 dB.

*Erbium doped fiber amplifiers (EDFA)*

Amplification in rare-earth doped fiber was demonstrated and analyzed as early as 1964 [12]. The increased interest in fiber-optic technologies in the 1980s led to the first demonstration of the EDFA in 1987 [13,14]. The gain spectrum of EDFAs coincides with the 1.55-μm low-loss window of standard silica fiber and their slow gain dynamics (about 10 ms) eliminate cross-talk. Furthermore, EDFAs can be fusion spliced to the transmission fiber resulting in very low coupling loss, and they show excellent noise properties. All these facts make EDFAs ideal as inline amplifiers in WDM systems. They are today by far the most commonly used optical amplifiers in communication systems. EDFAs can deliver polarization independent gain as high as 50 dB and saturation output power of +23 dBm. The noise figure is typically between 4 to 7 dB. The gain bandwidth normally spans from 1530 to 1560 nm but can be extended to 1620 nm by deploying special pumping schemes. The drawbacks are bulkiness, high cost, and high power consumption, which limit their usefulness in smaller, cost-sensitive networks. EDFAs are typically operated in saturation in order to maximize the output power. Gain transients when channels are dropped or added are therefore a difficult problem. Another limitation is the wavelength range. Extensive work has been done to develop fiber amplifiers that can cover other wavelength regions. Amplification around 1.3 μm can be achieved using

praseodymium ($Pr^{3+}$) or neodymium ($Nd^{3+}$) doping [15]. The best results have been reported for praseodymium-doped amplifiers (PDFAs) [16]. Thulium ($Tm^{3+}$) doping is used for amplification in the so-called S-band (1480-1530 nm) [17]. One of the major difficulties for these cases is the fact that silica fiber cannot be doped with these elements, and fluoride based fiber has to be used. Fluoride based fiber is expensive, very brittle, and difficult to fusion splice to the silica based transmission fiber. Consequently, these amplifiers are more expensive than EDFAs and their performance trails that of EDFAs. Furthermore, the poor pump conversion efficiency of these amplifiers makes them very inefficient.

*Erbium doped waveguide amplifiers (EDWA)*

Amplifiers based on erbium doped planar waveguides have attracted a lot of interest recently because of the increased need for compact, low-cost devices. The technology was extensively studied during the nineties [18,19] and EDWAs are now commercially available from several manufacturers. The main advantages of these devices are low manufacturing cost and a small form factor. The packaged size, including pump laser, is typically about $15 \times 2 \times 2$ cm. The technology also allows for integration of amplifiers with other waveguide devices such as splitters, combiners, modulators, etc. thereby creating loss-less devices [20]. Like EDFAs, EDWAs are limited to operation around 1.55 μm. They are also optically pumped and the cost of the pump laser limits the cost advantage EDWAs have over EDFAs. The gain and saturation power are typically lower than for EDFAs. It is possible to achieve higher gain by doping the glass higher but this also results in a higher noise figure. The doping levels typically used yield about 2 – 3 dB of gain per cm [21]. High gain could be achieved by using a very long waveguide. In practice, however, this is limited by the size of available substrates. Furthermore, a very large device would

eliminate the size advantage of this technology. EDWAs are polarization insensitive and typically provide about 15 dB of gain across the C-band. The noise figure is slightly higher than for EDFAs but lower than for SOAs.

*Raman amplification*

Raman amplification is based on stimulated Raman scattering, a nonlinear effect inherent to silica fiber where power from a high energy pump field is scattered and coherently added to a lower energy (longer wavelength) signal field [22]. The energy difference, known as the Stoke's shift, is emitted as an optical phonon. The fact that Raman amplification takes place in the existing transmission fiber and the possibility to achieve gain at any desired wavelength are two major advantages. The technology also shows very favorable noise properties. Low noise figure is not inherent to the Raman amplification process but stems from the fact that the gain is distributed along the fiber as opposed to lumped amplifiers. To achieve gain over a wide wavelength spectrum, several pumps have to be used, which, in combination with poor conversion efficiency makes the technology extremely power consuming. The need for multiple pump lasers also makes this a very expensive technology.

Raman amplification was studied in the mid-eighties for use in soliton systems [23] but interest faded when the EDFA was introduced in the late eighties. The technology is now gaining interest again as network engineers expand the WDM transmission window outside the C-band and seek to eliminate repeaters in long-haul and ultra long-haul (ULH) systems. Another important factor responsible for the booming interest is the maturation of high-power pump laser technology.

Raman amplification has been demonstrated at all important telecommunication wavelengths, including the short (S), conventional (C), long (L), and ultra-long (U) WDM band. The technology has been used in long

distance Tb/s transmission demonstrations as well as repeaterless ULH transmission experiment (se, for instance, references in [24]). ULH transmission is the most important application for this technology. Gain of over 40 dB and saturation output power of +30 dBm can be achieved but such high numbers are in general not necessary because of the distributed nature of this technology. Noise figures as low as 4 dB can be achieved. Flat gain over 100 nm was demonstrated using a 12 channel WDM pump source [25].

*Table 1.1. Comparison of optical amplifier technologies*

| | **SOA** | **EDFA** | **PDFA** | **EDWA** | **VCSOA** |
|---|---|---|---|---|---|
| Wavelength region | All telecom wavelengths | 1550 nm | 1310 nm | 1550 nm | All telecom wavelengths |
| Peak gain | 25 dB | 35 dB | 23 dB | 13 dB | 17 dB |
| 3-dB bandwidth | 40 nm | 30 nm | 25 nm | 30 nm | 0.12–0.6 nm |
| $P_{sat}$ (out) | +10 dBm | +23 dBm | +17 dBm | +6 dBm | -5 dBm |
| NF | 7 – 9 dB | 4 – 8 dB | 6.5 dB | 6 dB | 6 dB |
| PDG | 0.5 dB | 0.2 dB | 0.2 dB | 0.2 dB | 0 dB |
| Cost | Low | High | Very high | Medium | Low |
| Commercially available | Yes | Yes | Yes | Yes | No |
| Comment | | 80 nm bandwidth for split-band amplifiers | Gain-bandwidth trade-off Fluoride-based fiber Inefficient | 22 dB of gain over narrower bandwidth | Gain-bandwidth trade-off Parameters vary with mirror reflectivity |

Table 1.1. compares the performance of the most common optical amplifier technologies. The best results of the VCSOAs in this thesis are also included in the table for comparison. None of the technologies have an ultimate design; there are always trade-offs between different parameters, as well as between cost, practicality, and performance. The values given in the table are typical

values of commercially available amplifiers. Raman amplification is not included in the table as it is a distributed amplification technology that is difficult to comparable to discrete amplifiers.

## 1.3 History of vertical-cavity SOAs

Remarkably little work has been done on vertical-cavity SOAs. The first SOA was presented in 1963 [5] and the first VCSEL in 1979 [26]. Since then, extensive work has been done on both types of devices but the combination—VCSOAs—have attracted little interest. In 1991, finally, the first VCSOA was demonstrated by the same research group at Tokyo Institute of Technology that presented the first VCSEL. Koyama, Kubota, and Iga used an electrically pumped GaAs/AlGaAs VCSEL structure to amplify and filter an injected 885-nm signal [27]. The input signal was injected through the bottom mirror, which consisted of seven periods $SiO_2/TiO_2$. The output (top) mirror consisted of $Au/SiO_2/TiO_2/SiO_2$. It is interesting to note that electrical pumping and transmission mode operation was used. This design is advantageous for many applications but is not the easiest design to realize. The favorable filtering properties stemming from the high-finesse VCSEL cavity was recognized; the device was not presented as an amplifier but as an active filter. No fiber-to-fiber gain was obtained but about 4 dB internal gain was reported.

Two years later, in 1993, an optically pumped reflection mode device, also at 850 nm, was presented by Raj *et al.* at France Telecom. It was presented as an amplifying photonic switch. Only pulsed operation was reported [28]. The same group introduced resonant pumping in a following generation of 850-nm devices [29] and in 1996 they presented the first long-wavelength VCSOA [30]. The device was again presented as an amplifying switch. It was optically pumped and operated in reflection mode. The operating wavelength

was 1.55 μm. The sample consisted of an InP/InGaAs active region with two sets of 5 quantum wells, a gold bottom mirror and a two period Si-$SiO_2$ top mirror. 14 dB of gain was achieved in pulsed operation. Also in 1996, Wiedenmann *et al.* at University of Ulm presented an electrically pumped reflection mode VCSOA operating at 980 nm [31]. In 1998, they presented their second generation of devices: an electrically pumped, transmission mode VCSOA with an oxide aperture for current and mode confinement [32]. Whereas many VCSOAs before this were either merely VCSELs operated below threshold or very simple designs that required complicated experimental set-ups and pumping schemes, what Wiedenmann *et al.* presented was a very practical device because of the electrical pumping and transmission mode operation. They achieved 16 dB of gain. However, the operating wavelength was 980 nm, which is not the most interesting wavelength for telecomm applications. In 1998, Lewen *et al.* at KTH in Sweden used a 1.55 μm VCSEL structure for what was the first electrically pumped long wavelength VCSOA [33]. The device had an InP/InGaAsP bottom DBR and a Si/$SiO_2$ top DBR. They measured 18 dB of gain at 218 K not including coupling losses; fiber-to-fiber gain was not quoted. The device saturated very early (less than –25 dBm saturated output power) and the bandwidth was extremely narrow, most likely because the device was optimized as a VCSEL, not an amplifier.

It is interesting to note the wide variety of designs and fabrication technologies that have been used for these devices. The development of VCSOAs have clearly benefited greatly from VCSEL research over the past decade. Devices have been demonstrated with dielectric deposited mirrors, epitaxially grown mirrors, and wafer-bonded mirrors. Buried active regions, ion implantation, and oxide apertures have been incorporated. It is also remarkable that many researchers have stressed the multi-functionality of VCSOAs when presenting their devices. However, until a couple of years ago many aspects of

VCSOAs had sill not been characterized. For instance, the noise figure, which is one of the most important properties of optical amplifiers, had not been investigated. After we presented the first devices operating at 1.3 μm wavelength in 2000 [34], we tried to fill in some of the blanks on the VCSOA world map, and also demonstrate the usefulness of VCSOAs for practical applications.

## 1.4 This thesis

This thesis investigates the fundamental properties of vertical-cavity semiconductor optical amplifiers and explores a few possible applications of these devices to optical communication systems. Two generations of VCSOAs operating at 1.3 μm are presented. Both generations were fabricated by InP-GaAs wafer bonding. The devices were optically pumped and operated in reflection mode. The objectives of the first generation were to demonstrate the first VCSOA at 1.3 μm wavelength, to investigate basic VCSOA properties, and to develop theoretical models for these devices. The structure of these devices was, therefore, very simple. An InGaAsP/InP active region was wafer-bonded to two Al(Ga)As/GaAs DBRs forming a planar chip without any definition of individual devices. The lateral dimensions of the active region were defined by the spot size of the pump beam. Despite the simple structure, remarkable results were achieved thanks to a well-designed active region and excellent material quality. However, the efficiency of these devices was extremely low as carriers could diffuse laterally in the QWs, out of the active region. In the second generation of devices, a carrier confining structure was introduced. Pillars were etched through the active region in order to keep the carriers in the active region and improve the efficiency of the devices. Higher gain was achieved with the second generation and the efficiency was improved by a factor of three.

However, the etched pillar design also introduced anisotropic loss. This resulted in polarization dependent gain for the smaller devices of this generation.

Chapter 2 of this thesis gives general design rules for vertical-cavity SOAs, many of which also apply to in-plane Fabry-Perot SOAs. It introduces two theoretical models that are commonly used to aid device design and analyze SOAs: the Fabry-Perot model and the rate equation model. The fabrication processes and the design of the VCSOAs fabricated in this thesis are described in Chapter 3. Chapter 4 presents and analyzes the amplifier results. It covers amplifier gain, gain bandwidth, saturation, noise figure, and efficiency of both generations, under steady-state continuous wave (CW) conditions. The results are analyzed and compared to the theory developed in Chapter 2. Chapter 5 looks at possible applications for VCSOAs. Two applications are examined in detail: switching/modulation and optical preamplification of high speed receivers. Chapter 6, finally, summarizes the main contributions of the thesis, and gives suggestions for future work.

## References

[1] M. Ikeda, "Switching characteristics of laser diode switch," *IEEE Journal of Quantum Electronics*, vol. QE-19, no. 2, pp. 157-164, Feb. 1983.

[2] E. Almström, C. P. Larsen, L. Gillner, W. H. van Berlo, M. Gustavsson, E. Berglind, "Experimental and Analytical Evaluation of Packaged 4 x 4 InGaAsP/InP Semiconductor Optical Amplifier Gate Switch Matrices for Optical Networks", *IEEE Journal of Lightwave Technology*, vol. 14, no. 6, pp. 996-1004, June 1996.

[3] T. Durhus, B. Mikkelsen, C. Joergensen, S. L. Danielsen, K. E. Stubkjaer, "All-Optical Wavelength Conversion by Semiconductor Optical Amplifiers," *IEEE Journal of Lightwave Technology*, vol. 14, no. 6, pp. 942-954, June 1996.

[4] A. L. Schawlow, C. H. Townes, "Infrared and Optical Masers," *Physics Review*, vol. 112, no. 6, pp. 1940-1949, Dec. 1958.

[5] M. J. Coupland, K. G. Hambleton, C. Hilsum, "Measurement of amplification in a GaAs injection laser," *Physics Letters*, vol. 7, no. 4, pp. 231-232, Dec. 1963.

[6] T. Mukai, Y. Yamamoto, T. Kimura, "Optical Amplification by Semiconductor Lasers," in *Semiconductors and Semimetals*, vol. 22-E, R. K. Willardson and A. C. Beer, Eds. New York: Academic, 1985, pp. 265-318.

[7] C.-F. Lin, B.-R. Wu, L.-W. Laih, T.-T. Shih, "Sequence influence of nonidentical InGaAsP quantum wells on broadband characteristics of semiconductor optical amplifiers-superluminescent diodes," *Optics Letters*, vol. 26, no. 14, pp. 1099-1101, July 2001.

[8] B. Mason, J. Barton, G. A. Fish, L. A. Coldren, S. P. DenBaars, "Design of Sampled Grating DBR Lasers with Integrated Semiconductor Optical Amplifiers," *IEEE Photonics Technology Letters*, vol. 12, no. 7, pp. 762-764, July 2000.

[9] L. F. Tiemeijer, P. J. A. Thijs, T. van Dongen, R. W. M. Slootweg, J. M. M. van der Heiden, J. J. M. Binsma, M. P. C. M. Krijn, "Polarization insensitive

multiple quantum well laser amplifiers for the 1300 nm window," *Applied Physics Letters*, vol. 62, no. 8, pp. 826-828, Feb. 1993.

[10] T. Brenner, H. Melchior, "Integrated Optical Modeshape Adapters in InGaAsP/InP for Efficient Fiber-to-Waveguide Coupling," *IEEE Photonics Technology Letters*, vol. 5, no. 9, pp.1053-1059, Sept. 1993.

[11] L. Lablonde, I. Valiente, P. Lamouler, E. Delevaque, S. Boj, J. C. Simon, "Experimental and theoretical investigation of a gain clamped semiconductor optical amplifier," in *Proceedings to ECOC'94*, vol. 2, pp. 715-718, 1994.

[12] C. J. Koester, E. Snitzer, "Amplification in a Fiber Laser," *Applied Optics*, vol. 3, no. 10, pp. 1182-1186, Oct. 1964.

[13] R. J. Mears, L. Reekie, I. M. Jauncey, D. N. Payne, Low-noise erbium doped fibre amplifier operating at 1.54 μm," *Electronics Letters*, vol. 23, no.19, pp.1026-1028, Sept. 1987.

[14] E. Desurvire, J. R. Simpson, P. C. Becker, "High-gain erbium-doped traveling-wave fiber amplifier," *Optics Letters*, vol. 12, no. 11, pp. 888-890, Nov. 1987.

[15] A. Bjarklev, *Optical Fiber Amplifiers: Design and System Applications*, Boston: Artech House, 1993.

[16] Y. Nishida, M. Yamada, T. Kanamori, K. Kobayashi, J. Temmyo, S. Sudo, Y. Ohishi, "Development of an Efficient Praseodymium-Doped Fiber

Amplifier", *IEEE Journal of Quantum Electronics*, vol. 34, pp.1332-1339, Aug. 1998.

[17] T. Komukai, T. Yamamoto, T. Sugawa, Y. Miyajima, "Upconversion Pumped Thulium-Doped Fluoride Fiber Amplifier and Laser Operating at 1.47 μm," *IEEE Journal of Quantum Electronics*, vol. 31, no. 11, pp. 1880-1889, Nov. 1995.

[18] W. J. Wang, S. I. Najafi, S. Honkanen, Q. He, C. Wu, J. Glinski, "Erbium-doped composite glass waveguide amplifier," *Electronics Letters*, vol. 28, no. 20, pp. 1872-1873, Sept. 1992.

[19] R. N. Ghosh, J. Shmulovich, C. F. Kane, M. R. X. de Barros, G. Nykolak, A. J. Bruce, P. C. Becker, "8-mW Threshold Er3+-Doped Planar Waveguide Amplifier," *IEEE Photonics Technology Letters*, vol. 8, no. 4, pp. 518-520, Apr. 1996.

[20] D. Barbier, M. Rattay, F. Saint André, G. Clauss, M. Trouillon, A. Kevorkian, J.-M. P. Delavaux, E. Murphy, "Amplifying Four-Wavelength Combiner, Based on Erbium/Ytterbium-Doped Waveguide Amplifiers and Integrated Splitters," *IEEE Photonics Technology Letters*, vol. 9, no. 3, pp. 315-317, Mar. 1997.

[21] D. Barbier, "Erbium-doped waveguide amplifiers promote optical-networking evolution" in *LIGHTWAVE*, Nov. 2000.

[22] R. H. Stolen, E. P. Ippen, "Raman gain in glass optical waveguides," *Applied Physics Letters*, vol. 22, no. 6, pp. 276-281, Mar. 1973.

[23] L. F. Mollenauer, R. H. Stolen, M. N. Islam, "Experimental demonstration pf soliton propagation in long fibers: loss compensated by Raman gain," *Optics Letters*, vol. 10, no. 5, pp. 229-231, 1985.

[24] A. Evans, "Raman Amplification in WDM Systems," in *OFC 2001 Technical Digest*, pp. TuF4-1-TuF4-3, Mar. 2001.

[25] S. Namiki, Y. Emori, "Ultrabroad-Band Raman Amplifiers Pumped and Gain-Equalized by Wavelength-Division-Multiplexed High-Power Laser Diodes," *IEEE Journal of Selected Topics in Quantum Electronics*, vol. 7, no. 1, pp. 3-16, Jan./Feb. 2001.

[26] H. Soda, K. Iga, C. Kitahara, Y. Suematsu, "GaInAsP/InP surface emitting injection lasers," *Japanese Journal of Applied Physics*, vol. 18, no. 12, pp. 2329, Dec. 1979.

[27] F. Koyama, S. Kubota, K. Iga, "GaAlAs/GaAs active filter based on vertical cavity surface emitting laser," *Electronics Letters*, vol. 27, no. 12, pp. 1093-1095, June 1991.

[28] R. Raj, J. A. Levenson, J. L. Oudar, M. Bensoussan, "Vertical microcavity optical amplifying switch," *Electronics Letters*, vol. 29, no. 2, pp. 167-169, Jan. 1993.

[29] R. Raj, J. L. Oudar, M. Bensoussan, "Vertical cavity amplifying photonic switch," *Applied Physics Letters*, vol. 65, no. 18, pp. 2359-2361, Oct. 1994.

[30] N. Bouché, B. corbett, R. Kuszelewicz, R. Ray, "Vertical-cavity Amplifying Photonic Switch at 1.5 μm", *IEEE Photonics Technology Letters*, vol. 8, no. 8, pp. 1035-1037, Aug. 1996.

[31] D. Wiedenmann, B. Moeller, R. Michalzik, K. J. Ebeling, "Performance characteristics of vertical-cavity semiconductor optical amplifiers," *Electronics Letters*, vol. 32, no. 4, pp. 342-343, Feb. 1996.

[32] D. Wiedenmann, C. Jung, M. Grabherr, R. Jäger, U. Martin, R. Michalzik, K. J. Ebeling, "Oxide-confined vertical-cavity semiconductor optical amplifier for 980 nm wavelength", in *CLEO 98 Technical Digest*, Paper CThM5, p. 378, 1998.

[33] R. Lewén, K. Streubel, A. Karlsson, S. Rapp, "Experimental Demonstration of a Multifunctional Long-Wavelength Vertical-Cavity Laser Amplifier-Detector", *IEEE Photonics Technology Letters*, vol. 10, no. 8, pp. 1067-1069, Aug. 1998.

[34] E. S. Björlin, B. Riou, A. Keating, P. Abraham, Y-J Chiu, J. Piprek, J. E. Bowers, "1.3-μm Vertical-Cavity Amplifier," *IEEE Photonics Technology Letters*, vol. 12, no. 8, pp. 951-953, Aug. 2000.

# Chapter 2

# VCSOA Design

The design of VCSOAs naturally has a lot in common with the design of in-plane Fabry-Perot (FP) SOAs, VCSELs, and FP filters. These devices have been studied extensively for many years (see, for instance Refs. [1-3]). The theoretical models that have been developed provide a solid foundation on which VCSOA theory is built. For the particular case of the VCSOAs presented in this thesis, the design also relied heavily on previous VCSEL work done at UCSB. The first theoretical paper on VCSOAs was published in 1994 by Tombling *et al.* [4]. The performance predictions presented in that paper were largely based on work by Mukai *et al.* [5]. Since then, VCSOAs have been theoretically examined in a handful of papers [6-9]. The models developed in this thesis leverage off the theoretical work presented in those publications. Section 2.1 of this chapter outlines some general design issues and limitations specific to VCSOAs. Section 2.2 examines the optical cavity, the active region and the mirrors of VCSOAs. Section 2.3 presents the theoretical model in detail, and explains the most important modeling tools—the FP equations and the rate equations. In Section 2.4, theoretical results for gain, gain bandwidth,

gain saturation, and noise properties of VCSOAs are presented. This chapter covers both general theory and the specific cases of the devices fabricated in this thesis.

## 2.1 General design issues and limitations

The fundamental geometrical differences between the vertical-cavity and the in-plane designs result in very different amplifier characteristics. In an in-plane SOA, the mode volume is relatively large, the cross-section of the mode normal to the direction of propagation is oval in shape, and the single-pass gain is large. In a VCSOA, on the other hand, the mode volume is small, the mode is circular-symmetric around the axis of propagation, and the single-pass gain is very small. The optical signal in a VCSOA passes perpendicularly through the different material layers. The optical field is therefore always parallel to the plane of the active layers, which makes it easier to achieve polarization independent gain. The circular-symmetric mode in a VCSOA yields high coupling efficiency to optical fiber, which is beneficial for achieving a low noise figure. The most striking difference between VCSOAs and in-plane devices is the length of the active region. In a VCSOA, the combined thickness of the QWs is on the order of a few hundred nm. In an in-plane device on the other hand, the length of the active region is typically a few hundred μm—three orders of magnitude larger. This naturally results in a very small single-pass gain in VCSOAs, on the order of a few percent, and VCSOAs therefore use feedback, provided by highly reflective mirrors, to enhance the gain. The feedback constricts the gain bandwidth to the linewidth of the Fabry-Perot mode, which typically is on the order of a nanometer or less. (The term gain bandwidth is used throughout this thesis referring to the optical width of the gain spectrum. It is defined as the full width, half maximum (FWHM) of the gain spectrum. The gain bandwidth

should not be confused width the term *modulation* bandwidth, which will be introduced in Chapter 5.)

Depending on the reflectivity of the two mirrors, a VCSOA can be operated in two different configurations: transmission mode operation where both mirrors are slightly transmissive and the signal is injected from one side and collected from the other side, or reflection mode operation where the signal is injected and collected through a slightly transmissive top mirror and the bottom mirror has very high reflectivity. These two configurations are shown schematically in Figure 2.1. There are different advantages and issues with each and the choice of operational mode might ultimately depend on the intended application of the VCSOA.

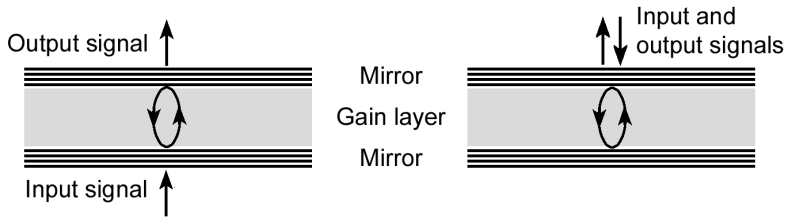


*Figure 2.1. Schematic of VCSOAs showing transmission mode (left) and reflection mode (right) operation.*

The small single-pass gain makes VCSOAs extremely sensitive to losses. In order for any optical amplifier to provide useful signal gain, the internal gain has to overcome all internal losses in the device. However, if the amplifier uses feedback the total loss including mirror loss must not be compensated by the gain, or the device will start lasing. Denoting internal loss per pass $\alpha'_i$ (which includes absorption, scattering and diffraction), mirror loss per pass $\alpha'_m$, and internal gain per pass g', this can be summarized in a few simple relations. (The apostrophes are used here to distinguish the gain and loss terms *per pass* from

$\alpha_i$, $\alpha_m$, and g, which are reserved for internal loss, mirror loss and material gain *per unit length*.)

$g' < \alpha'_i$ ➔ loss

$\alpha'_i < g' < \alpha'_i + \alpha'_m$ ➔ gain

$g' = \alpha'_i + \alpha'_m$ ➔ lasing threshold

Since it is desirable to have as high amplifier gain as possible, it can be seen from the third relation that the total loss also has to be high to keep the device from lasing. High amplifier gain requires high internal gain and low internal loss, and hence the mirror loss should be high. In other words: the more signal power that we couple out of the device, the more we can increase the gain by increasing the drive current or pump power. This is fundamental in the optimization of the mirror reflectivites of VCSOAs. It also leads us to the differences between VCSELs and VCSOAs. In a VCSEL, low threshold current is desirable, which requires strong feedback, *i.e.* high mirror reflectivity. The opposite is true for VCSOAs; using low mirror reflectivity allows for higher single-pass gain without the occurrence of lasing. Another important difference is the cavity length. A VCSEL cavity needs to be short for high frequency modulation. A VCSOA cavity needs to fit a large number of QWs to achieve as high single-pass gain as possible. It is, in fact, desirable to use several stacked multiple-QW active regions in a VCSOA, which requires a longer cavity.

Proper balance between active-region gain and mirror reflectivity is paramount in the design of VCSOAs. The mirror reflectivities have a profound effect on all amplifier parameters—gain, gain bandwidth, saturation power, and noise figure. This will be described in detail in the following sections, and explained briefly in this section. To develop a good understanding for how the amplifier properties change with mirror reflectivity, it is helpful to look individually at the two different regimes where lasing threshold can and cannot

be reached. In the first regime, high mirror reflectivity and high active-region gain makes it possible to reach a round-trip net gain of unity and the device starts lasing. In this case, the carrier density and active-region gain clamp at lasing threshold. This sets the limit for the maximum amplifier gain that can be obtained. Depending on the available active-region gain (which is not fully utilized in this regime) this might prevent operation at high population inversion, which is needed for low noise performance. High mirror reflectivity also leads to increased photon density in the cavity, which results in early gain saturation.

Low reflectivity on the other hand allows for operation at higher carrier density and higher single-pass gain. If lasing threshold cannot be reached, the carrier density can be maximized and the gain of the active region can be used to its full potential. The amplifier has to be pumped harder in this case and the maximum obtainable amplifier gain is limited by the maximum carrier density and maximum material gain. Low mirror reflectivity leads to wider gain bandwidth, higher saturation power, and a lower noise figure. If the reflectivity is *too* low, there will not be enough feedback to reach sufficient signal gain. This simple analysis shows that there is an optimum reflectivity for a given active region. This makes it easier to optimize VCSOAs than VCSELs. In VCSEL design, there is a trade-off between high output power and low threshold. For a VCSOA, it is ideal to use a mirror reflectivity that is just low enough to allow operation at high carrier density without lasing to occur. It is simply desirable to find the breaking point between the two regimes described above. This condition gives the highest possible amplifier gain and gain-bandwidth product, the highest saturation power, and the lowest noise figure.

## 2.2 The amplifier cavity

The resonant cavity of a VCSOA consists of two mirrors enclosing the active region. The mirrors provide feedback of the optical signal and the intensity of the signal grows exponentially as it passes through the gain medium. Interference between the fields traveling back and forth inside the cavity creates a standing wave between the mirrors. The design of the cavity, *i.e.* length, mirror reflectivity, etc., affects the shape of the optical mode, the spectral dependence of the amplifier gain, and the free spectral range (FSR) of the VCSOA. The amplified spontaneous emission (ASE) is also enhanced by the feedback. This can have a detrimental effect on the noise figure of the amplifier if the mirror reflectivities are not chosen properly. The ASE can also cause gain saturation if the device is operated very close to lasing threshold.

One important difference between VCSOAs and VCSELs is the input signal that is injected through one of the mirrors in the VCSOA. The mirror on the input side has optical signals traversing it in both directions, and the interference between these signals has to be accounted for when analyzing the device. If not taken into account properly, this interference leads to a discrepancy between results obtained using different models [1,7]. This was neglected for many years in the analysis of FP amplifiers. In 2002, Royo *et al.* realized the problem and showed that this interference leads to a different expression for the mirror loss compared to the expression commonly used when analyzing lasers [8,9]. The loss through the mirrors actually depends on the gain of the amplifier. This can be qualitatively illustrated by a simple example. Consider a cavity made of two mirrors with reflectivities $R_1$ and $R_2$ as depicted in Figure 2.2, and an incoming field of a wavelength that corresponds to the cavity resonance. The fields are labeled as follows. Incoming field: $E_1$; reflected of the first mirror: $E_2$; entering through the first mirror: $E_3$; reflected of

the second mirror: $E_4$; exiting through the second mirror: $E_5$; reflected of the inside of the first mirror: $E_6$; exiting through first mirror: $E_7$. Fields $E_6$ and $E_3$ will add up in phase and thereby build up the intensity inside the cavity. If $R_1 = R_2$, this intensity is high enough so that $E_7$ exactly cancels out $E_2$ by destructive interference (these two fields are 180° out of phase) and $E_5$ is of the same intensity as $E_1$. The resonator appears to be transparent to the cavity resonance wavelength.

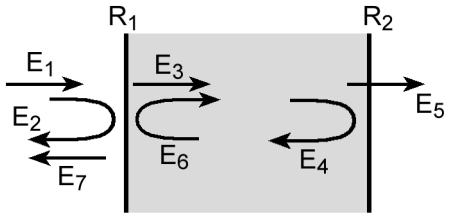


*Figure 2.2. FP cavity with mirror reflectivities $R_1$ and $R_2$. Mirror $R_1$ has fields traversing it in both directions. This has to be considered when analyzing VCSOAs.*

If $R_1 > R_2$, $E_7$ will not quite cancel out $E_2$ and there will be a back reflection. However, if $R_1 > R_2$ and there is gain in the cavity, the intensity inside the cavity is amplified and $E_7$ can cancel out $E_2$ (if the gain has precisely the right value). Looking at the cavity from the left, it is impossible to distinguish between the last case and the case of equally reflective mirrors. This example is quite simple but it serves its purpose of pointing out that the phase information of the signal cannot be neglected. A rigorous derivation of the proper expression for the mirror loss can be found in Ref. [8]. Another instance where the interference between the input and output signals is important is when using VCSOAs for modulation applications. In a reflection mode device, the output signal vanishes when the field reflected off the input mirror cancels out the field exiting the cavity. This effect can be used to greatly enhance the extinction ratio. This will be discussed in more detail in Chapter 5.

### *2.2.1 Active region*

Active region designs that have been developed for VCSELs are in many cases directly applicable to VCSOAs. For example, strained multiple quantum well (MQW) active regions have been standard for VCSELs for many years. Indeed, all VCSOAs presented to date, except the very first one, used MQW active regions. InGaAsP/InP is the most commonly used material system for long-wavelength VCSEL active regions. It is also the material system used in all long-wavelength VCSOAs that have been presented. The development of long-wavelength VCSELs has trailed that of short-wavelength VCSELs. The main reasons for this are the difficulties to make good mirrors that can be grown lattice matched on InP, the high Auger recombination in narrow bandgap materials, and the small conduction band offset in InGaAsP/InP. Significant progress has been made recently using AlInGaAs QWs for 1.55 μm emission [10], GaInNAs grown on GaAs for 1.3 μm [11], and Sb-based structures [12]. AlInGaAs provide improved high temperature performance due to its larger conduction band offset and GaInNAs has the advantage of being lattice matched to GaAs. No VCSOAs have yet been reported using these materials.

Of major importance for VCSOA active regions is that the gain is independent of the polarization of the signal. Because of the symmetry of the zinc blende crystal, III-V compound semiconductors grown on (001) substrates exhibit the symmetry needed to provide isotropic gain in the (001) plane. Fortunately, (001) is the most common crystallographic orientation for III-V substrates. Because of the this, QWs grown on regular InP substrates provide gain that is independent of the polarization angle of the signal, as long as the polarization is in the plane of the wells [2]. Since the net modal gain is given by the gain less the loss, polarization dependent signal gain can result from polarization dependent loss, *e.g.* from anisotropic mirror reflectivity or non-

circular mesas [13]. Care has to be taken to not introduce any anisotropic loss in the subsequent processing of the VCSOAs.

VCSOAs require much higher single-pass gain than VCSELs and therefore need more QWs. There does not exist an optimum active region design in the same way as for lasers; there are no trade-offs between the different amplifier properties. In the design of a VCSOA active region, one has to set a target performance level and then from an estimate of the material gain calculate the number of QWs that is needed. The modeling tools needed to do this will be described in Section 2.3. An example will be given here. Assume that the goal is a reflection mode VCSOA with 25 dB of amplifier gain and at least 0 dBm of saturated output power. Furthermore, assume that the QW material can provide a maximum gain of 3000 $cm^{-1}$ at full inversion. The VCSOA QWs should be pumped as close to full inversion as possible, in order to achieve the lowest possible noise figure. To reach the desired performance level, the mirror reflectivities should be about 0.9 for the top mirror and as close to unity as possible for the bottom mirror. That would give a single-pass gain at threshold of 5.4%. The VCSOA needs to be operated a little bit away from threshold. 5% single-pass gain is therefore a good target value. This requires about 100 nm of active material, which corresponds to about 16 QWs using the QW thickness that was used in the devices in this thesis. The desired value of gain is only reached if the QWs are positioned on one or more of the standing wave peaks in the cavity. By careful positioning of the QWs on the standing wave peaks, the gain can be enhanced by up to a factor two [14]. For the large number of QWs needed in VCSOAs, it is desirable to use a long cavity with the QWs grouped into two or more sets that provide periodic gain that matches the standing wave pattern in the cavity. The standing wave effect (gain enhancement) increases with decreased number of QWs per standing wave peak. If the spacer layers are doped, such as in an electrically pumped device, there is

a trade-off between gain enhancement and absorption loss. In that scenario the ideal design (for 16 wells) is two sets of 8 QWs or, perhaps, $4 \times 4$, depending on the exact value of the absorption loss. If optical pumping is used, the absorption loss is significantly lower, and it is advantageous to split up the QWs into sets of two wells each.

If higher gain is desired, the maximum number of QWs that can be used is limited by the pumping. Even the 16 QWs in the example above would be difficult to pump uniformly using electrical injection. Optical pumping is an attractive way to pump VCSOAs for a number of reasons. Optical pumping generates carriers in the QWs, without the need of transporting the carrier through the structure. This results in very uniform carrier distribution throughout a large number of QWs. As mentioned above, using optical pumping allows the entire structure to be undoped. This simplifies growth and processing, and minimizes optical losses. Furthermore, optical pumping can generate uniform carrier distribution across a laterally large active region. This makes it possible to obtain high output power from a cavity that still supports the fundamental Gaussian mode. Optical pumping is not just a tool for the lab. Device and pump laser can be packaged in the same package, or even integrated into the same structure [15]. Several high-performance long-wavelength VCSELs have been presented that use optical pumping [15,16]. To continue the example above of 16 QWs, and assuming a pump efficiency of 10% (which is slightly better than what was achieved in this thesis), a carrier density of $3 \times 10^{18}$ can be reached with about 35 mW of pump power. If the pump power is increased to 100 mW, the same carrier density can be reached in 45 QWs.

If a very large number of QWs is desired, the limiting factor might ultimately be what is practical to fabricate. The limitations for how thick an active region can be grown depends on many factors, such as what materials are

used, the amount of strain in the different layers, what growth technology is used, and so on. An analysis of this is outside the scope of this thesis.

The two generations of VCSOAs fabricated in this thesis used the same active region material. Since this active region was to be used for the first VCSOAs fabricated on this project it was designed to have significantly more gain than what is needed according to calculations. The extra gain compensated for unexpected loss, and produced good results even from the simple design of the very first generation of devices. The active region design was based on experience from previously designed VCSEL active regions at UCSB. It was an InGaAsP/InP active region grown by MOCVD. It consisted of 21 compressively strained 60 Å thick $InAs_{0.5}P_{0.5}$ QWs (strain: 1.5%) surrounded by strain compensating 76 Å thick $In_{0.8}Ga_{0.2}P$ barriers. The QWs were grouped together in three sets of 7 wells each. 74 nm thick InP spacing layers were used to position the three sets on the three central standing wave peaks in the cavity. 241 nm thick InP cladding layers made the total thickness of the active region 5/2 times the internal wavelength. The refractive index profile and standing wave distribution in the cavity is shown in Figure 2.3. The wafer-bonded interfaces were placed at standing-wave nulls in order to minimize scattering and absorption losses at the rough interfaces.

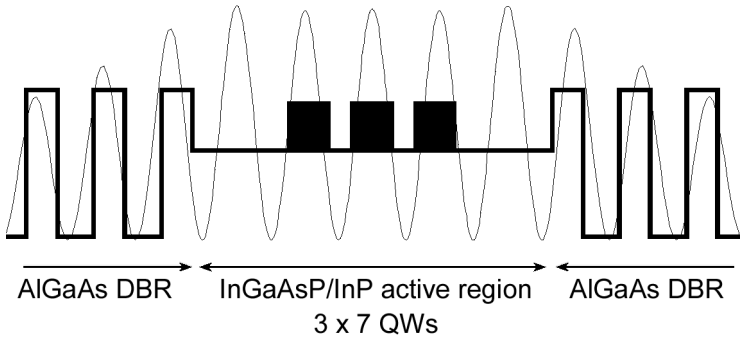


*Figure 2.3. Refractive index profile and standing wave distribution in 5/2-λ cavity of wafer-bonded VCSOA. Quantum wells are positioned at peaks; bonded interfaces at nulls.*

The active region was designed so that the QWs were the only layers in the structure that allowed band-to-band absorption of the 980-nm pump light. The total thickness of the QWs is only 126 nm. Consequently, a substantial fraction of the pump light is transmitted through the device, resulting in rather low efficiency. On the other hand, the excess pump power throughout the wells ensures uniform carrier generation in all wells. Furthermore, having wider-bandgap material surrounding the wells leads to improved carrier confinement. Since optical pumping is employed, population of the wells does not rely on carrier transport. This allowed for the use of $In_{0.8}Ga_{0.2}P$ barriers, which have a wider bandgap than the InP cladding layers. The alternative would be to have lower-bandgap absorption layers surrounding the QWs. This would improve the efficiency of the devices, but not lead to the desired uniform distribution of carriers or good carrier confinement. The band diagram of one set of QWs is shown in Figure 2.4.

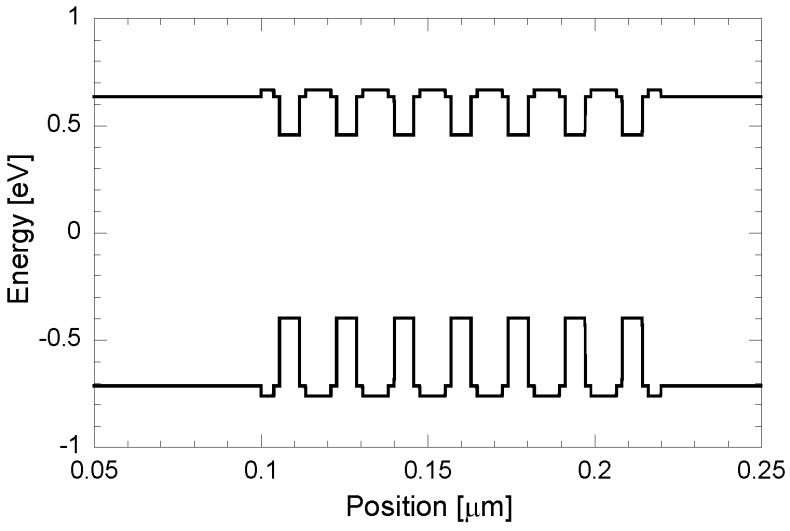


*Figure 2.4. Band diagram of one set of QWs in the active region used in this thesis. The QW design is optimized for optical pumping.*

### *2.2.2 Mirrors*

The reflectivity of the top and bottom mirrors are two of the most important parameters in the design of a VCSOA. For the case of reflection mode operation, a bottom mirror reflectivity close to one is desired, and only the top mirror reflectivity needs careful optimization. The most commonly used type of mirror in VCSELs and VCSOAs is the distributed Bragg reflector (DBR). A DBR consists of alternated $\lambda/4$-thick layers of high and low refractive index materials where constructive interference between the fields reflected off the multiple interfaces throughout the stack leads to very high reflectivity. DBRs can be made of either semiconductor or dielectric material. They can be made either conductive or insulating. DBRs have been the mirrors of choice in VCSELs for many years and extensive publications are available on different types, different materials, and the properties of these mirrors [2,17]. The mirror reflectivity used in VCSOAs is typically significantly lower than what is used in VCSELs. Fewer mirror periods are therefore needed. The exception is the as-high-as-possible reflectivity of the bottom mirror in reflection mode devices. The choice of materials to be used depends on the desired mirror reflectivity, if the devices are to be electrically or optically pumped, the operation wavelength, and available fabrication technologies.

The use of wafer bonding in the fabrication of the VCSOAs in this thesis gives the freedom of optimizing mirrors and active region separately. The mirrors do not have to be lattice matched to the active region. Undoped AlGaAs/GaAs DBRs grown by molecular beam epitaxy (MBE) were used. The technology of wafer bonding this type of DBRs to an InP-based active region has been used to fabricate state-of-the-art long-wavelength VCSELs [18]. DBRs in the same material system are also used in commercially available short-wavelength VCSELs, where the whole structure is grown lattice matched on GaAs. The properties of these mirrors are therefore well known. Their

advantages include good thermal properties and high index contrast, which leads to high reflectivity from relatively few mirror periods. As the VCSOAs fabricated here are optically pumped, undoped material can be used, which minimizes loss associated with free-carrier absorption. The interfaces do not have to be graded, which simplifies the growth considerably. A 25-period $Al_{0.99}Ga_{0.01}As$/GaAs DBR was used as bottom mirror in all devices fabricated in this thesis. The top mirrors used for the devices in this thesis had between 10.5 and 15.5 mirror periods.

The peak reflectivity of a loss-less DBR is easily calculated from the number of periods and the refractive indices of the materials. In reality however, losses in the DBR, including absorption, scattering, and diffraction, lead to lower reflectivity. The magnitude of these losses depends on doping, growth quality, etc. Including absorption in the calculation of the reflectivity is fairly straightforward. To take scattering and diffraction into account is a little bit more involved [17]. An exact number for the total loss in a DBR is difficult to obtain and one typically has to do with a more or less reliable estimate. An example of an important source of loss in the DBRs used in this project is the roughness of the DBR surface. The reflectivity of the top mirror of the VCSOAs was adjusted after the fabrication of the devices was completed. This was done by selectively etch off individual mirror periods. The reflection of the semiconductor-air interface is quite important to the reflectivity of the DBR because of the large refractive index contrast. In several cases the etch resulted in a rough mirror surface, which decreased the reflectivity substantially. A practical and accurate way to calculate the reflectivity of a mirror is from the transfer-function of a Fabry-Perot cavity made from the mirror material. This can be a Fabry-Perot cavity without gain (a filter) or one with gain, *i.e.* a VCSOA. This method was used to calculate the reflectivity of the top mirrors used for the VCSOAs in this thesis. The procedure was the following: the

bottom mirror reflectivity was calculated using Vertical, a VCSEL simulation software that uses one-dimensional transmission matrices. The calculated reflectivity spectrum of the bottom DBR is shown in Figure 2.6. The peak reflectivity is 0.999. (Since the bottom mirror reflectivity is close to unity, and there is no semiconductor air interface, the estimate of the loss is less critical as compared to the case of the top mirror). The gain spectrum of the finished VCSOA was then measured and Equation 2.4 was fitted to the data. Such a curve fit is shown in Figure 2.5 for the case of a VCSOA with a 10.5-period top DBR. The previously calculated bottom mirror reflectivity of 0.999 was used, and top mirror reflectivity, single pass gain, and coupling loss were used as fitting parameters. It is important to measure the peak as well the tails in order to obtain reliable values from the fit. For the device in this example, the top mirror reflectivity was determined to be 0.918.

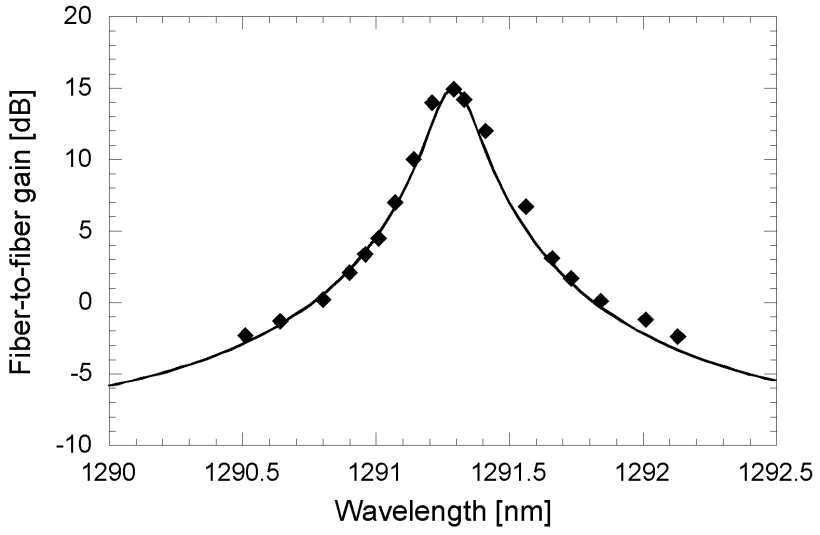


*Figure 2.5. Gain spectrum used to calculate top mirror reflectivity. For this VCSOA the top mirror reflectivity was determined to be 0.918.*

The top-mirror reflectivity of all devices fabricated in this thesis was calculated using this method, and determined to be between 0.91 and 0.98. Another important reason why the above-mentioned method is recommended for determining the reflectivity is evident from the shape of the reflectivity spectra shown in Figure 2.6. The high reflectivity mirror has a flat stopband over about 100 nm. For this case, it is clearly sufficient to simply calculate the peak reflectivity. Also shown in Figure 2.6 is a calculated reflection spectrum for a 8.5-period DBR. The peak reflectivity of this mirror is about 0.9, which is a typical top mirror reflectivity for the VCSOAs fabricated in this thesis. However, the stopband of mirrors with such low reflectivity tend to have a rounder shape. This results in variations in reflectivity if devices with different cavity lengths are fabricated using the same mirror material. For a 10.5 period stack the reflectivity difference between the center wavelength and 10 nm off-center is 0.5%.

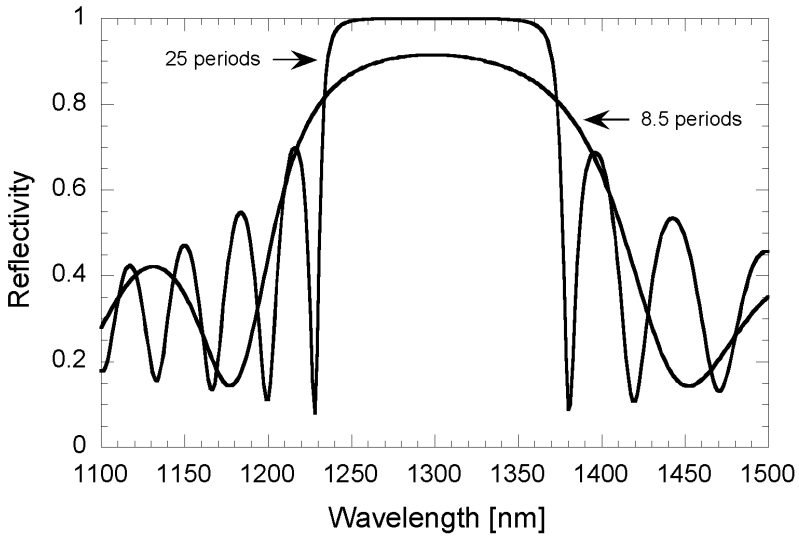


*Figure 2.6. Calculated reflectivity spectra for typical top and bottom DBRs used for VCSOAs in this thesis. Note the round shape of the reflectivity spectrum of the DBR with the lower reflectivity.*

## 2.3 Modeling tools

Several different models have been developed to predict and analyze optical amplifier performance. Rate equations have been used to model the balance and interaction between carriers and photons in SOAs [1,5] as well as fiber amplifiers [19]. The FP approach, where the well-known FP theory is expanded to cover a cavity with gain, is naturally very useful for FP amplifiers. Traveling wave equations have been used to take the spatial distribution of carriers, gain, and photons into account [20]. The traveling wave approach is useful for long devices where different parts of the active region see different signal intensities. In a VCSOA the signal passes through an extremely thin gain region multiple times, and experiences the same gain each time. The traveling wave approach is therefore not necessary for VCSOAs. The noise properties of optical amplifiers have been described using several different approaches, either quantum mechanical or semiclassical [1,5,19].

These models were developed with fiber amplifiers and/or in-plane laser amplifiers in mind, long before the first VCSOA was presented. In most cases the models can be applied to VCSOAs with little or no modification. The first theoretical paper on VCSOAs by Tombling *et al.* [4] was largely based on in-plane FPSOA work by Mukai *et al.* [5]. Both rate equations and the FP equations were used to predict VCSOA performance. Karlsson *et al.* used a similar approach, but also analyzed the detector characteristics of VCSOAs [6]. In 2000, Piprek *et al.* presented a more detailed rate equation model [7]. However, in these early theoretical VCSOA papers—as well as in even older in-plane publications—the results obtained using rate equation analysis and the FP approach did not agree. As mentioned earlier, this problem stemmed from an incorrect expression for the mirror loss, and was solved in 2002 by Royo *et al.* [8,9]. The noise figure of VCSOAs has been investigated recently [21]. Noise

theory developed for in-plane FPSOAs was applied to VCSOAs, and compared to experimental results.

### *2.3.1 Gain model*

The models presented here contain a number of unknown parameters. To show general trends using an established model, typical values from the literature can be used for any unknowns. However, in order to validate the accuracy of a theoretical model that is being developed, it has to be compared to real data. For this purpose realistic values for unknown parameters are essential. Depending on the complexity of the model, one or a few unknowns may be used as fitting parameters; too many unknowns makes the model less useful, albeit easier to fit to the data. One of the more central unknowns in VCSOA modeling is the gain model, which describes the relation between carrier density and material gain. For the active region used in the this project, the gain as a function of carrier density was calculated by J. Piprek using PICS3D laser simulation software [7]. The calculation suggested a transparency carrier density of 1.1 x $10^{18}$ $cm^{-3}$ and gain that saturates to a value of 5100 $cm^{-1}$ for very high carrier densities. Over a limited carrier density range, the gain can be described by the following three-parameter logarithmic function, as described in Ref. [22].

$$g = g_0 \ln\left[\frac{N + N_S}{N_{tr} + N_S}\right] \tag{2.1}$$

N is the carrier density, $N_{tr}$ is the transparency carrier density, and $g_0$ and $N_s$ are fitting parameters. Good agreement with the calculated gain was found using $g_0$ = 1580 $cm^{-1}$ and $N_s$ = -0.63 $cm^{-3}$. This calculation assumed perfect material. In reality however, it is well known that QWs can be damaged by the high temperature and high pressure during wafer bonding if they are not protected by a superlattice defect blocking layer [23].

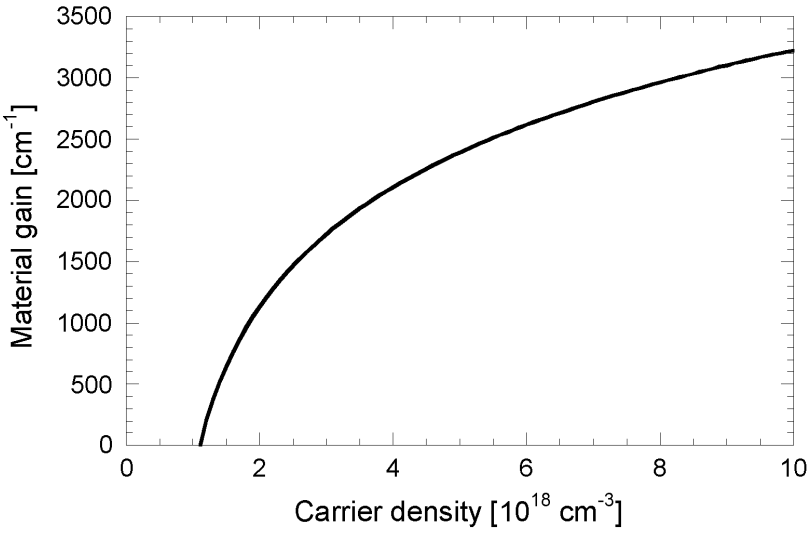


*Figure 2.7. Gain versus carrier density modeled using a three-parameter logarithmic function.*

Heavily strained QWs, as those used in this active region, are especially vulnerable. It is therefore safe to assume that the gain in the real devices after two wafer bonds has been substantially degraded. Indeed, it was found from rate-equation modeling that better agreement with experimental data could be obtained if $g_0$ was decreased to about 1100 cm$^{-1}$. The adjusted three-parameter logarithmic gain function is plotted in Figure 2.7. It is evident from the graph that the three-parameter fit is no good for high carrier densities—it does not suggest any gain saturation. This should be kept in mind when using the gain model in attempts to predict performance at very high carrier densities.

From the material gain, the single pass gain is given by

$$g_s = \exp(\Gamma_{enh} \cdot g \cdot L_a - \alpha_i \cdot L) \tag{2.2}$$

where $\Gamma_{enh}$ is the enhancement factor, $L_a$ is the total length of the active region, $\alpha_i$ is the internal loss, and L is the cavity length. $\Gamma_{enh}$ describes the gain enhancement due to the standing wave effect as described in [22]. For our

structure we calculated $\Gamma_{enh}$ = 1.75. $L_a$ is simply the combined thickness of the QWs, which in our case is 126 nm. $\alpha_i$ is difficult to estimate, but based on measurements on VCSELs made from similar material it can be concluded to be between 5 and 20 $cm^{-1}$. In the modeling here, we used a value of 15 $cm^{-1}$. L is the cavity length including the penetration depth into the mirrors. It is in our case 2.2 μm.

### *2.3.2 Fabry-Perot equations*

The gain spectrum of a VCSOA can be easily modeled using the well-known FP equations for a cavity with gain [1]. In this model, the VCSOA structure is simplified considerably. The DBRs are replaced by two hard mirrors, separated by a cavity of length L with refractive index n. It is important that the penetration depth into the DBRs is included in L. The top mirror reflectivity is $R_t$ and the bottom mirror reflectivity is $R_b$. The signal traversing the cavity experiences a single-pass gain $g_s$. An incoming field entering the cavity through the top mirror is considered, and all fields exiting the cavity are summed up to give the output field. The output field is then divided by the input field and the fields are squared to obtain the power gain. The amplifier gain in transmission mode ($G_t$) and reflection mode ($G_r$) operation are given by

$$G_t = \frac{(1-R_t)(1-R_b)g_s}{(1-\sqrt{R_t R_b}\,g_s)^2 + 4\sqrt{R_t R_b}\,g_s \sin^2\phi} \tag{2.3}$$

$$G_r = \frac{(\sqrt{R_t} - \sqrt{R_b}\,g_s)^2 + 4\sqrt{R_t R_b}\,g_s \sin^2\phi}{(1-\sqrt{R_t R_b}\,g_s)^2 + 4\sqrt{R_t R_b}\,g_s \sin^2\phi} \tag{2.4}$$

$\phi$ is the round-trip phase detuning normalized to the cavity resonance. The phase term contains the cavity length and refractive index, and the signal wavelength. Note that the gain of a transmission mode device is independent of the direction of signal propagation through the device. If $\phi$ is set equal to zero,

Equations 2.3 and 2.4 can be used to calculate the peak gain. The peak gain depends only on three parameters—$R_t$, $R_b$, and $g_s$. From Equations 2.3 and 2.4, formulas for calculating the gain bandwidth are readily obtained. The gain bandwidth (FWHM) for the two cases are given by

$$\Delta f_t = \frac{c}{\pi n L} \cdot \arcsin\left[ \frac{(1-\sqrt{R_t R_b}\, g_s)^2}{4\sqrt{R_t R_b}\, g_s} \right]^{1/2} \tag{2.5}$$

$$\Delta f_r = \frac{c}{\pi n L} \cdot \arcsin\left[ 4\sqrt{R_t R_b}\, g_s \left( \frac{1}{(1-\sqrt{R_t R_b}\, g_s)^2} - \frac{2}{(\sqrt{R_t}-\sqrt{R_b})^2} \right) \right]^{-1/2} \tag{2.6}$$

(c is the velocity of light in vacuum). For a given value of single-pass gain, the amplifier gain increases and the bandwidth decreases with increased reflectivity. A good figure of merit is the gain-bandwidth product—the square root of the gain times the gain bandwidth. It can be shown that the gain-bandwidth product for the two cases are given by the following expressions [24].

$$\Delta f_t \sqrt{G_t} = \frac{c}{2\pi n L} \cdot \left[ \frac{(1-R_t)(1-R_b)}{\sqrt{R_t R_b}} \right]^{1/2} \tag{2.7}$$

$$\Delta f_r \sqrt{G_r} = \frac{c}{2\pi n L} \cdot \left[ \frac{1}{\sqrt{R_t}} - \sqrt{R_t} \right] \tag{2.8}$$

The FP model is a very convenient tool to model general trends in VCSOA behavior. Only a few parameters are needed and the general shape of the curves does not change if the values are varied.

### *2.3.3 Rate equations*

To model the interaction between photons and carriers in the amplifier cavity rate equations are used. This model is more complex than the FP approach. There are more unknown parameters, and the results are more sensitive to the values of these parameters. Rate equation analysis is well known and commonly used to analyze lasers [22]. To analyze amplifiers, the input signal

has to be taken into account. This is done by adding a term in the photon-density equation for the input signal and modifying the mirror loss to account for interference between the input signal and light exiting the amplifier [8]. The rate equations for carriers, N, and photons, S, then take the following form.

$$\frac{dN}{dt} = G_{gen} - \Gamma_{enh} v_g gS - (AN + BN^2 + CN^3) \tag{2.9}$$

$$\frac{dS}{dt} = \frac{\eta_s P_s}{h\nu_s V_s} + \beta\Gamma BN^2 + \Gamma_{enh}\Gamma v_g gS - (\alpha_i + \alpha_m) v_g S \tag{2.10}$$

The first term on the right-hand side of Equation 2.9, $G_{gen}$, is a generation term that is different depending on if electrical or optical pumping is used. For optical pumping, $G_{gen} = \eta_p P_p / h\nu_p V_p$ with $P_p$ the pump power, $h\nu_p$ the energy of the pump photons, and $V_p = L_a A_p$ ($A_p$ is the area of the pump spot) is the pumped volume. The pump efficiency $\eta_p$ is one of the most difficult parameters to estimate and is therefore typically used as a fitting parameter. The second term is the stimulated recombination and the last term summarizes all recombination processes that do not contribute to amplification of the signal. AN is the defect recombination, $BN^2$ is the spontaneous emission, and $CN^3$ is Auger recombination. A has a large impact on the results, it is difficult to estimate, and is generally used as a fitting parameter. B and C have a smaller impact at moderate carrier densities but are important at high carrier densities. Diffusion of carriers can be a substantial loss term, which is not explicitly included here. For large devices, or if some carrier confinement scheme is used, the diffusion loss is small and can be neglected. For the VCSOAs fabricated here however, diffusion turned out to be a major loss term. The diffusion is proportional to the carrier gradient, dN/dr, and the spatial distribution of carriers has to be considered to analyze it rigorously. However, a simpler alternative is to increase one of the loss terms to account for diffusion. If optical pumping is used, the carrier distribution can be assumed to be Gaussian. This makes dN/dr,

and hence the diffusion, proportional to N. Diffusion loss can therefore be included in A. In the small signal regime, well below saturation, the stimulated recombination term in Equation 2.9 can be neglected and it can be solved independently of Equation 2.10. In that case, the lateral distribution of carriers can be more easily analyzed, as explained in Ref. [25]. This will be used to analyze carrier confined VCOSAs in Section 4.3.

The first term on the right-hand side of Equation 2.10 describes the injection of the input signal into the cavity. The second term is the spontaneous recombination, the third term the stimulated recombination, and the last term is the loss of photons. $\alpha_m$ is the mirror loss, which depends on the mirror reflectivity and on the amplifier gain. It is defined as [8]

$$\alpha_m = \left( \frac{G_r + G_t}{G_r + G_t - 1} \right) \cdot \ln g_s \tag{2.11}$$

The rate equations were fitted to measured gain saturation data in order to find viable values for the unknown parameters. All parameters used in the rate equations are summarized in Table 2.1. The parameters that were varied in the curve fit were the pump efficiency $\eta_p$, and the loss terms A and B. The experimental data was from a Generation-1 VCSOA. Due to the high diffusion loss in this generation of devices, a very high value of A ($6.2 \times 10^8$ $s^{-1}$) and a very low pump coupling efficiency ($\eta_p$ = 0.032) was used. It was experimentally determined that only about 20% of the pump light was absorbed in the active region (the rest being transmitted through the VCSOA or reflected back). The internal pump efficiency is thus about 16%. The efficiency of the two generations of VCSOAs will be further discussed in Chapter 4. After the rate equations have been validated by curve fitting to experimental results, they can be used to model how the pump power and signal power affects the gain. Efficiency parameters can be extracted and the gain saturation can be predicted.

*Table 2.1 Parameters used in rate equation model.*

| Parameter | Description | Value | Comment |
|---|---|---|---|
| $\eta_p$ | Pump coupling efficiency | 0.032 | Fitting parameter |
| $P_p$ | Pump power | | |
| $h\nu_p$ | Energy of signal photons | $2.03 \times 10^{-19}$ J | |
| $L_a$ | Length of active region | $1.26 \times 10^{-5}$ cm | Combined QW thickness |
| $A_p$ | Pumped area | $6.08 \times 10^{-7}$ cm$^2$ | Pump beam spot size |
| $V_p$ | Pumped volume | $7.66 \times 10^{-12}$ cm$^3$ | $L_a \times A_p$ |
| $\eta_s$ | Signal coupling efficiency | 0.71 | 1.5 dB coupling loss |
| $P_s$ | Input signal power | | |
| $h\nu_s$ | Energy of signal photons | $1.53 \times 10^{-19}$ J | |
| L | Cavity length | $2.2 \times 10^{-4}$ cm | (Includes penetration into DBRs) |
| $A_s$ | Area of signal mode cross section | $5.41 \times 10^{-7}$ cm$^2$ | |
| $V_s$ | Signal mode volume | $1.19 \times 10^{-10}$ cm$^3$ | $L \times A_s$ |
| $\Gamma$ | Confinement factor | 0.057 | $L_a/L$ |
| $\Gamma_{enh}$ | Enhancement factor | 1.75 | |
| $v_g$ | Group velocity | $9 \times 10^9$ cm/s | |
| g(N) | Material gain | | From gain model |
| A | Defect recombination coefficient | $6.2 \times 10^8$ s$^{-1}$ | Fitting parameter Diffusion loss included |
| B | Bimolecular recombination coefficient | $2.2 \times 10^{-10}$ cm$^3$/s | Fitting parameter |
| C | Auger recombination coefficient | $1 \times 10^{-29}$ cm$^6$/s | From Ref. [22] |
| $\beta$ | spontaneous emission factor | 0.02 | |
| $\alpha_i$ | Internal loss | 15 cm$^{-1}$ | Estimate |
| $\alpha_m(R_t, R_b, g_s)$ | Mirror loss | | From Ref. [8] |

## 2.4 Theoretical results

The theoretical models outlined in the previous section can now be used to plot a number of design curves. General trends for variations with pump level and mirror reflectivity are presented below. The dimensions of the VCSOAs fabricated in this thesis, and the gain model for the active region that was used, were used in some of the calculations. Aside from that, efforts were made to keep the modeling as general as possible. Operation in both transmission mode and reflection mode are covered.

### *2.4.1 Gain and gain bandwidth*

The balance between gain and reflectivity is central in VCSOA design. By plotting the amplifier gain versus mirror reflectivity for different values of single-pass gain, and for operation as close to threshold as desired, the best operating point for a given active region design can be found. Figure 2.8 shows gain (bottom) and gain bandwidth (top) versus mirror reflectivity for a transmission mode VCSOA. One mirror reflectivity is held constant at 0.95 and the reflectivity of the other mirror is represented on the x-axis. The material gain is assumed to saturate at a maximum value of 3500 $cm^{-1}$, which gives a maximum single-pass gain of 8%. Four pairs of curves representing constant single-pass gains of 2%, 4%, 6%, and 8% are shown. These curves were calculated using Equations 2.3 and 2.5. The FP model is only valid below lasing threshold, which is given by the condition $g_s R_1 R_2 = 1$. The gain goes toward infinity and the gain bandwidth goes to zero at lasing threshold. Also shown are gain curves at 95% and 90% of the pump power required to reach lasing threshold. Those curves were calculated using the rate equations. The curve corresponding to a single-pass gain of 8%, together with the 95%-of-threshold curve, mark the maximum amplifier gain that can be obtained. These curves are

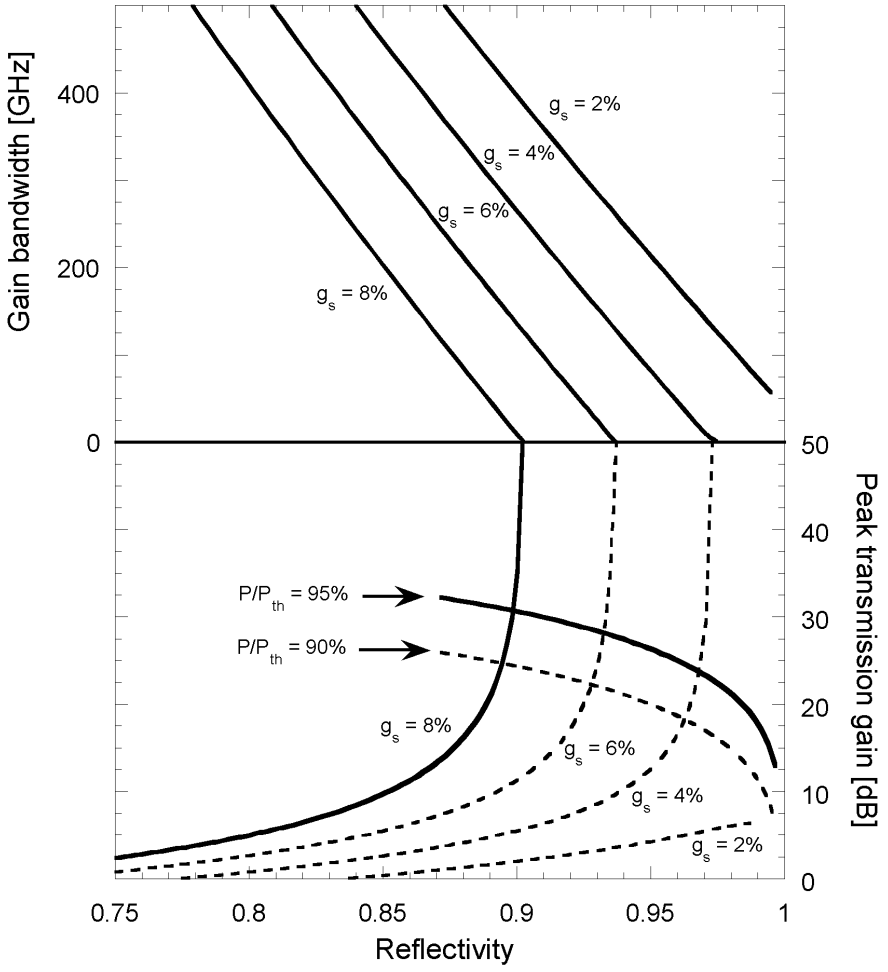


*Figure 2.8. Peak gain and gain bandwidth versus mirror reflectivity for transmission mode operation. The reflectivity of one mirror is held constant at 0.95. The solid lines in the bottom half of the figure indicate maximum achievable gain. The dashed curves indicate trends.*

shown as solid lines. The point where they cross represent the optimum mirror reflectivity and the highest possible gain. For the case of transmission mode operation and the active region used here, the optimum reflectivity is 0.9, which gives a gain of about 30 dB. To the left of this point, the maximum gain is limited by the maximum material gain of 3500 $cm^{-1}$. Lasing threshold cannot be

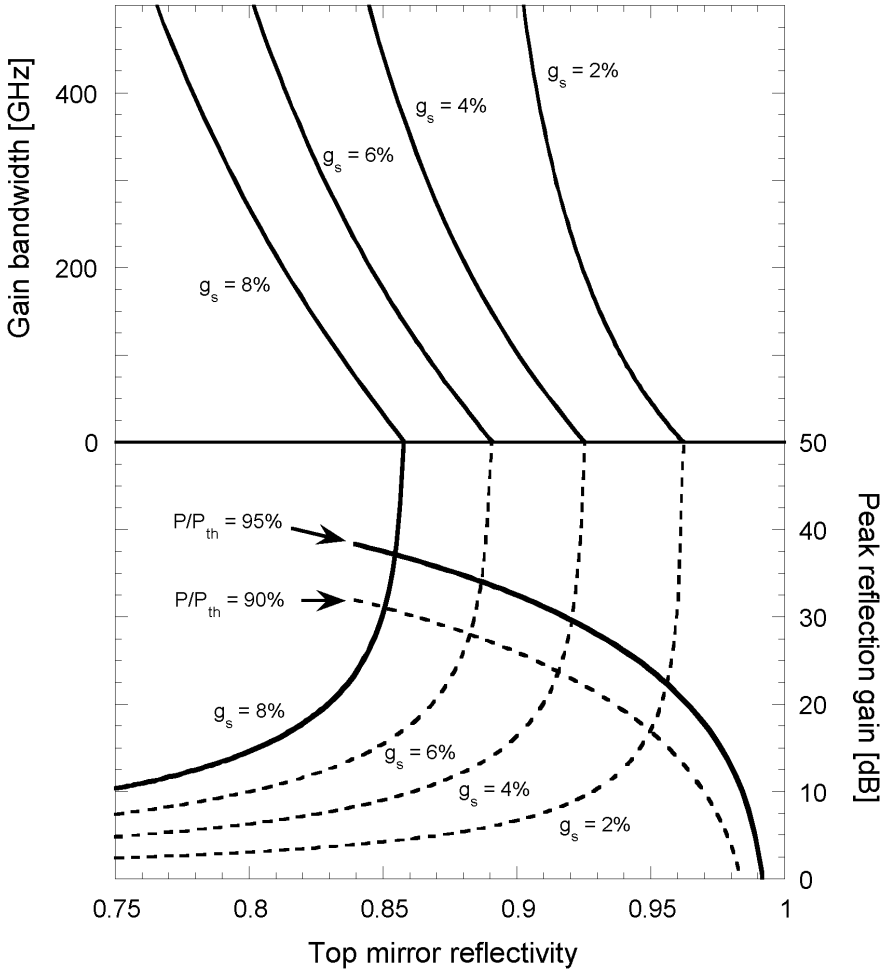


*Figure 2.9. Peak gain and gain bandwidth versus top mirror reflectivity for reflection mode operation. The bottom mirror reflectivity is 0.999.*

reached, and the active region can be pumped to full population inversion for low noise performance. To the right of the crossing point, the VCSOA performance is limited by lasing threshold. The dashed curves show performance trends for lover values of single-pass gain and operation further away from lasing threshold. The gain curves for constant single-pass gain are the most general ones as they only need three input parameters—$R_t$, $R_b$, and $g_s$.

The bandwidth curves are not as general as they require values for the length and refractive index of the cavity. The curves calculated using the rate equations are the least general ones as they involve a number of material and design specific parameters. Figure 2.9 shows gain and gain bandwidth versus top mirror reflectivity for the case of reflection mode operation. For this case, the bottom mirror reflectivity is 0.999. Optimum mirror reflectivity and highest possible gain as suggested by the graph are in this case about 0.85 and 35 dB. The single pass gain needed to achieve high amplifier gain is higher for transmission mode operation because of the higher combined mirror loss.

Figures 2.8 and 2.9 give the impression of a trade-off between gain and bandwidth. However, this is only true for a constant single-pass gain, such as the maximum gain in the low-reflectivity regime. In the high-reflectivity regime, where the performance is limited by lasing threshold, decreased reflectivity allows for stronger pumping and thereby higher gain. Because of this apparent trade-off situation, the gain-bandwidth product is a good figure of merit for VCSOAs. It is defined as the square-root of the gain times the bandwidth. The gain-bandwidth product for both reflection and transmission mode operation are plotted in Figure 2.10 versus reflectivity of one of the mirrors. These curves are calculated using Equations 2.7 and 2.8. For transmission mode operation, the gain-bandwidth product is independent of the direction of signal propagation through the VCSOA. Curves are shown for one mirror reflectivity constant at 0.8 and 0.95, and the other mirror varied. For the case of reflection mode operation, the gain-bandwidth product is independent of the bottom mirror reflectivity; the x-axis represents top-mirror reflectivity. It is clear from the figure that the gain-bandwidth product increases with decreased mirror reflectivity for both operational configurations.

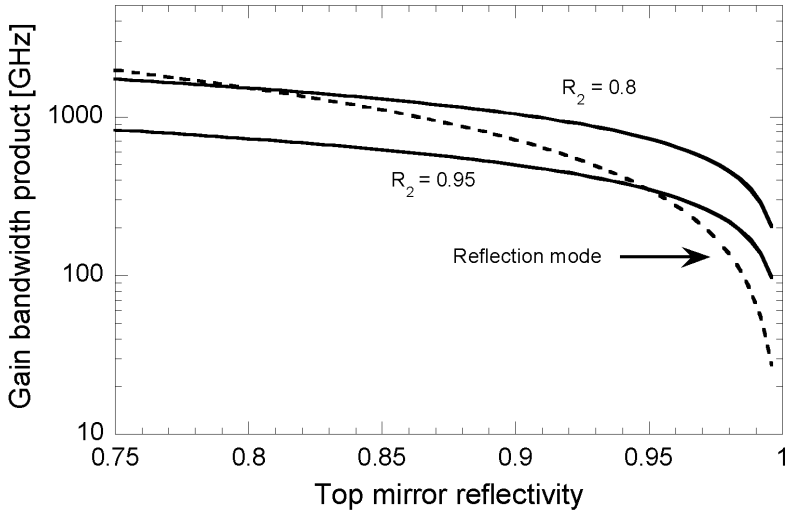


*Figure 2.10. Gain-bandwidth product for reflection mode (dashed line) and transmission mode operation (solid line). For reflection mode operation, the gain-bandwidth product is independent of the bottom mirror reflectivity.*

### *2.4.2 Gain saturation*

As the input signal power is increased, the active region gain eventually saturates. The saturation input power is defined as the input signal power for which the gain drops by 3 dB from its small signal value. The gain saturation is governed by the balance between photons and carriers inside the cavity. To model the saturation properties of VCSOAs, the rate equations (Equations 2.9 and 2.10) are solved for steady state (time derivatives equal zero). The photon density equation is easily solved for S, which is then inserted into the carrier density equation. The carrier density equation is then solved for N, which is used in the gain model to calculated the single-pass gain. Finally, the amplifier gain is calculated from Equations 2.3 and 2.4. The input signal power is varied in order to find the saturation power. Saturation input power versus unsaturated gain for transmission mode and reflection mode operation are shown in figure

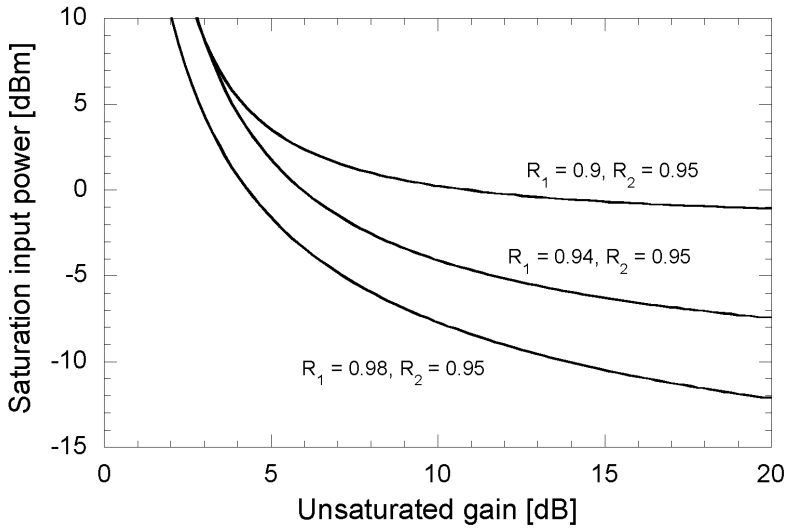


*Figure 2.11. Saturation input power versus unsaturated gain for transmission mode operation.*

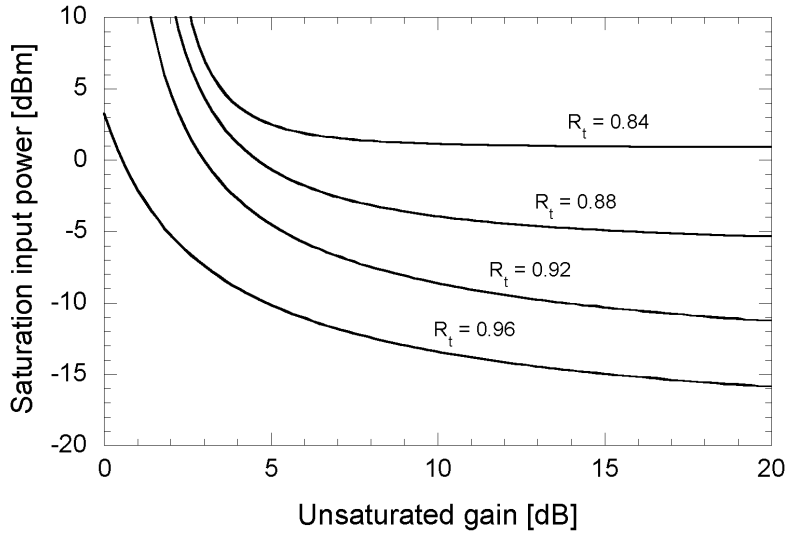


*Figure 2.12. Saturation input power versus unsaturated gain for reflection mode operation. The bottom mirror reflectivity is 0.999.*

2.11 and 2.12, respectively. As the pump power is increased, the gain increases due to the increased carrier density. The increase in gain results in increased photon density. This causes the gain to saturate earlier, except for the case of high gain at very low mirror reflectivities. Depending on the slope of the curve the saturation *output* power may decrease, stay constant, or increase. This varies along the curves, but depends also on the specific VCSOA design (or the model used to describe it).

### *2.4.3 Noise*

Amplification of an optical signal adds undesired power fluctuations to the signal. These power fluctuations are unavoidable as they are inherent to the randomness of the amplification process. The power fluctuations degrade the signal to noise ratio (SNR), ultimately leading to undetectable information. The noise figure is a figure of merit for the SNR degradation, and hence for the power penalty associated with the introduction of the device into a transmission system. The total output noise from an optical amplifier consists of several different noise terms of different origin. The terms contributing to the total noise are: beating between ASE components and the coherent signal light, beating between different ASE components, and shot noise due to both signal and ASE. The input signal might also have some excess noise and the receiver adds thermal noise. Spontaneous-spontaneous beat noise is independent of the input signal power and is the dominating term at low signal power. This term depends on the optical bandwidth of the ASE spectrum. For this reason, a bandpass filter is normally used after the optical amplifier in order to minimize the amount of ASE reaching the detector. This is not needed for a VCSOA as the spontaneous emission bandwidth is limited by the FP cavity. Signal-spontaneous beat noise and shot noise increase with input signal power. At high signal powers signal-spontaneous beat noise is the main contributor to the output

noise. The output ASE, and hence the signal-spontaneous beat noise is greatly affected by the mirror reflectivity.

The noise in VCSOAs can be analyzed using the same methods as for in-plane FPSOAs [26-28]. Considering signal-spontaneous beat noise to be dominant, the noise factor, F, defined as input SNR over output SNR (the noise *figure* is defined as NF = 10log(F) and expressed in decibels), is given by $F = 2n_{sp}\chi(G-1)/G$ [5]. For high signal gain (G>>1) this reduces to

$$F = 2n_{sp}\chi \tag{2.12}$$

Here, $n_{sp}$ is the population inversion parameter and $\chi$ is the excess noise coefficient, which describes signal-spontaneous beat noise enhancement due to finite mirror reflectivity. $\chi$ takes a value of one for zero reflectivity (the case of traveling wave amplifiers) and values higher than one for finite mirror reflectivities. Using photon statistics master equations as described by Shimoda *et al*. [29], it can be shown that $\chi$ is given by [26]:

$$\chi = \frac{(1+R_b g_s)(1-R_t)(g_s-1)}{(1-\sqrt{R_t R_b}\, g_s)(G-1)} \tag{2.13}$$

where G is the amplifier gain. Reflection and transmission mode operation are associated with significantly different expressions for $\chi$. (It is here assumed that the signals exits the VCSOA through the top mirror in both cases, i.e. the signal enters the transmission mode VCSOA through the bottom mirror. This makes the analysis of $\chi$ a little bit simpler). Inserting Equations 2.3 and 2.4 into Equation 2.13, the excess noise coefficient for the two cases can be shown to be:

$$\chi_t = \frac{(1+R_b g_s)(1-R_t)(g_s-1)}{(1-R_b)(1-R_t)g_s - (1-\sqrt{R_t R_b}\, g_s)^2} \tag{2.14}$$

$$\chi_r = \frac{(1+R_b g_s)(g_s-1)}{(R_b g_s^2-1)} \tag{2.15}$$

For transmission mode and high gain (G>>1), $\chi$ simplifies to

$$\chi_t = \frac{(1+R_b g_s)(g_s - 1)}{(1-R_b)g_s} \tag{2.16}$$

The excess noise coefficient versus amplifier gain for both cases is plotted in Figure 2.13 and 2.14, for different mirror reflectivities. For transmission mode operation (Figure 2.13), $\chi_t$ equals one when the single pass gain is $g_s = R_b^{-1/2}$. It is obviously desirable to operate the VCSOA close to this ideal value of $g_s$, but at the same time be able to vary the signal gain G. It is also desirable to maximize $g_s$ in order to achieve high signal gain. This can be achieved by using low input mirror reflectivity and high output mirror reflectivity. This is evident from Figure 2.13; a value of $\chi_t$ close to one over a wide range of signal gain is achieved using $R_{in}$=0.85 and $R_{out}$=0.95. For symmetrical devices, $\chi_t$ is independent of mirror reflectivity. For the case of reflection mode operation (Figure 2.14), $\chi_r$ is a function of bottom mirror reflectivity only. $\chi_r$-values close to one can be achieved for bottom mirror reflectivities higher than 0.99, which is easily obtained using DBR mirrors.

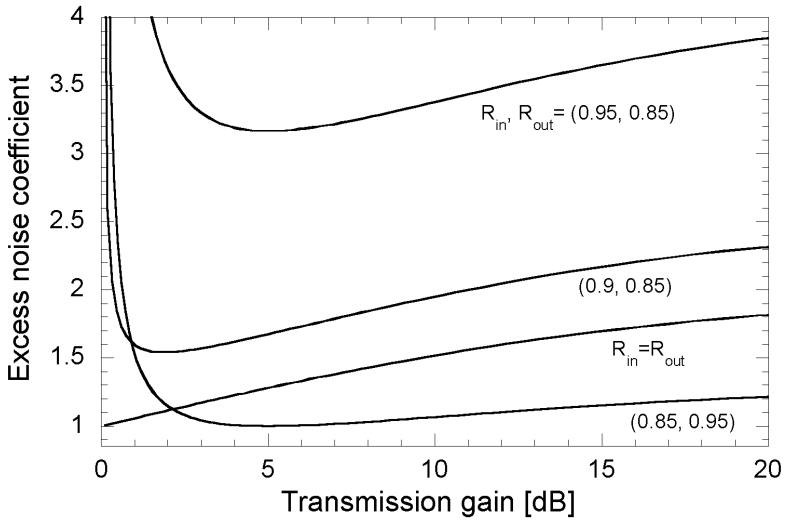


*Figure 2.13. Excess noise coefficient versus amplifier gain for transmission mode operation.*

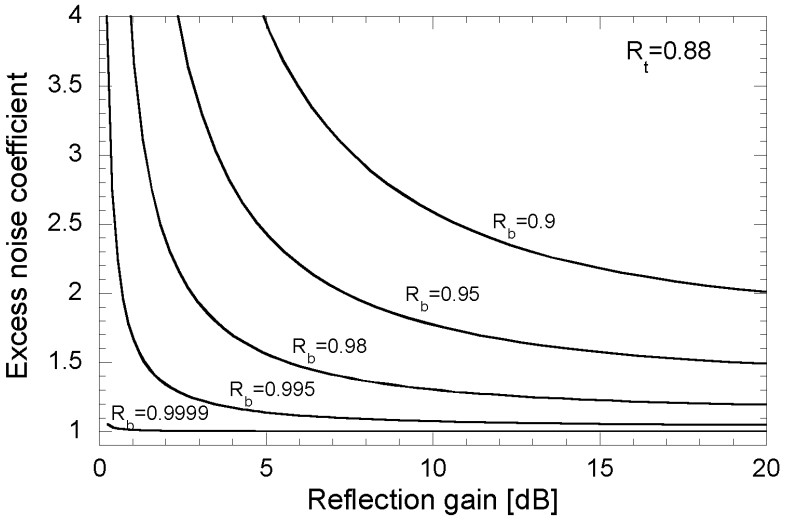


*Figure 2.14. Excess noise coefficient versus amplifier gain for reflection mode operation.*

It is desirable to operate an optical amplifier with as high population inversion as possible in order to minimize reabsorption of the signal light, which is detrimental to the noise figure. The population inversion parameter is defined as [28]:

$$n_{sp} = \frac{N}{N - N_{tr}} \tag{2.17}$$

$n_{sp}$ takes values greater than one for low carrier densities and reaches unity at complete inversion. A delicate problem inherent to FPAs is that strong pumping is desired to reach high carrier density, and thereby minimize $n_{sp}$, while the amplifier still has to be operated in the regime below lasing threshold. The mirror reflectivity governs how hard the amplifier can be pumped before it reaches lasing threshold. Figure 2.15 shows a plot of the calculated population inversion parameter at threshold, and at 90% and 70% of threshold, versus mirror reflectivity ($R_t \times R_b$). The rate equations (Equations 2.9 and 2.10) were

used in these calculations and the precise values are therefore specific to the devices fabricated in this thesis. However, the curves illustrate a very general obstacle that hinders low-noise operation of VCSOAs, and the shape of the curves do not change for different designs. The plot is valid for both transmission and reflection mode operation. For a reflection mode device with bottom mirror reflectivity close to unity the x-axis in the plot simply represents top mirror reflectivity. It is evident from this graph that too high mirror reflectivity makes low noise operation impossible. To achieve an $n_{sp}$ below 1.5 the reflectivity has to be on the order of 0.9 or less.

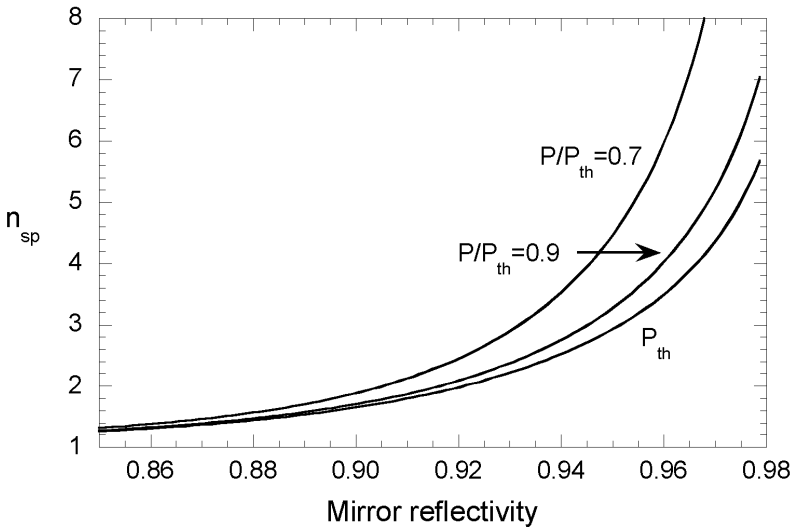


*Figure 2.15. Population inversion parameter versus mirror reflectivity ($R_t \times R_b$) for three different pumping levels.*

The noise figure of the devices fabricated in this thesis can now be calculated using Equation 2.12. These VCSOAs were operated in reflection mode with a bottom mirror reflectivity of 0.999. The excess noise coefficient is thus 1 (Figure 2.14). The population inversion parameter at 90% of the pump power required to reach lasing threshold shown in Figure 2.15 is used. The

resulting noise figure is plotted as a function of top mirror reflectivity in Figure 2.16. A noise figure of 5 dB can be obtained using a top mirror reflectivity of 0.9. To achieve a noise figure smaller than 4 dB, the top mirror reflectivity has to be less than 0.85.

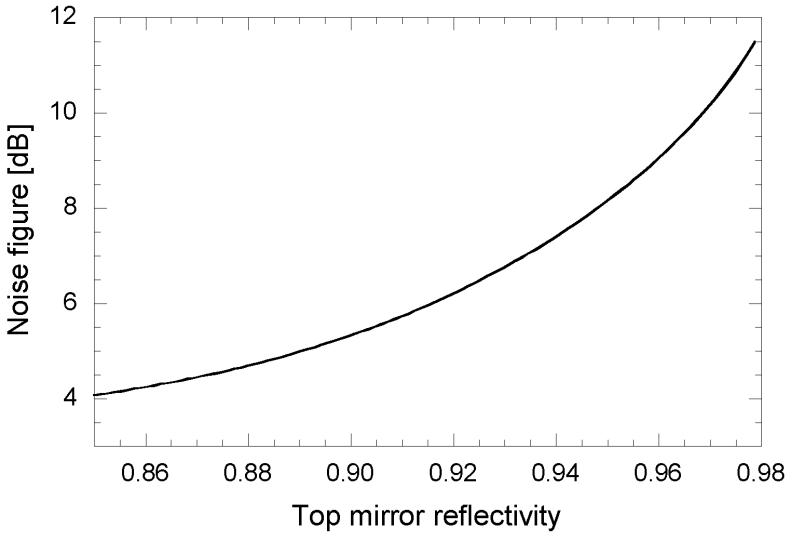


*Figure 2.16. Calculated noise figure at $P/P_{th} = 0.9$ versus top mirror reflectivity for the devices fabricated in this thesis.*

## 2.5 Summary

VCSOA design theory was presented in this chapter. The properties of long-wavelength active regions and DBR mirrors were outlined. A theoretical model for analyzing VCSOAs was presented. It was based on the FP equations for a cavity with gain, and carrier and photon rate equations. It was showed that the reflectivity of the mirrors affect all parameters of the VCSOA, and that for a given active region, there is an optimum mirror reflectivity that yields the best performance. The reflectivity should be just low enough so that lasing threshold cannot be reached. This gives the highest gain, highest gain-bandwidth product, highest saturation power, and the lowest noise figure. The ASE is enhanced by

the feedback in the VCSOA. The noise figure can therefore be rather high if the reflectivities are not chosen properly. For a reflection mode device, the bottom mirror reflectivity should be close to unity for the lowest possible noise figure. For operation in transmission mode, the input mirror reflectivity should be low and the output mirror reflectivity high in order to minimize the noise figure. The theoretical model developed in this chapter will be used to analyze the results in Chapter 4.

## References

[1] H. Ghafouri-Shiraz, *Fundamentals of laser diode amplifiers*, West Sussex, England: Wiley, 1996.

[2] C. Wilmsen, H. Temkin, L. A. Coldren, *Vertical-Cavity Surface-Emitting Lasers*, Cambridge, UK: Cambrige University Press, 1999.

[3] E. Hecht, *Optics*, Addison-Wesley, 1987.

[4] C. Tombling, T. Saito, T. Mukai, "Performance Predictions for Vertical-Cavity Semiconductor Laser Amplifiers," *IEEE Journal of Quantum Electronics*, vol. 30, no. 11, pp. 2491-2499, Nov. 1994.

[5] T. Mukai, Y. Yamamoto, T. Kimura, "Optical Amplification by Semiconductor Lasers" in *Semiconductors and Semimetals*, vol. 22, part E, pp. 265-319, London, UK: Academic, 1985.

[6] A. Karlsson, M. Höijer, "Analysis of a VCLAD: Vertical-Cavity Laser Amplifier Detector," *IEEE Photonics Technology Letters*, vol. 7, no. 11, pp. 1336-1338, Nov. 1995.

[7] J. Piprek, S. Björlin, J. E. Bowers, "Design and Analysis of Vertical-Cavity Semiconductor Optical Amplifiers," *IEEE Journal of Quantum Electronics*, vol. 37, no. 1, pp.127-134, Jan. 2001.

[8] P. Royo, R. Koda, L. A. Coldren, "Vertical Cavity Semiconductor Optical Amplifiers: Comparison of Fabry-Pérot and Rate Equation Approaches," *IEEE Journal of Quantum Electronics*, vol. 38, no. 3, pp. 279-284, Mar. 2002.

[9] P. Royo, R. Koda, L. A. Coldren, "Rate equations of vertical cavity semiconductor optical amplifiers," *Applied Physics Letters*, vol. 80, no. 17, pp. 3057-3059, Apr. 2002.

[10] C. E. Zah, R. Bhat, B. N. Pathak, F. Favire, W. Lin, M. C. Wang, N. C. Andreadakis, D. M. Hwang, M. A. Koza, T. P. Lee, Z. Wang, D. Darby, D. Flanders, J. J. Hsieh "High-performance uncooled 1.3-μm $Al_xGa_yIn_{1-x-y}As$/InP strained-layer quantum-well lasers for subscriber loop applications", *IEEE Journal of Quantum Electronics*, vol. 30, no.2, pp. 511-523, Feb. 1994.

[11] A. W. Jackson, R. L. Naone, M. J. Dalberth, J. Smith,K. J. Malone, D. W. Kisker, J. F. Klem, K. D. Choquette, D. Serkland, K. Geib, "OC-48 capable InGaAsN vertical cavity laser", *Electronics Letters*, vol. 37, no. 6, pp. 355-356, Mar. 2001.

[12] S. Nakagawa, E. Hall, G. Almuneau, J. K. Kim, D. A. Buell, H. Kroemer, L. A. Coldren, "1.55-μm InP-Lattice-Matched VCSELs With AlGaAsSb-AlAsSb DBRs", *IEEE Journal of Selected Topics in Quantum Electronics*, vol. 7, no. 2, pp. 224-230, Mar./Apr. 2001.

[13] T. Mukaihara, N. Ohnoki, Y. Hayashi, N. Hatori, F. Koyama, K. Iga, "Polarization Control of Vertical-Cavity Surface-Emitting Lasers Using a Direfringent Metal/Dialectric Polarizer Loaded on Top Distributed Bragg Reflector", *IEEE Journal of Selected Topics in Quantum Electronics*, vol. 1, no.2, pp. 667-673, June. 1995.

[14] S. W. Corzine, R. S. Geels, J. W. Scott, R.-H. Yan, L. A. Coldren, "Design of Fabry-Perot Surfacce-Emittong Lasers with a Periodic Gain Structure," *IEEE Journal of Quantum Electronics*, vol. 25, no.6, pp. 1513-1524, June 1989.

[15] V. Jayaraman, T. J. Goodnough, T. L. Beam, F. M. Ahedo, R. A. Maurice, "Continuous-wave operation of single-transverse-mode 1310-nm VCSELs up to 115 degrees C," *IEEE Photonics Technology Letters*, vol. 12, no. 12, pp. 1595-1597, Dec. 2000.

[16] D. Vakhshoori, J.-H. Zhou, M. Jiang, M. Azimi, K. McCallion, C.-C. Lu, K. J. Knopp, J. Cai, P. D. Wang, P. Tayebati, H. Zhu, P. Chen, "C-band tunable 6 mW vertical-cavity surface-emitting lasers", *OFC 2000 Technical Digest Postconference Edition*, Paper PD13, pp. PD13-1-PD13-3, 2000.

[17] D. I. Babic, "Double-fused long-wavelength vertical-cavity lasers," Ph.D. Dissertation in *Electrical and Computer Engineering*, University of California, Santa Barbara, 1995.

[18] A. Karim, J. Piprek, P. Abraham, D. Lofgreen, Y.-J. Chiu, J. E. Bowers, "1.55-μm Vertical-Cavity Laser Arrays for Wavelength-Division Multiplexing," *IEEE Journal of Selected Topics in Quantum Electronics*, vol. 7, no.2, pp. 178-183, Mar./Apr. 2001.

[19] E. Desurvire, *Erbium-Doped Fiber Amplifiers, Principles and applications*, New York, USA: Wiley, 1994.

[20] D. Marcuse, "Computer model of an injection laser amplifier," *IEEE Journal of Quantum Electronics*, vol. QE-19, no. 1, pp. 63-73, Jan. 1983.

[21] E. S. Björlin, J. E. Bowers, "Noise Figure of Vertical-Cavity Semiconductor Optical Amplifier," *IEEE Journal of Quantum Electronics*, vol. 38, no. 1, pp. 61-66, Jan. 2002.

[22] L. A Coldren, S. W. Corzine, *Diode Lasers and Photonic Integrated Circuits*, New York, NY: Wiley, 1995.

[23] K. A. Black, P. Abraham, A. Karim, S. K. Mathis, J. E. Bowers, E. L. Hu, "Improved Luminescence from InGaAsP/InP MQW Active Regions Using a Wafer Fused Superlattice barrier," in *Proceedings to IPRM'99*, Davos, Switzerland, May 1999.

[24] J. Piprek, S. Björlin, J. E. Bowers, "Optical Gain-Bandwidth Product of Vertical-Cavity Laser Amplifiers," *Electronics Letters*, vol. 37, no. 5, pp. 298-299, Mar. 2001.

[25] N. K. Dutta, "Analysis of current spreading, carrier diffusion, and transverse mode guiding in surface emitting lasers," *Journal of Applied Physics*, vol. 68, no. 5, pp. 1961-1963, Sept. 1990.

[26] T. Mukai, Y. Yamamoto, "Noise in AlGaAs Semiconductor Laser Amplifier" *IEEE Journal of Quantum Electronics*, vol. QE-18, pp. 564-575, Apr. 1982.

[27] Y. Yamamoto, "Noise and Error Rate Performance of Semiconductor Laser Amplifiers in PCM-IM Optical Transmission systems" *IEEE Journal of Quantum Electronics*, vol. QE-16, pp. 1073-1081, Oct. 1980.

[28] T. Mukai, Y. Yamamoto, T. Kimura, "S/N and Error Rate Performance in AlGaAs Semiconductor Laser Amplifier and Linear Repeater Systems" *IEEE Transactions on Microwave Theory and Technology*, vol. MTT-30, pp. 1548-1556, Oct. 1982.

[29] K. Shimoda, H. Takahasi, C. H. Townes, "Fluctuations in Amplification of Quanta with Application to Maser Amplifiers," *Journal of the Physical Society of Japan*, vol. 12, no. 6, pp. 686-700, June 1957.

# Chapter 3

# VCSOA Fabrication

The devices presented in this thesis were fabricated using wafer bonding. InGaAsP/InP active regions were bonded to AlGaAs/GaAs DBRs, in order to utilize the high reflectivity and favorable thermal properties of the AlGaAs material system. The processing was fairly simple; for instance, no metallization was needed, since the devices were optically pumped. The first generation of devices required only two bonding steps and two substrate removals. The processing of the second generation of amplifiers was slightly more involved, requiring a dry-etch step and a wet-etch step in addition to the wafer bonding.

## 3.1 VCSOAs fabricated in this thesis

Two generations of VCSOAs were fabricated in this thesis. Both generations were optimized for reflection mode operation, *i.e.* they had a bottom mirror reflectivity close to unity and significantly lower top mirror reflectivity. The devices were designed for optical pumping—the entire structure was undoped. The difference between the two designs was a carrier confining structure in

Generation 2. The same InGaAsP/InP active region (as described in Chapter 2) was used in both generations. In fact, active region material from the same wafer was used for all devices fabricated throughout the project. This enabled a quantitative comparison of the two designs. The active region had three sets of 7 compressively strained $InAs_{0.5}P_{0.5}$ QWs surrounded by strain compensating $In_{0.8}Ga_{0.2}P$ barriers. InP spacing layers were used to position the three sets on the three central standing wave peaks in the cavity. The bottom mirror was also the same in all devices. It was a 25-period $Al_{0.99}Ga_{0.01}As$/GaAs DBR with a calculated reflectivity of 0.999.

A schematic of the first generation VCSOAs is shown at the top in Figure 3.1. It was a planar structure consisting of the active region sandwiched between the two DBRs. No individual devices were formed on the chip. The only patterning that was done on the sample was the channel etch that facilitates wafer bonding. The spot size of the pump beam was used to define the lateral dimensions of the devices. Several Generation-1 chips ware fabricated, with different $Al_{0.99}Ga_{0.01}As$/GaAs top DBRs. The number of top mirror periods was varied in the characterization of the devices. The top mirror reflectivities for Generation 1 ranged from 0.91 to 0.98.

The planar structure of Generation 1 allowed the generated carriers to diffuse laterally in the QWs, out of the active region. This resulted in very low efficiency. In order to improve the efficiency in Generation 2, carrier confinement was introduced. A simple way to achieve carrier confinement is to etch mesas through the active layers of the device. However, the etched sidewalls allow carriers to recombine at surface states, which can compromise the effectiveness of the carrier confinement. The degree to which surface recombination affects the carrier density in the active region depends on the materials in the active region, the quality of the sidewall surface, and the dimensions of the etched mesa. The sidewall recombination is lower in

InGaAsP/InP than in the AlGaAs/GaAs material system [1]. The surface recombination states are created by the termination of the lattice. The dry-etch used to form the mesas and the subsequent surface treatment are therefore crucial to minimizing the number of recombination sites. The number of recombination states can be reduced by chemical passivation of the sidewalls [2] or semiconductor regrowth [3].

The processing of the second generation VCSOAs began with bonding the active region to the bottom DBR. After bonding, the InP substrate was removed. Prior to the second bond, circular mesas were defined on the active region using reactive ion etching (RIE). The etch was stopped after the third set of QWs leaving the bottom InP cladding intact. In addition to etching vertical mesas, the QWs were under-etched. This resulted in a step-like sidewall profile where the InP cladding layers had a slightly larger diameter than the QWs. Finally, the top DBR was bonded to the active region. The second wafer bond takes place at a higher temperature than the growth temperature of the QWs. During the second bond, InP from the layers surrounding the QWs migrates to smoothen the steps in the sidewalls, thereby covering the QW edges. If successful, this mass transport of InP creates a buried heterostructure. Under-etching the QWs is desirable for other reasons as well. In addition to the intended creation of a buried heterostructure, it is advantageous for thermal reasons to have large InP layers surrounding the QW. Any heat generated in the QWs will spread to the surrounding InP layers. A larger volume of InP is simply a more efficient heat sink. Devices were fabricated with mesa sizes ranging from 5 μm to 36 μm. The mesas were positioned fairly close together in order to support the top mirror; the distance between the centers of adjacent mesas was 40 μm. The bottom mirror and active region were the same in Generation 2 as in Generation 1. The top mirror was a 10.5 period

$Al_{0.9}Ga_{0.1}As$/GaAs DBR with a calculated reflectivity of 0.918. A schematic of a Generation-2 VCSOA is shown at the bottom in Figure 3.1.

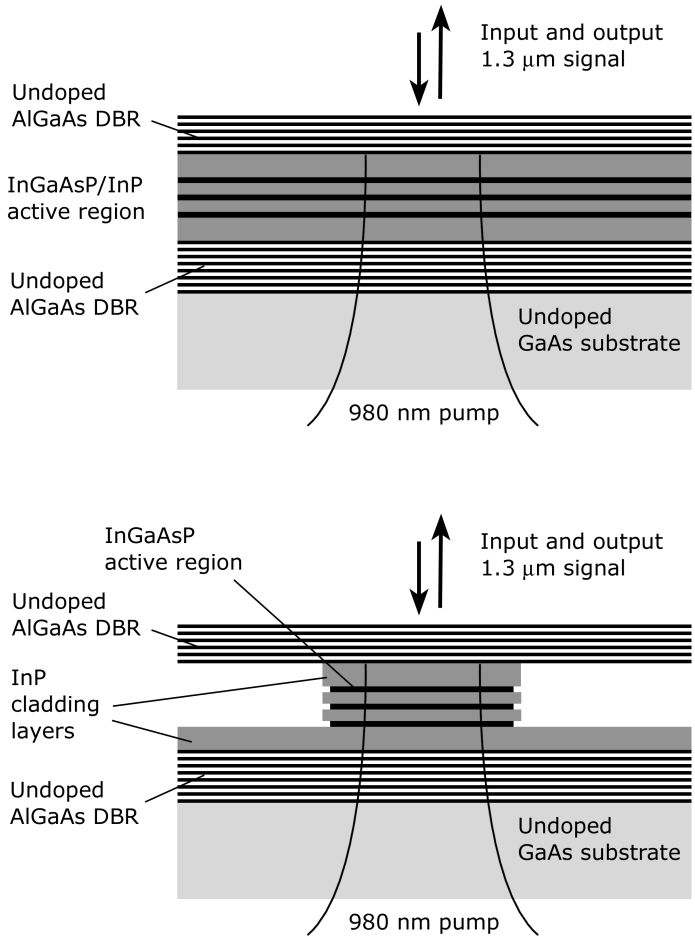


*Figure 3.1 Schematic of VCSOAs fabricated in this thesis. In Generation 1 (top) the lateral dimensions of the devices were defined by the pump beam. In Generation 2 (bottom) devices were formed by etching carrier confining mesas.*

## 3.2 Wafer bonding

The requirements on the bonded interface are fairly relaxed for optically pumped devices. A smooth interface is desirable in order to minimize optical loss due to scattering, but the electrical conductivity across the interface is not relevant. In order to minimize scattering loss in the devices, the bonded interfaces were positioned at nulls in the standing wave pattern in the cavity, thereby minimizing the interaction between the signal field and the rough material at the interface. The wafer bonding process previously developed at UCSB [4] was used without further process development. The surface preparation process consisted of a solvent clean followed by an oxygen plasma oxidation and oxide removal in $NH_4OH$. The samples were brought into contact while immersed in methanol. It is well known that high temperature and high pressure lead to improved yield (bonded area) and improved electrical properties of the bonded interface. However, high temperature and high pressure can also be detrimental to the QW gain, significantly degrading the peak gain and altering the gain spectrum. This problem is more severe for highly strained QWs. Since the devices fabricated here were to be pumped optically, both pressure and temperature were decreased compared to what has been reported for the fabrication of electrically pumped VCSELs [4,5]. The pressure used during the bonding varied from 1.5 MPa to 3.6 MPa, and the annealing temperature varied between 575°C and 590°C. The annealing time was about 30 minutes. Slight variations in pressure, annealing temperature, and annealing time had no apparent effect on the performance of the devices. A detailed description of the wafer-bonding process and an in-depth analysis of the wafer bonded InP-GaAs interface are given in Ref. [4].

## 3.3 Mirror reflectivity adjustment

In order to fully characterize the VCSOAs, device properties were measured for different top mirror reflectivities. The first sample of the Generation-1 devices was fabricated with 15.5 top mirror periods. The top mirror reflectivity was then adjusted by etching off single mirror periods, and measurements of device parameters were repeated for different number of top mirror periods. As one mirror period consists of one layer of GaAs and one layer of AlGaAs, two selective etch steps were used to remove one period. The GaAs layers were etched in a 5:1 solution of citric acid and hydrogen peroxide ($H_2O_2$). The etch times used was about 1.5 minutes for the first layer (it takes a while to etch through some oxide on the outermost layer) and about 1 minute for subsequent layers. Surface color changes were observed in order to monitor the etch. The AlGaAs layers were etched in 1:10 solution of hydrofluoric acid (HF) and water for about 20 seconds. Both etches are fairly selective and timing was not critical. The same technique was used to optimize the performance of the amplifiers in later processing runs when the desired reflectivity was known but different from that of the mirror material at hand.

## 3.4 Mesa definition

To create the carrier confining structure in the second generation of VCSOAs, mesas were formed in the active region prior to the second bonding. For this step, RIE in a $CH_4/Ar/H_2$ chemistry was used. All three sets of QWs were etched, and the etch was stopped right after the third set, leaving the bottom InP cladding intact. The large number of very thin layers resulted in a rather weird looking signal from the in-situ laser monitoring. Therefore, the etch was based on timing. (The timing is critical here, as there is no stop-etch layer.) A

scanning electron micrograph (SEM) of the etched mesas, before the second bond, is shown in Figure 3.2.

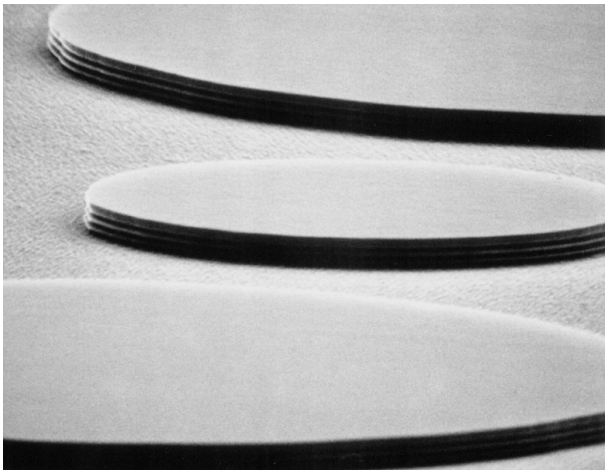

*Figure 3.2 Etched mesas on Generation 2 VCSOAs, half-way through the processing.*

## 3.5 Active region under-etch

After the mesas were defined, the QWs were under-etched. It is desirable to use a highly selective etch that is also isotropic. Because of the compositions of the wells and barriers it was difficult to find an etch that showed high selectivity toward InP. The etch that was chosen for the task was a 3:1:5 solution of $H_2SO_4$:$H_2O_2$:$H_2O$ heated to 75ºC. A SEM of the cross section of a finished device is shown in Figure 3.3. The under-etched QWS are clearly visible, but the sidewalls appears smoothened from the mass transport during the second wafer bond. Unfortunately, this wet etch was not as isotropic as desired, resulting in noncircular active regions. This introduced anisotropic optical loss, which lead to polarization dependent gain (PDG) in the smaller devices. PDG will be further discussed in Chapter 4. To avoid the polarization dependent loss, the etch must be made diffusion limited instead of reaction limited, without

loosing the selectivity towards InP. This might be hard with the present composition of QWs and barriers, which should be considered in the design of future VCSOA active regions.

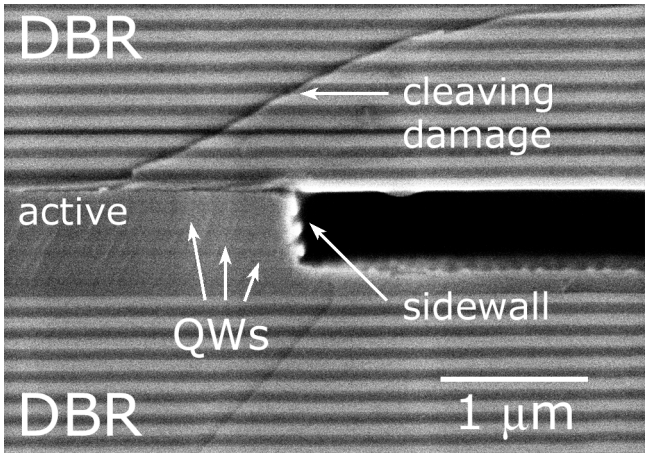


*Figure 3.3 SEM of cross section of finished Generation 2 VCSOA.*

## 3.6 Summary

This chapter described the design and fabrication of two generations of VCSOAs. Both generations were designed to be pumped optically and operated in reflection mode. The difference between the two designs was the carrier confining structure in Generation 2. Both generations were fabricated by wafer bonding an InGaAsP/InP active region to two AlGaAs/GaAs DBRs. The same active region material was used in both generations in order to enable an quantitative evaluation of the designs, which will be presented in Chapter 4.

# References

[1] L. A Coldren, S. W. Corzine, *Diode Lasers and Photonic Integrated Circuits*, New York, NY: Wiley, 1995.

[2] E. Yablonovitch, C. J. Sandroff, R. Bhat, T. Gmitter, "Effects of passivating ionic films on the photoluminescence properties of GaAs," *Applied Physics Letters*, vol. 51, no. 24, pp. 2022-2024. Dec. 1987.

[3] J. J. Hsieh, C. C. Shen, "Room-temperature CW operation of buried-stripe double-heterostructure GaInAsP/InP diode lasers," *Applied Physics Letters*, vol. 30, no. 8, pp. 429-431, Apr. 1977.

[4] K. A. Black, "Fused Long-Wavelength Vertical-Cavity Lasers," Ph.D. Dissertation in *Materials*, University of California, Santa Barbara, 2000.

[5] A. Black, A. R. Hawkins, N. M. Margalit, D. I. Babic, A. L. Holmes, Jr., Y.-L. Chang, P. Abraham, J. E. Bowers, E. L. Hu, "Wafer Fusion: Materials Issues and Device Results," *IEEE Journal of Selected Topics in Quantum Electronics*, vol. 3, no. 3, pp. 943-951, June 1997.

# Chapter 4

# Results and Analysis

Analyzing an all-optical, active device such as an optically pumped VCSOA is not trivial. The main source of uncertainty lies in the extreme sensitivity of the coupling efficiency—for both pump light and signal—into and out of the device. Even though it is possible to estimate the coupling efficiency of the signal and what fraction of the pump light is being absorbed in the active region, small adjustments in the alignment of the experimental setup causes major changes in the coupling efficiency and pump efficiency. This naturally leads to difficulties in comparing data taken on different occasions. To minimize these problems, a great portion of the results will be presented for a certain pump level relative to threshold instead of absolute pump power. In those cases where the pump power is of specific interest, *e.g.* to determine the efficiency of a device, several measurements were taken and the best reproducible values are presented. Whenever possible, complete sets of data were taken without adjusting the alignment of the system.

## 4.1 Experimental setup

A schematic of the experimental setup that was used for characterization of the VCSOAs is shown in Fig. 4.1. It consists of a pump source, a signal source, and various optical elements to guide the light into and out of the device under test. All devices fabricated in this thesis were operated in reflection mode with the signal injected through the top DBR and the optical pump beam injected through the bottom DBR and GaAs substrate. Therefore, the sample was mounted vertically to provide access to both sides of the devices. A 980-nm laser diode, kindly donated by Dr. S Mohrdiek and Dr. C. Harder at Nortel, was used as an optical pump. The pump beam was focused on the active region of the VCSOA using free-space optics. Experiments were made to find the optimal pump spot size. This is largely dictated by the size of the input signal. A small pump spot size naturally leads to higher intensity, but the pump spot must, off course, not be smaller than the signal. A spot size larger than the signal leads to compromised efficiency but gives some leeway for alignment. It was found that a spot just 0.5 μm larger than the signal spot size gave all the leeway needed, and the best results. The signal and pump spot sizes were 8.3 μm and 8.8 μm, respectively. A 1.3-μm external cavity tunable laser diode was used as a signal source. The input signal power was controlled by a variable optical attenuator (VOA). A single-mode fiber and a lens were used to inject the 1.3-μm signal through the top mirror of the device and to collect the output signal. The input and the output signals were separated by means of an optical circulator. The total coupling loss (including loss in the circulator, which was measured to be 3.5 dB) varied between 5 dB and 7 dB. The output signal was monitored using an optical spectrum analyzer (OSA) or an optical power meter. This was the basic setup; variations in the setup were made to accommodate different experiments such as noise figure measurements, modulation response, etc.

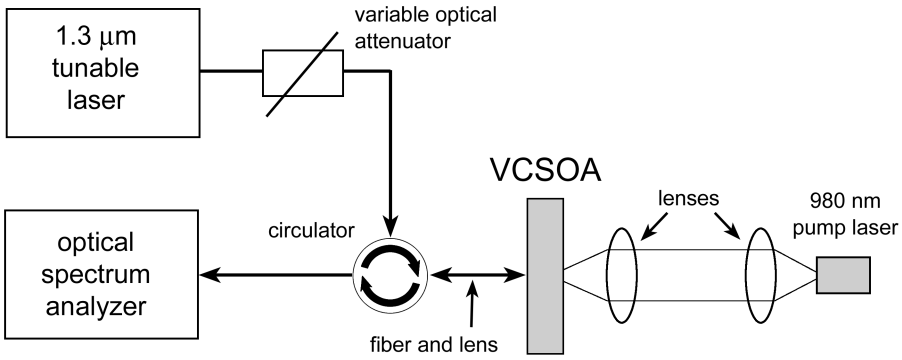


*Figure 4.1. Experimental setup for VCSOA characterization.*

## 4.2 Generation 1

The first generation of VCSOAs was a planar, gain guided design. The main goal of this generation of devices was to do a complete characterization of the amplifier properties, which included varying the mirror reflectivity, and developing/validating the theoretical model that was presented in Chapter 2. Gain, gain bandwidth and saturation power were measured for different pump powers and different top mirror reflectivities. VCSOAs were for this purpose fabricated with numbers of top mirror periods ranging from 15.5 to 12.5. This yielded calculated reflectivities between 0.98 and 0.945 for smooth mirror surfaces. The sample with 12.5 mirror periods started out with 14.5 top mirror periods, which were subsequently removed one at the time during characterization of the device. The repeated removal of mirror periods resulted in a nonuniform sample surface and consequently a nonuniform reflectivity. Efforts were made to find a spot on the sample with the lowest reflectivity possible in order to extend the range of investigated mirror reflectivities. The lowest mirror reflectivity that was found on that sample, and thus the lowest reflectivity investigated, was deduced to be 0.91. Due to technical difficulties the noise figure was only measured on one sample with $R_t = 0.955$.

### *4.2.1 Gain and gain bandwidth*

Fiber-to-fiber gain versus pump power for two Generation-1 VCSOAs is shown in Figure 4.2. The two samples had 13.5 and 12.5 top mirror periods, which gives reflectivities of 0.965 and 0.945, respectively. For $R_t$ = 0.965 lasing threshold was reached at a pump power of $P_{th}$ = 90 mW. A fiber-to-fiber gain of 11 dB was measured for $P/P_{th}$ = 0.88. For the case of $R_t$ = 0.945, lasing threshold occurred at $P_{th}$ = 125 mW. Maximum gain obtained in this case was 13 dB, at $P/P_{th}$ = 0.89. This clearly demonstrates that in the high reflectivity regime, decreasing $R_t$ allows for stronger pumping, which results in higher gain. The slope efficiencies as indicated by the dashed lines are 0.14 dB/mW for the higher reflectivity, and 0.12 dB/mW for the lower reflectivity. The efficiency will be further discussed below, in Section 4.3.3.

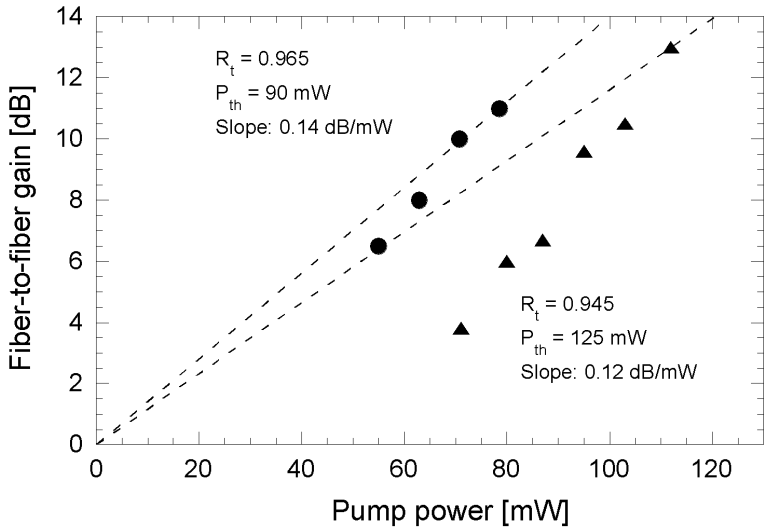


*Figure 4.2. Fiber-to-fiber gain versus pump power for two Generation-1 VCSOAs. The dots are measurements and the dashed lines indicate maximum slope efficiency. Lower reflectivity allows for stronger pumping and higher gain, but leads to reduced slope efficiency.*

Figure 4.3 shows gain bandwidth versus gain. Dots are measurements and the lines are curve fits based on the FP equations (Equations 2.3 - 2.6). The relation between gain and gain bandwidth (the *shape* of the curves) clearly demonstrates good agreement between measurements and theory. The fact that the measurements fall right on top of the curves is, of course, because FP theory was used to determine the reflectivity of the VCSOA mirrors. Figure 4.4 shows the gain-bandwidth product versus $R_t$ for all samples in Generation 1.

A gain spectrum measured on the sample from Generation 1 with the lowest top mirror reflectivity is shown in Figure 4.5. The number of top mirror periods was 12.5, but the reflectivity was deduced to be as low as 0.91. This is attributed to surface roughness as explained above. The gain bandwidth for a

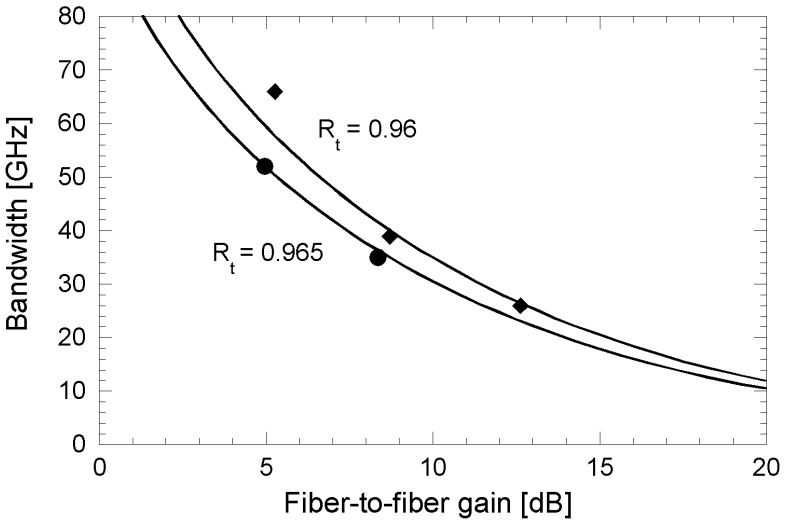


*Figure 4.3. Gain bandwidth versus Fiber-to-fiber gain for Generation 1. Dots are measurements, lines are curve fits based on the FP equations.*

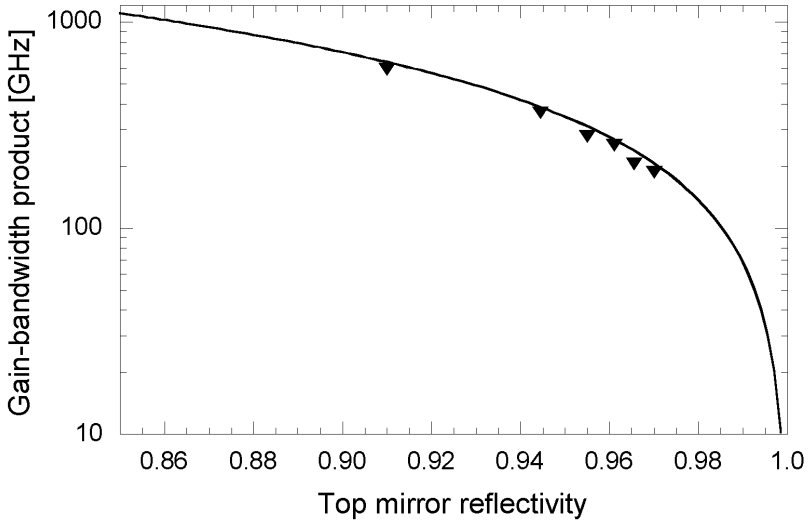


*Figure 4.4. Gain bandwidth product versus top mirror reflectivity for all Generation-1 VCSOAs. Dots are measurements, the line is calculated using Equation 2.8.*

fiber-to-fiber gain of 11.3 dB was measured to be 0.6 nm, which corresponds to 100 GHz. The curve fit is based on Equation 2.4. The parameters used in the fit is $R_b = 0.999$, $R_t = 0.91$, and $g_s = 1.035$. The maximum gain measured at this spot of the sample was 12.7 dB for 140 mW of pump power. Lasing threshold could not be reached. To achieve 12.7 dB fiber-to-fiber gain with $R_b = 0.999$ and $R_t = 0.91$, a single pass gain of 3.7% is required. From the gain model in Chapter 2 it can be deduced that the material gain and carrier density was about 1725 $cm^{-1}$ and $3 \times 10^{18}$ $cm^{-3}$, respectively. This is the highest gain and carrier density that was achieved for Generation 1. It was predicted in Chapter 2 that the active region could provide gain up to 3500 $cm^{-1}$, which would yield 8% single-pass gain. The discrepancy is attributed to high carrier loss through lateral diffusion in the QWs. This causes the carrier density to saturate before the gain saturates, which limits the achievable amplifier gain.

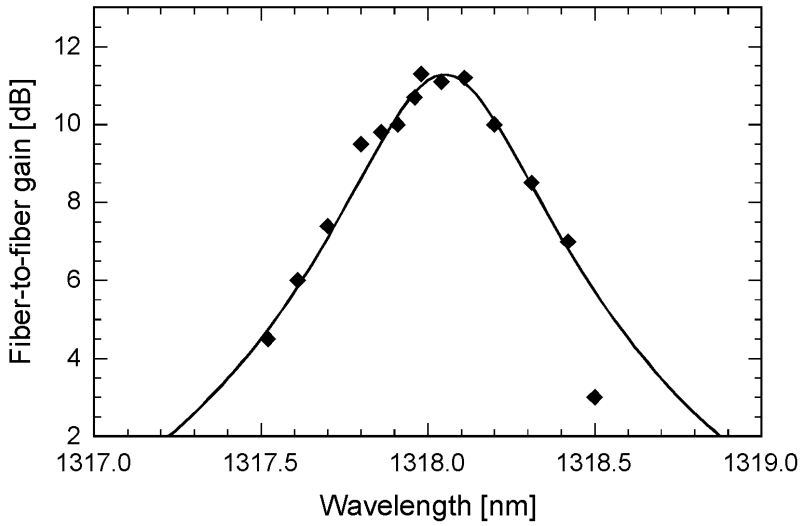


*Figure 4.5. Gain spectrum demonstrating 0.6 nm (100 GHz) gain bandwidth. Dots are measurements, the line is a curve fit based on Equation 2.4.*

### *4.2.2 Saturation*

Figure 4.6 and 4.7 show the saturation characteristics of two Generation-1 VCSOAs with top mirror reflectivities 0.96 and 0.91. The dots are measurements and the lines are curve fits based on the relation $G = G_0 \times (1 + P_{in}/P_{sat})^{-1}$. $G_0$ is the unsaturated gain value and $P_{sat}$ is the input signal power for which the gain drops by 3 dB. For the higher reflectivity, gain versus input signal power is shown for three different pump levels relative to lasing threshold. For the lower reflectivity, the VCSOA could not be brought to lasing threshold. Gain versus input signal power is shown for 120 mW and 140 mW pump power. The gain saturates earlier with increased pump power. This is in agreement with the predictions in Chapter 2. The output saturation power is in both cases constant. For the higher reflectivity the output saturation power was about –9 dBm. Theory predicts higher saturation power for lower

reflectivity. Indeed, for the case of $R_t$ = 0.91 the saturation output power was –3.5 dBm. This is the highest saturation output power reported for any VCSOA to date.

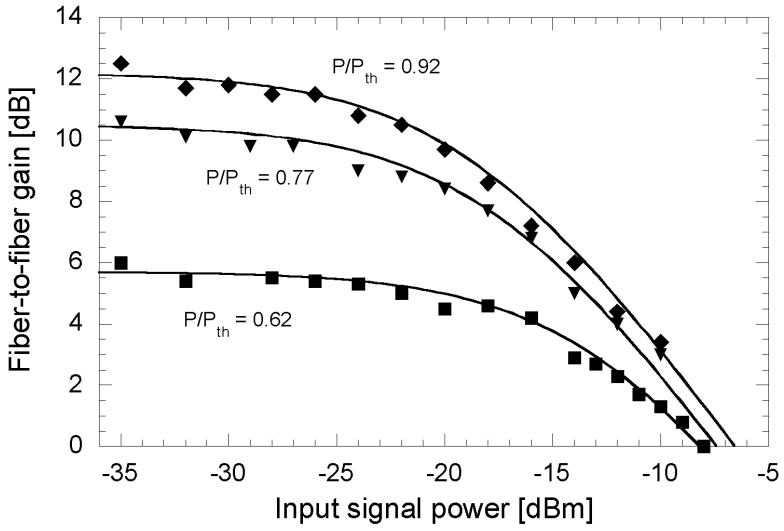


*Figure 4.6. Fiber-to-fiber gain versus input signal power for a VCSOA with $R_t$ = 0.96.*

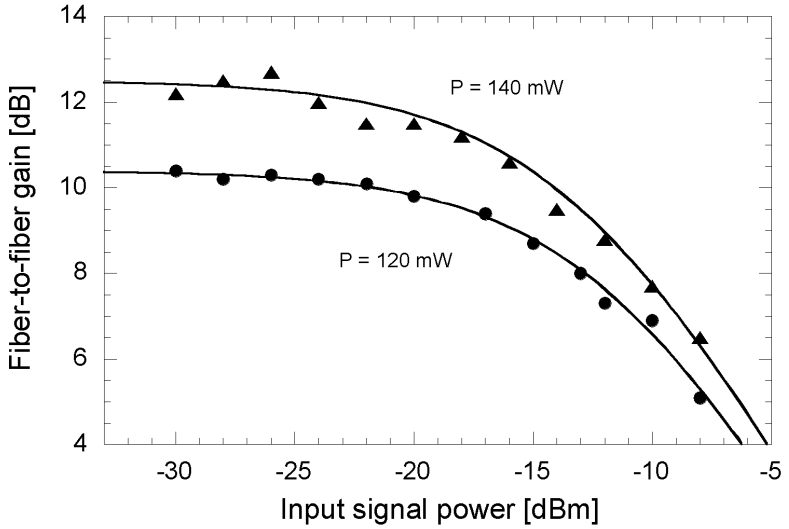


*Figure 4.7. Fiber-to-fiber gain versus input signal power for a VCSOA with $R_t$ = 0.91. The saturated output power was –3.5 dBm.*

### *4.2.3 Noise*

The noise figure was measured on a Generation-1 VCSOA with $R_t = 0.955$ and $R_b = 0.999$. The noise figure of this device, at 90% of threshold, was calculated in Chapter 2 (Figure 2.16). For $R_t = 0.955$ the calculation gives a noise figure of 8.4 dB. For any practical application, the often critical parameter is not the intrinsic noise figure of a device but rather its fiber-to-fiber noise figure. The noise figure is degraded by loss associated with coupling of signal into and out of the device. The fiber-to-fiber noise factor can be calculated using the equation for the noise factor of cascaded devices as explained in Ref. [1]. It can be shown that the input coupling loss directly degrades the noise factor (in logarithmic units, the input coupling loss is simply added to the noise figure), whereas the output coupling loss is only significant when the gain is very small. The input coupling loss in the experiments presented here was estimated to be between 1 and 2 dB. A fiber-to-fiber noise figure around 10 dB can thus be expected from the present device.

Both electrical and optical methods as described in Ref. [2] were used to characterize the noise figure of the VCSOAs. Using optical measurement techniques, the noise figure is calculated from the spectral density of the ASE at the signal frequency, the amplifier gain and the energy of the signal photons. The noise factor in linear units is given by the following equation.

$$F = \frac{2\rho_{ase}}{Gh\nu} + \frac{1}{G} \tag{4.1}$$

The first term represents signal-spontaneous beat noise and the second term represents shot noise. G is the amplifier gain, h is Planck's constant, $\nu$ is the frequency of the signal, and $\rho_{ase}$ is the ASE density in the same polarization state as the signal. Spectra of the ASE and the output signal from a Generation-1 VCSOA are shown in Figure 4.8. The pump power was 93 mW (corresponding to $P/P_{th} = 0.9$) and the input signal power was –30 dBm. 13.5 dB fiber-to-fiber

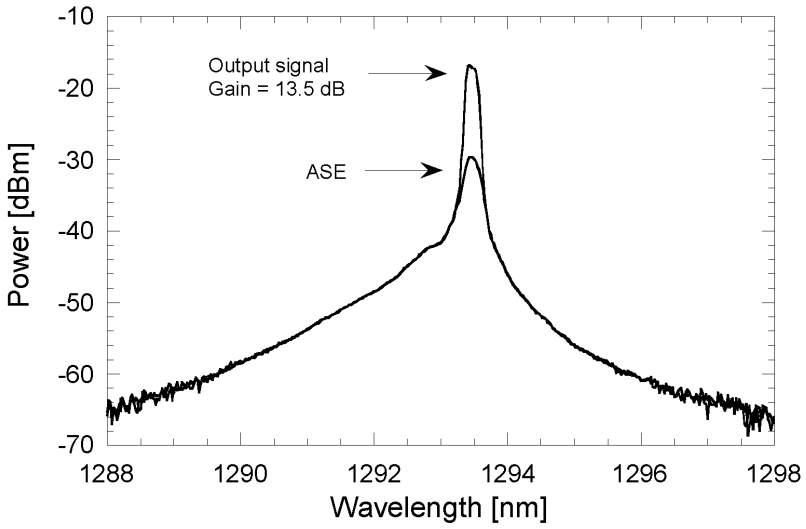


*Figure 4.8. Output spectra from a VCSOA with $R_t$ = 0.955. Output signal and ASE are shown for $P/P_{th}$ = 0.9 and –30 dBm input signal power.*

gain was measured and the output ASE was $2.78 \times 10^{-17}$ W/Hz. As the OSA measures the total optical power in both polarization states, the factor $2\rho_{ase}$ in Equation 4.1 is simply replaced by the measured value. This yields a fiber-to-fiber noise figure of 9.12 dB, calculated from Equation 4.1. This value is in good agreement with the theoretical prediction. It should be noted that using a standard OSA, it is rather difficult to measure the ASE density over the small frequency interval of interest. The low frequency noise, which is the most important part of the noise spectrum, is caused by beating with the ASE close to the signal frequency. For example, only beating with ASE components within a 20 GHz (0.11 nm) region around the signal frequency will show up in a 10 Gbit/s receiver. The OSA has a resolution bandwidth of 0.1 nm. It is evident from the shape of the ASE spectrum (Figure 4.8), the resolution of the OSA, and the frequency range of interest that these measurements are associated with some uncertainty. Furthermore, when the VCSOA is operated in the

saturated regime, the spectral hole burning caused by the signal results in a dip in the ASE spectrum. This makes it difficult to determine the value of the ASE using a standard OSA. In this regime other methods have to be used to measure the ASE density. Since an OSA was the available tool for the measurements presented here, the optical method was used only for small input signal powers when the ASE spectrum is unaffected by the signal.

Electrical measurement techniques give a more complete characterization of the noise figure. The output noise from the amplifier is measured using a calibrated receiver and electrical spectrum analyzer. The thermal noise from the detector and shot noise is subtracted from the measured noise and an ideal shot noise term (1/G) is added. The noise figure is given by the following equation [2]:

$$F(f) = \frac{S_p(f)}{2h\nu G^2 P_{in}} + \frac{1}{G} \tag{4.2}$$

$S_p(f)$ is the measured and corrected electrical noise spectrum in $W^2/Hz$ as a function of electrical frequency, and $P_{in}$ is the input signal power. Using a VOA to control the input signal power minimizes the excess noise of the signal that could otherwise affect the measurements. Noise spectra were measured from 0 to 10 GHz, for different input signal powers, and the noise figure was calculated using Equation 4.2. Noise figure and Fiber-to-fiber gain for $P/P_{th} = 0.9$ is shown in Figure 4.9. Results from optical measurements are also shown in the figure. For low input signal power (-30 dB and –25 dB), gain of about 13 dB was measured. The noise figure given by the electrical method was about 9 dB, which is slightly lower than the results from the optical method and about 1 dB lower than the calculated value. The discrepancy between theory and measurements can be attributed to the gain model (Chapter 2, Section 2.3.1), which was used to calculated the population inversion parameter. As the input signal power increases the amplifier gain starts to saturate. In this regime the

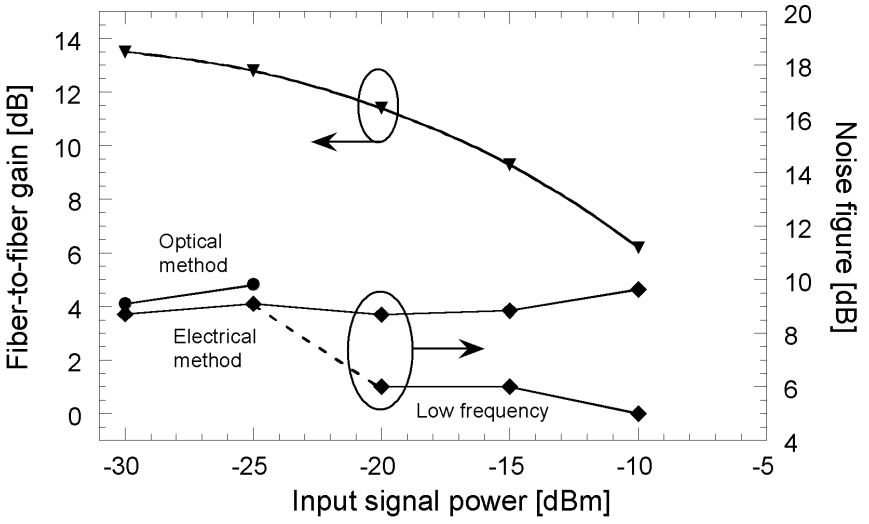


*Figure 4.9. Gain and noise figure versus input signal power for $P/P_{th}$ = 0.9.*

carrier density in the QWs is depleted by the signal. The reduction in carrier density naturally causes a decrease in gain and yields an increased population inversion parameter. This results in a degradation of the noise figure. It has been shown that at low electrical frequencies, the gain saturation causes a decrease in output noise resulting in a low frequency noise figure considerably lower than the broad band noise figure [3]. The bandwidth of the low frequency dip in the noise spectrum is inversely proportional to the carrier lifetime and hence more significant in SOAs compared to fiber amplifiers. A spectrum of the output noise and the noise figure for $P/P_{th}$ = 0.9 of pump power and –10 dBm of signal is shown in Figure 4.10. A noise figure smaller than 5 dB for frequencies below 1 GHz is demonstrated. The broadband noise figure is in this case about 10 dB. Because of the high top mirror reflectivity, the noise figure of this VCSOA is clearly limited by a high population inversion parameter. Reduced mirror reflectivity would allow for stronger pumping and thereby a more favorable population inversion.

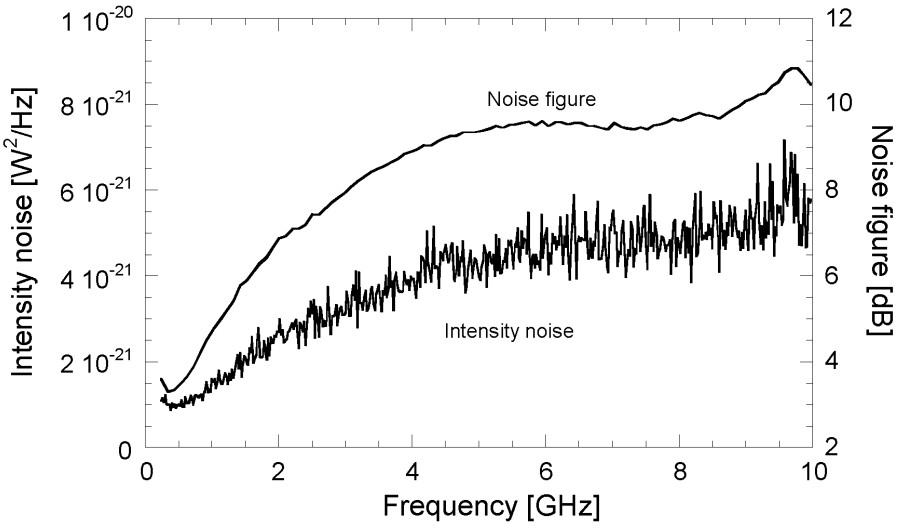


*Figure 4.10. Noise spectrum and noise figure for $P/P_{th}$ = 0.9 and –10 dBm input signal power.*

## 4.3 Generation 2

The highest gain-bandwidth product and highest saturation output power achieved for Generation 1 was measured for the device with the lowest top mirror reflectivity ($R_t$ = 0.91). However, lasing threshold could not be reached at this reflectivity, and higher gain was measured for higher reflectivity ($R_t$ = 0.955). This indicates that the ideal top mirror reflectivity for this design is somewhere between those numbers. If the maximum carrier density can be increased, the top mirror reflectivity can be further reduced.

The second generation VCSOAs had carrier confining mesas etched through the active region. The purpose of this design was to decrease carrier loss through diffusion and thereby achieve two goals: to increase the efficiency of the devices and make it possible to reach higher carrier densities and, thereby, higher gain. Modeling suggested that 8% single-pass gain could be reached with increased carrier density, which would allow for a $R_t$ as low as 0.86.

However, based on the results of Generation 1, it was decided that a more modest reflectivity reduction was more appropriate. A 10.5 period $Al_{0.9}Ga_{0.1}As/GaAs$ with a calculated reflectivity of 0.918 was used as top mirror for Generation 2.

### *4.3.1 Size dependence*

The optimum size of the VCSOA depends on the mode size of the input signal. A larger mode leads to lower intensity per unit area and, consequently, to higher saturation power. This is analogous to large mode—high output power in VCSELs. A larger area has to be pumped to support a larger mode, which obviously leads to higher power consumption. A small mode on the other hand, requires less pump power but leads to increased optical losses through diffraction and scattering. The size and shape of the input signal mode are determined by the optics that are used to couple the signal into the device. For fiber optic applications, this is typically done by either butt coupling the single mode fiber directly to the facet of the device or by using some sort of lens. For the case of butt coupling, the input mode will be of the same size as the mode in the single mode fiber, which is about 9 μm. In the present work, a lens was used for the coupling between the devices and fiber. The $1/e^2$-diameter of the of the input signal was measured to be 8.3 μm.

The mesa-sizes of Generation-2 devices ranged from 5 μm to 36 μm. For mesas of exactly the same size, or smaller, than the signal mode, the scattering loss is substantial. If the difference between the mesa diameter and diameter of the pumped area is larger than the diffusion length of the carriers, the carriers will recombine before they reach the barrier, and the carrier confinement will have no effect. The diffusion length in strained 1.3-μm InGaAsP QWs is about 1 – 2 μm [4]. The $1/e^2$-diameter of the pump beam that

was used in this thesis was measured to be 8.8 μm. It can be concluded from this that the optimum mesa size for the present devices is between 8.3 and about 13 μm. Figure 4.11 shows peak fiber-to-fiber gain versus mesa diameter. The dots represent average of at least three devices and the error bars indicate the extreme values. For mesas larger than 15 μm, size-independent gain was observed (*i.e.* no difference from the planar design of Generation 1). For devices smaller than 15 μm, the peak gain increased since the carrier confinement made it possible to reach higher carrier densities. The highest fiber-to-fiber gain of 17 dB was measured for an active region diameter of 9 μm. When the mesa diameter approaches the signal spot size, optical loss through scattering off the mesa sidewalls causes the gain to decrease. For mesa diameters smaller than the signal and pump spot sizes the gain dropped drastically.

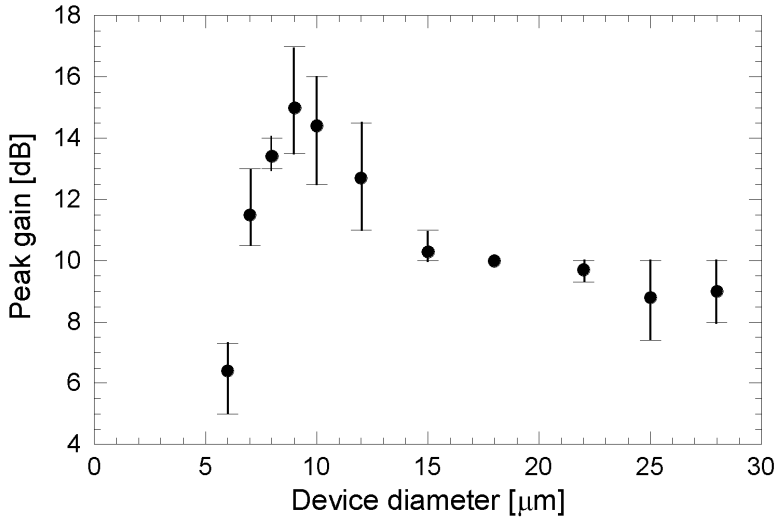


*Figure 4.11 Size dependence of amplifier gain. The carrier confinement makes it possible to achieve higher carrier density, which increases the gain. For diameters smaller than the signal (8.3 μm) the loss increases dramatically.*

To demonstrate extremely small devices was not the goal of this thesis; devices smaller than the input signal mode are obviously not of any interest. The performance of the smallest devices will therefore be only briefly analyzed. For a thorough analysis of excess losses in minute vertical cavities and scaling of parameters in miniature VCSELs, the reader is referred to Refs. [5,6]. The size dependent excess loss is plotted versus mesa radius in Figure 4.12. The increased coupling loss for smaller devices has been accounted for by simply calculating what fraction of the power in the input signal mode overlaps the device. It has been shown that the scattering loss in air-post VCSELs follows $1/r^{\gamma}$ where $\gamma$ varies between 2 and 2.8, depending on the model that is used [7]. For the VCSOAs analyzed here, the excess loss follows a $1/r^{2.8}$ dependence as shown by the curve fit in the figure. The high value for $\gamma$ is expected since the pillars are etched in the active region, instead of in the mirror as was the case in the devices in Ref [7]. This leads to a stronger interaction between the rough sidewall and the optical field.

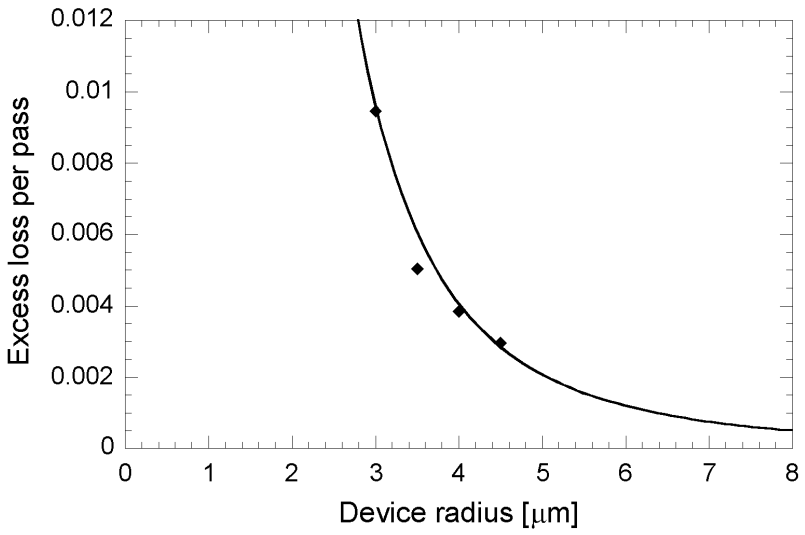


*Figure 4.12 Excess loss versus device radius. As the radius is decreased, the loss increases as $1/r^{2.8}$.*

The decreased carrier loss through diffusion resulted in increased maximum carrier density and increased gain compared to Generation 1. The decreased carrier loss also resulted in higher carrier density at lower pump powers. The pump power required to reach 10 dB fiber-to-fiber gain is plotted versus mesa diameter in Figure 4.13. Dots are measurements, the solid line is a calculated curve. For large devices pump power in excess of 100 mW was required to reach 10 dB gain. For devices larger than 20 μm, no difference between device diameters was observed; in this regime the properties of the devices are identical to the planar design. As the mesa size decreases, the required pump power decreases because of the carrier confinement. For device sizes 10, 9, and 8 μm, 10 dB of gain was obtained for less than 50 mW of pump power. For the 7-μm VCSOA, higher pump power (70 mW) was needed. This device is smaller than the input signal, and higher material gain is required to compensate for the increased loss.

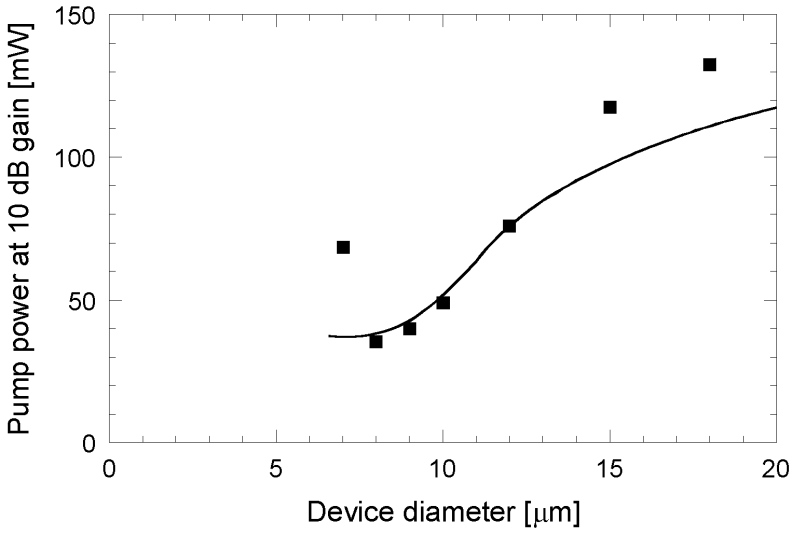


*Figure 4.13 Pump power required to reach 10 dB fiber-to-fiber gain versus mesa diameter. The solid line is a calculation that includes diffusion of carriers and heating, but not decreased pump power absorption due to bleaching.*

The calculated curve is based on the carrier rate equation including diffusion and sidewall recombination. The simplest way to do this is to assume that the carriers are uniformly distributed over the entire cross-section of the mesa. This simplification is only valid for mesa sizes close to the size of the pump beam, and was used for devices up to 10 μm in diameter. For larger devices, the spatial distribution of carriers must be taken into account. This is done by solving the carrier rate equation in cylindrical coordinates as described in Ref [8]. A diffusion coefficient of 12 $cm^2/s$, an average carrier lifetime of 2 ns, and a sidewall recombination velocity of 1000 cm/s were used in the calculations. The effect of heating at higher pump powers is also included in the calculation. The energy of the pump photons is 25% larger than the bandgap of the QWs. 25% of the pump power therefore goes to heat generation. It has been shown that the signal gain decreases by about 0.2 dB/K [9]. A thermal resistance of 0.5 K/mW was used in the calculation. There are too many unknowns in these calculation to extract any materials parameters; the values that were used are typical values found in the literature. The high pump power needed for large devices can not be explained by this model only. The discrepancy between the calculated pump power and the actual pump power used (about 20 mW for a 15-μm device) can be attributed to a decrease in the absorption of pump power due to bleaching of the QWs. This has not been included in the model, nor has optical guiding, which may have an effect for small device sizes.

A small polarization dependence in the gain was observed for the smaller devices. 4 dB polarization dependence was measured for 9 μm devices; devices of 15 μm diameter and larger were polarization independent. The polarization dependence is attributed to slightly non-circular mesas caused by the anisotropic wet-etch. This can be avoided by optimizing the QW under-etch process.

### *4.3.2. Results, 9-μm VCSOA*

The best results of Generation 2 were produced by a 9-μm diameter device. This device showed the highest gain at the lowest pump power. No size dependence was observed in the saturation power of the devices. Fiber-to-fiber gain and noise figure for this device are plotted versus pump power in Figure 4.14. The input signal power was –30 dBm. The maximum fiber-to-fiber gain was 17 dB, which means that the intrinsic gain was about 24 dB. This is the highest gain reported to date for a long wavelength VCSOA. The pump power needed to reach this value of gain was 50 mW, which corresponds to $P/P_{th} = 0.86$. The efficiency as indicated by the dashed line was 0.34 dB/mW. A noise figure of 6.1 dB was measured for 17 dB gain. This is in good agreement with predictions in Chapter 2. The gain spectrum for an input signal power of –30 dBm and a peak fiber-to-fiber gain of 15 dB is shown in Figure 4.15. The triangles are measurements and the line is a curve-fit based on Equation 2.4. The gain bandwidth was measured to be 0.2 nm (32 GHz).

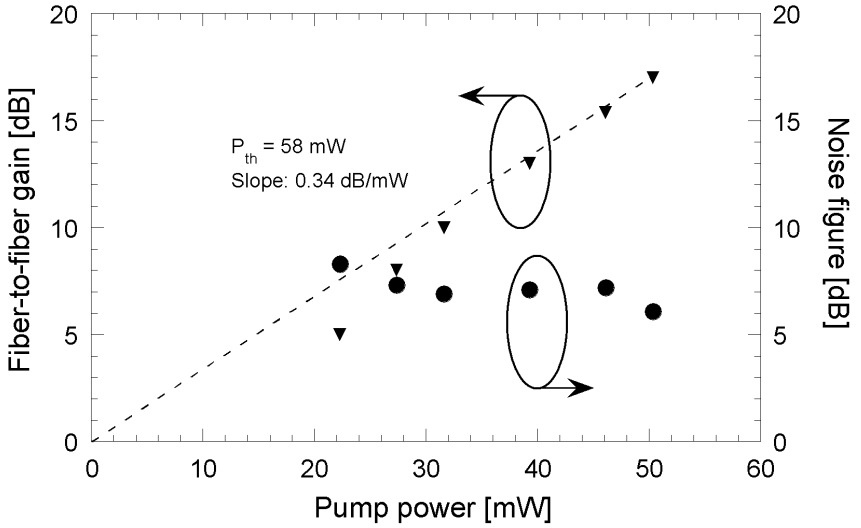


*Figure 4.14 Fiber-to-fiber gain and noise figure versus pump power for a 9-μm diameter VCSOA. The dots are measurements and the dashed line shows maximum slope efficiency.*

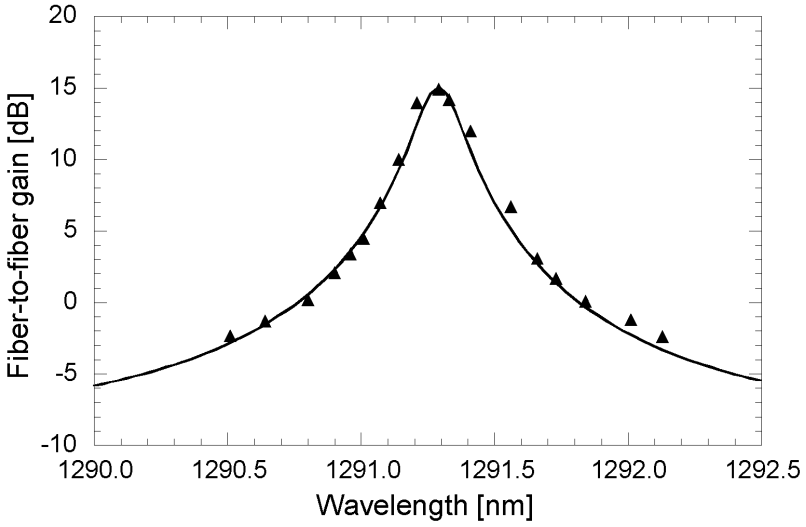


*Figure 4.15 Gain spectrum of 9-$\mu$m VCSOA. The gain bandwidth for15 dB gain was 0.2 nm.*

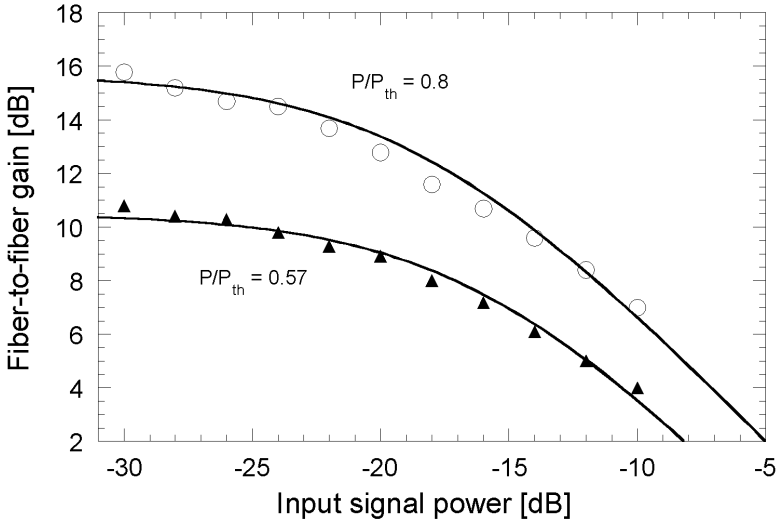


*Figure 4.16 Saturation characteristics for 9-$\mu$m VCSOA. For 15.5 dB of small-signal gain, the saturation output power was –5 dBm.*

The saturation characteristics of this device are shown in Figure 4.16. Due to the slightly higher reflectivity, the saturation power is slightly lower than the best result of Generation 1. For a $P/P_{th} = 0.57$ the small-signal gain was 10.5 dB and the saturation output power was measured to be –8.5 dBm. For a $P/P_{th} = 0.8$ the small-signal gain increased to 15.5 dB and a saturation output power of –5 dBm was measured. The fact that lasing threshold can be reached suggests that the QW gain is now high enough so that the reflectivity could be even lower. This would result in higher saturation power, lower noise figure, and even higher amplifier gain.

### *4.3.3 Efficiency comparison: Generation 1—Generation 2*

The efficiency of Generation 2 was improved dramatically compared to Generation 1. This can be quantified by comparing the pump power required to reach a certain gain level. This is shown in Figure 4.17 for both generations of VCSOAs. The pump power required to reach 10 dB of fiber-to-fiber gain (solid lines and triangles) and lasing threshold (dashed lines and circles) are plotted versus top mirror reflectivity. For Generation 1, the lowest pump power needed to achieve 10 dB gain was about 70 mW (measured for high mirror reflectivity). The top mirror reflectivity of Generation 2 was 0.918. At that reflectivity, the planar design would need over 100 mW of pump power to give 10 dB gain, whereas the carrier confined design needed only 33 mW. This corresponds to a threefold improvement in efficiency. The planar design could not be brought to lasing threshold at reflectivities lower than 0.945. The 9-μm diameter carrier confined device lased at 60 mW of pump power, clearly demonstrating that higher carrier density can be obtained than what was possible for Generation 1.

A comparison of the pump power required to reach a certain gain level clearly shows the efficiency improvement in Generation 2. However, is does not give a number for the efficiency of the VCSOAs. The efficiency of an

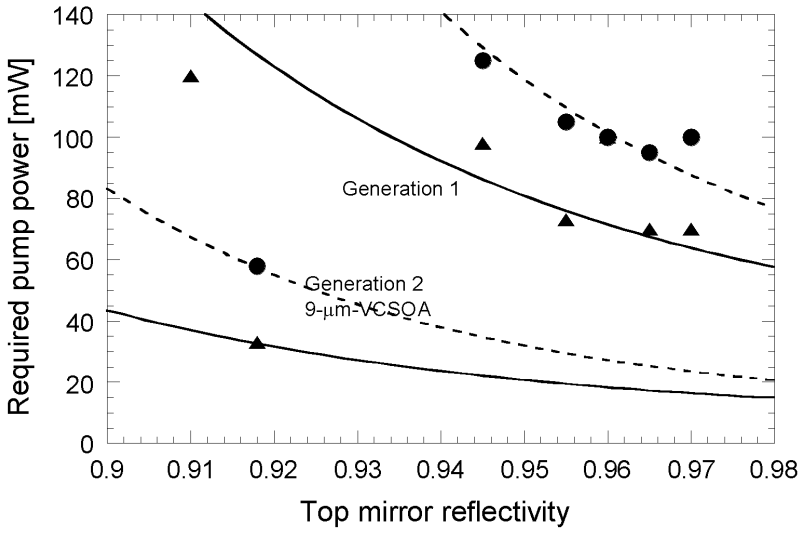


*Figure 4.17. Comparison of power consumption of Generation 1 and Generation 2. The circles and dashed lines represent pump power required to reach lasing threshold. The triangles and solid lines represent pump power required to reach 10 dB gain. A threefold improvement is demonstrated.*

optical amplifier is not a commonly used figure of merit, and consequently there is not a standard definition for it used in the literature. If the amplifier is optically pumped, like the case of EDFAs and EDWAs, the efficiency is sometimes defined as the amplification in dB per mW of pump power as shown in Figures 4.2 and 4.14. This efficiency is sometimes called the gain coefficient but will here be referred to as the *slope efficiency*. The highest slope efficiency measured for Generation 1 was 0.14 dB/mW. For a 9-μm device from Generation 2 a slope efficiency of 0.34 dB/mW was measured. This improvement is slightly less than a factor of three. However, these values represent different top mirror reflectivities: 0.965 for Generation 1 and 0.918 for Generation 2. The slope efficiency increases with increased reflectivity. The true improvement is, therefore, larger than indicated by these numbers. These

numbers are similar to what has been reported for EDWAs. It is also similar to the efficiency of commercial EDFAs, but significantly lower than the highest value reported for EDFAs of 11 dB/mW [10]. However, the slope efficiency does not take the signal power or the number of signal channels into account. Consequently, it does not provide a fair means to compare different amplifiers. Alternatively, the *quantum efficiency* can be defined as the number of signal photons (output power minus input power divided by energy per photon) produced per pump photon. The quantum efficiency increases as the signal power is increased, until the amplifier saturates. The maximum quantum efficiency obtained for Generation 1 was measured to be 0.5%. This was obtained for $R_t = 0.91$. The carrier confining structure in Generation 2 increased the quantum efficiency threefold, to 1.5%.

The threefold improvement in efficiency and the fact that higher amplifier gain was obtained with Generation 2 confirms that the carrier confinement had a great impact on the lateral carrier loss. The exact composition and crystalline structure of the material covering the QW edges could not be established, and the reduction in surface recombination can therefore not be quantified. Nor was it possible to quantitatively evaluate the decreased sidewall recombination from the calculated curve in Figure 4.13. However, the reduced carrier loss is evidence of very low sidewall recombination. This indicates that InP from the cladding layers filled in the steps in the sidewalls during the second wafer bond, effectively creating a buried heterostructure. In-plane buried heterostructure lasers fabricated by mass transport have already been demonstrated [11]. Wafer bonding provides an attractive way to fabricate buried heterostructure VCSOAs and VCSELs, as it gives the freedom to process the active region before the structure is completed.

The threefold improvement is remarkable, but the efficiency is still very low, indicating substantial losses. As mentioned previously, only about 20% of

the pump power is absorbed in the active region of the devices. Taking this into account, the quantum efficiencies increase to 2.5% for Generation 1 and 7.5% for Generation 2. These number are still very low, indicating that less than one out of 10 carriers actually contributes to amplification of the signal. The rest is lost through non-radiative recombination and lateral diffusion of carriers out of the active region, and through poor overlap of the pump spot and the signal. The efficiency is further degraded by optical loss through absorption, scattering and diffraction. In order to improve the efficiency further, the optical pumping scheme has to be improved, and the optical losses must be addressed. Diffraction and scattering losses can be reduced by introducing better index guiding. The pump beam/carrier distribution—signal mode overlap can be further optimized to yield more efficient gain guiding.

## 4.4 Summary

Two generations of optically pumped VCSOAs were presented and analyzed in this chapter. Generation 1 was a planar design where the lateral dimensions of the devices were defined by the diameter of the pump beam. It was the first demonstration of a VCSOA operating at 1.3-μm wavelength. The top mirror reflectivity ($R_t$) was varied in the characterization of these devices. The highest reflectivity was 0.98 and the lowest was 0.91. It was demonstrated that for high reflectivities the VCSOA performance is limited by lasing threshold. In this regime better performance is achieved for reduced reflectivities. If lasing threshold cannot be reached, the performance is limited by the maximum carrier density that can be obtained. This is in agreement with theoretical predictions. The highest fiber-to-fiber gain of Generation 1 was 13.5 dB measured for $R_t = 0.955$. The widest gain bandwidth was 0.6 nm (100 GHz), for 11.3 dB gain, and the highest saturation output power was –3.5 dBm. These values were

measured for a top mirror reflectivity of $R_t$ = 0.91. The noise figure was measured for a device with $R_t$ = 0.955. The fiber-to-fiber noise figure was determined to be about 9 dB. It was limited by the high mirror reflectivity, which prevented operation at high population inversion. The efficiency of Generation 1 was very low, mainly due to carrier loss through lateral diffusion in the QWs.

In Generation 2 carrier confinement was introduced. This generation was fabricated from the same material as Generation 1. The carrier confinement resulted in threefold efficiency improvement. It also produced higher maximum carrier density, resulting in higher gain than for Generation 1. The maximum fiber-to-fiber gain was 17 dB for a pump power of 50 mW. A noise figure of 6.1 dB was measured for the same pump level. This is the best performance presented for a long-wavelength VCSOA to date. The results of both generations are summarized in Table 4.1.

*Table 4.1 Summary of results.*

| | **Generation 1** | **$R_t$ (Gen 1)** | **Generation 2 ($R_t$ = 0.918)** |
|---|---|---|---|
| Fiber-to-fiber gain | 13.5 dB | 0.955 | 17 dB |
| Gain bandwidth | 0.12 – 0.6 nm | | 0.15 – 0.3 nm |
| GBW-product | 590 GHz | 0.91 | 400 GHz |
| Noise figure | 9 dB | 0.955 | 6.1 dB |
| Saturation power | -3.5 dBm | 0.91 | -5 dBm |
| Quantum efficiency | 0.5% | 0.91 | 1.5% |

# References

[1] D. M. Baney, P. Gallion, R. S. Tucker, "Theory and Measurement Techniques for the Noise Figure of Optical Amplifiers", *Optical Fiber Technology*, vol. 6, pp. 122-154, 2000.

[2] R. S. Tucker, D. M. Baney, "Optical Noise Figure: Theory and Measurements" in *OFC 2001 Technical Digest*, paper WI1, 2001.

[3] M. Shtaif, G. Eisenstein, "Noise Characteristics of Nonlinear Semiconductor Optical Amplifiers in the Gaussian limit", *IEEE Journal of Quantum Electronics*, vol. 32, pp. 1801-1809, Oct. 1996.

[4] D. X. Zhu, S. Dubovitsky, W. H. Steier, J. Burger, D. Tishinin, K. Uppal, P. D. Dapkus, "Ambipolar diffusion coefficient and carrier lifetime in a compressively strained InGaAsP multiple quantum well device," *Applied Physics Letters*, vol. 71, no. 5, pp. 647-649, Aug. 1997.

[5] B. J. Thibeault, T. A. Strand, T. Wipiejewski, M. G. Peters, D. B. Young, S. W. Corzine, L. A. Coldren, J. W. Scott, "Evaluating the effects of optical and carrier losses in etched-post vertical cavity lasers," *Journal of Applied Physics*, vol. 78, no. 10, pp.5871-5875, Nov. 1995.

[6] E. R. Hegblom, D. I. Babic, B. J. Thibeault, L. A. Coldren, "Scattering Losses from Dielectric Apertures in Vertical-Cavity Lasers," *IEEE Journal of Selected Topics in Quantum Electronics*, vol. 3, no. 2, pp. 379-389, Apr. 1997.

[7] D. I. Babic, "Double-fused long-wavelength vertical-cavity lasers," Ph.D. Dissertation in *Electrical and Computer Engineering*, University of California, Santa Barbara, 1995.

[8] N. K. Dutta, "Analysis of current spreading, carrier diffusion, and transverse mode guiding in surface emitting lasers," *Journal of Applied Physics*, vol. 68, no. 5, pp. 1961-1963, Sept. 1990.

[9] T. Kimura, S. Björlin, John E. Bowers, "High Temperature Characteristics and Tunability of Long-Wavelength Vertical-Cavity Semiconductor Optical Amplifiers," submitted to *IEEE Photonics Technology Letters*, Dec. 2002.

[10] M. Shimizu, M. Yamada, M. Horiguchi, T. Takeshita, M. Okayasu, "Erbium-doped fibre amplifiers with an extremely high gain coefficient of 11.0 dB/mW," *Electronics Letters*, vol. 26, no. 20, pp. 1641-1643, Sept. 1990.

[11] Z.-L. Liau, J. N. Walpole, "Mass-Transported GaInAsP/InP Lasers," *Lincoln Laboratory Journal*, vol. 2, no. 1, pp. 77-94, 1989.

# Chapter 5

# VCSOA Applications

Optical amplifiers are used extensively in today's fiber-optic communication networks. The EDFA has been the dominant technology since it was commercialized in the late eighties. However, fiber-optic networks are constantly expanding and evolving, and many new amplifier applications have appeared that require very different amplifier properties. Extensive research is being conducted toward the development of amplifier technologies that suit these new applications. Most notably, there is currently significant interest in amplifier technologies that can provide compact, low-cost devices.

This chapter looks into possible applications for VCSOAs. These applications are, of course, dictated by the special properties of VCSOAs. A few potential applications are outlined in Section 5.1. The feasibility of using VCSOAs for switching or modulation is investigated in Section 5.2. Optical preamplification is covered in Section 5.3. An optical preamplification experiment at 10 Gb/s is presented and analyzed.

## 5.1 Potential VCSOA applications

VCSOAs have a number of potential applications in optical communication systems. Compared to other amplifier technologies, the VCSOA bandwidth is very narrow and the saturation power relatively low. The noise figure of VCSOAs can be much lower than for in-plane SOAs. They can be designed to operate at any desired telecommunication wavelength. The vertical-cavity geometry is compatible with low-cost fabrication and packaging techniques. A property that is a disadvantage for one application might be the enabler of another. The narrow gain bandwidth, for instance, hinders amplification of multiple channels but provides filtering and channel selection. VCSOAs can potentially be used wherever a compact, low-cost, single-channel amplifier is needed. There are many instances in WDM networks where the channels are split up and amplified or processed individually. A reason for this is the importance of maintaining equal signal power in all channels. VCSOAs are ideal for these applications. VCSOAs can also be integrated in high-density 2D array architectures. This is not possible with in-plane SOAs or fiber amplifiers. Proposed applications for VCSOAs include optical interconnects, switching and modulation, and optical pre-amplification of high-speed receivers.

Free-space optical interconnections are the most promising way to solve the wiring bottleneck between silicon chips in computers [1,2]. The transmitters in these interconnections can be either VCSEL arrays or modulator arrays with an external laser source. The attributes of VCSOAs that make them attractive for use in optical interconnects are their circular beam profile, low power consumption and compatibility with 2D array architectures. Proposed applications are as modulators, preamplifiers, or buses. As modulators, they are an alternative to MQW electro-optic modulators. Better extinction ratio and low voltage operation are here foreseen advantages [3]. An array of preamplifiers

integrated with a receiver array would ease the requirements on both transmitters and receivers. This would lead to decreased power dissipation, which in turn would enable higher interconnect density [4]. The optical bus, or repeater, can serve as detector and amplifier in interconnects between multiple boards. Part of the signal is detected and part is passed through to the next board. The amplifier compensates for the coupling loss and the power absorbed by the detector [5].

Using SOAs for switching or modulation is attractive because of their fast gain dynamics, typically large extinction ratio, and the fact that amplifier gain compensates coupling losses. For switching applications the signal is divided and fed through a matrix of SOAs. An amplifier that is turned off naturally absorbs the signal. By turning a combination of amplifiers on, a path through the grid opens up that routs the signal to the desired output port. For all-optical packet-switched networks, the switching time must be small compared to the packet duration. Switching times on the order of a few ns or less are needed [6]. This is easily obtained with SOA-based switches. For modulation applications, SOAs are not as fast as electroabsorption modulators or $LiNbO_3$ Mach-Zehnder modulators. However, the amplifier gain gives very precise control of the output power, which is an advantage in many applications. Amplifying modulators are attractive for a number of applications. For example, the gain could compensate for losses associated with division of a signal for transmission to multiple recipients. Another application is the use of SOAs as remote modulators in networks with a centralized light source. Several proposed solutions for access and fiber to the home (FTTH) networks take this approach, instead of using conventional transceivers, in order to minimize component cost [7-9]. The polarization independent gain and potential low manufacturing cost of VCSOAs would be major advantages for these applications. In the configuration in Ref. [8] SOAs are used both to detect the

incoming signal at the remote nodes and to modulate a continuous wave (CW) signal for the upstream information. A VCSOA showing amplifier-detector dual functionality has already been demonstrated [10].

Optical preamplification of high-speed receivers might be one of the most interesting applications for VCSOAs. Desired properties for this application are good noise performance and polarization independent gain, which are areas of difficulty for in-plane devices. Also desired are low power consumption, compactness, and low cost, properties that are not associated with fiber amplifiers. VCSOAs can meet all these criteria. Furthermore, an optical filter is normally added after the amplifier for this application, something not needed if VCSOAs are used since their narrow bandwidth makes them function as amplifying filters. The low saturation power of VCSOAs is not a problem for optical preamplification as the signal power reaching the receiver is typically optimized at a lower level than the saturation power of a VCSOA.

## 5.2 Switching and Modulation

Extensive work has been done investigating the possible use of in-plane SOAs for optical switching [11-13] and for modulation [7,14,15]. Limiting factors for switches based on in-plane SOAs are the polarization dependent gain and accumulation of ASE as SOAs are cascade into switch matrices [13]. The polarization independent gain of VCSOAs would be a significant advantage for these application. The accumulation of ASE would be suppressed by the typically narrow VCSOA bandwidth. The narrow bandwidth provides wavelength selection, which may be an advantage or a limitation depending on the specific switch architecture and application. When using SOAs as external modulators, both transmission mode and reflection mode operation are possible, with different advantages and considerations for each. Operation in reflection

mode has the advantage of minimizing difficult and costly fiber alignment. This is indeed the configuration chosen in Refs. [7,8]. For the case of switching, were several amplifiers are cascaded, operation in transmission mode is clearly advantageous. No multiport switches based on VCSOAs have yet been demonstrated but the switching/modulation properties of individual VCSOA elements have been briefly studied. A vertical-cavity amplifying switch operated in reflection mode at 1.55-mm wavelength has demonstrated a switching time of 10 ps and an extinction ratio of 14 dB [16].

The VCSOAs fabricated in this thesis were optimized for reflection mode operation. Previously reported reflection mode VCSOA switches turn off completely in the off-state thereby limiting the extinction ratio to the gain of the amplifier [16]. However, the unique properties of the Fabry-Perot structure can be used to significantly increase the extinction ratio. For a single pass gain of $g_s = \sqrt{R_t} \big/ \sqrt{R_b}$ , the reflection gain equals zero. The origin of this effect lies in the fact that the field reflected off the front facet is 180º out of phase with the fields exiting the cavity. When the two fields are of the same amplitude, the output signal vanishes due to destructive interference. Using this level as off-state greatly increases the extinction ratio.

In order to investigate the maximum extinction ratio of our devices, amplifier gain as a function of pump power was measured under CW conditions. These measurements were done on a Generation-1 VCSOA with a top mirror reflectivity of 0.955. Figure 5.1 shows fiber-to-fiber gain as a function of pump power. The dots are measurements and the line is a curve fit based on Equation 2.4. Rate-equation analysis was used to link the single-pass gain to the pump power. The input signal wavelength is 1291.5 nm and the input signal power ($P_{in}$) is –25 dBm. Without pump power the 1.3 μm signal is reflected off the top mirror of the VCSOA without entering the cavity. 10 dB attenuation of the

signal is observed. At about 13 dBm (22 mW) of pump power the condition for output signal cancellation is met and the output signal power decreases drastically. An attenuation of –27 dB is measured. As the pump power is increased further, the intensity of the cavity mode increases and the VCSOA eventually shows gain. At about 20 dBm (93 mW) of pump power a fiber-to-fiber gain of 8 dB was measured. For higher pump powers the gain rolls over, as the cavity resonance frequency is red-shifted due to heating and the gain spectrum drifts away from the input signal wavelength. An extinction ratio of 35 dB for 7 dB modulation of pump power is demonstrated. The small pump power modulation needed to produce a large signal extinction ratio ensures fast switching. Spectra of the output signal at maximum amplification, as well as maximum attenuation is shown in Figure 5.2. No extinction ratio degradation was observed as the input signal power was increased and the VCSOA saturated; 35 dB extinction ratio was measured up to $P_{in}$ = –10 Bm.

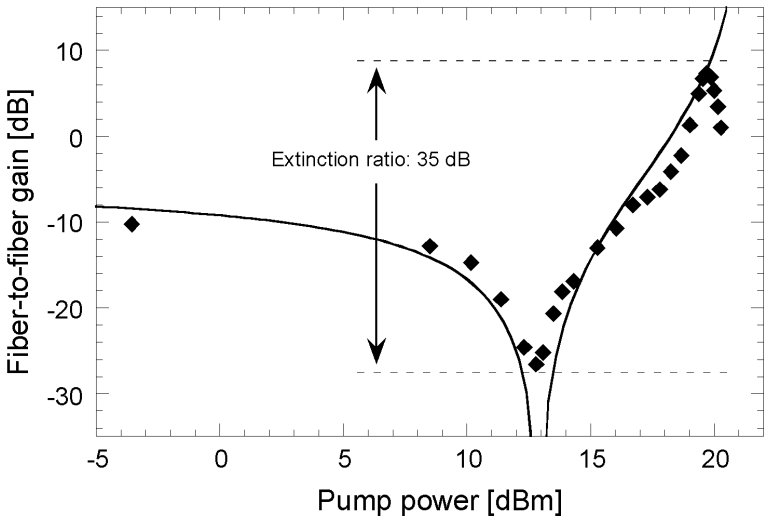


*Figure 5.1. Fiber-to-fiber gain versus pump power. The input signal power was –25 dBm. The solid line is a curve fit based on Equation 2.4.*

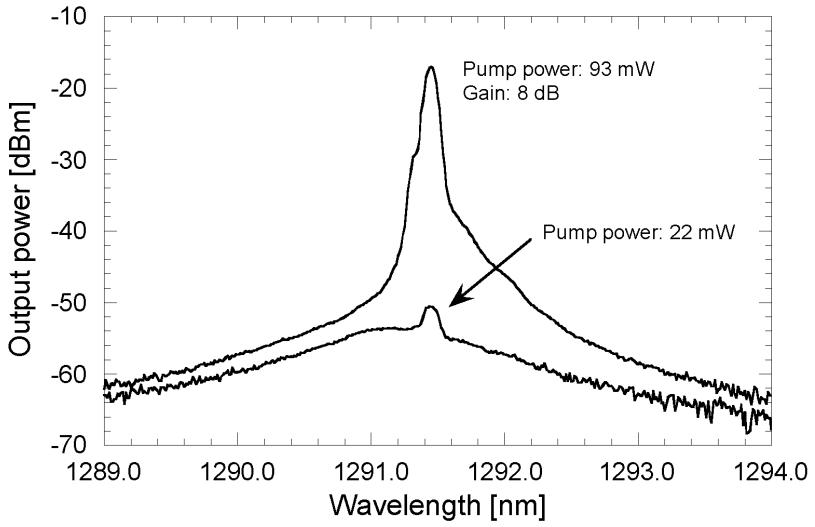


*Figure 5.2. Output spectra at peak gain and maximum attenuation.*

The increased temperature sensitivity at higher pump powers is shown in Figure 5.3. The graph shows spectral dependence of gain for three different pump powers, corresponding to the dip, the maximum gain, and after roll-over in Figure 5.1. The dots are measured data and the lines are curve fits based on Equation 2.4. Maximum attenuation, occurring at 22 mW of pump power, has its minimum around 1291.4 nm. For a pump power of 93 mW the peak gain is 8 dB. For this increase in pump power, the cavity resonance frequency, and hence the gain peak, is red-shifted less than 0.1 nm. The gain bandwidth for a peak gain of 8 dB is 0.25 nm, so the signal stays within the bandwidth. At higher pump power the heating is more pronounced. Over 10 dB of fiber-to-fiber gain was measured for a pump power of 110 mW. For this pump level however, the peak of the gain spectrum occurs at 1291.8 nm, making modulation up to this level impossible. For high modulation speed, thermal effects will not modulate the cavity resonance frequency. For switching however, when the VCSOA might be in the on-state for longer times, heating of

the device can be detrimental to the performance. Optical pumping minimizes heating of the device as joule-heating is eliminated. It is still necessary to operate in a regime where the device can effectively dissipate the generated heat.

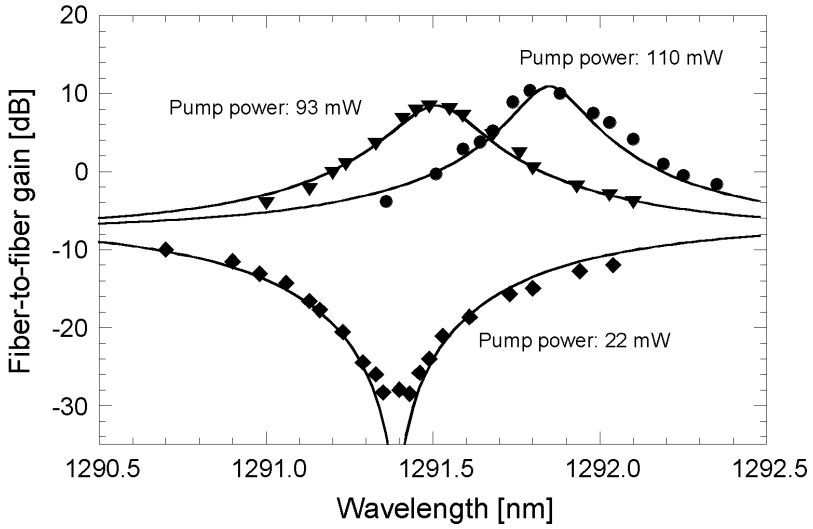


*Figure 5.3. Gain spectra for different pump powers. Dots are measurements and the solid lines are curve fits based on Equation 2.4. The heating of the active region at high pump powers causes a red-shift of the gain spectrum, which sets a limit to the obtainable extinction ratio.*

Using optical pumping eliminates electrical parasitics and carrier transport issues since carriers are generated in the QWs. The rise time in an optically controlled switch is therefore extremely fast. The fall time is determined by the carrier lifetime and the change in carrier density that is needed to go from the on-state to the off-state. The carrier lifetime varies with the carrier density and the input signal power. The difference in carrier density between the on and off states depends on the mirror reflectivity. This dependence is shown in figure 5.4. For low top mirror reflectivity, lower single-pass gain is needed to achieve full extinction, and higher single-pass gain is needed to achieve high amplifier gain. A larger modulation swing is therefore

needed, which results in slower switching. Using a highly reflective top mirror on the other hand, enables faster switching. However, high top mirror reflectivity also leads to narrow gain bandwidth, which makes the modulator/switch more wavelength selective and more sensitive to temperature variations.

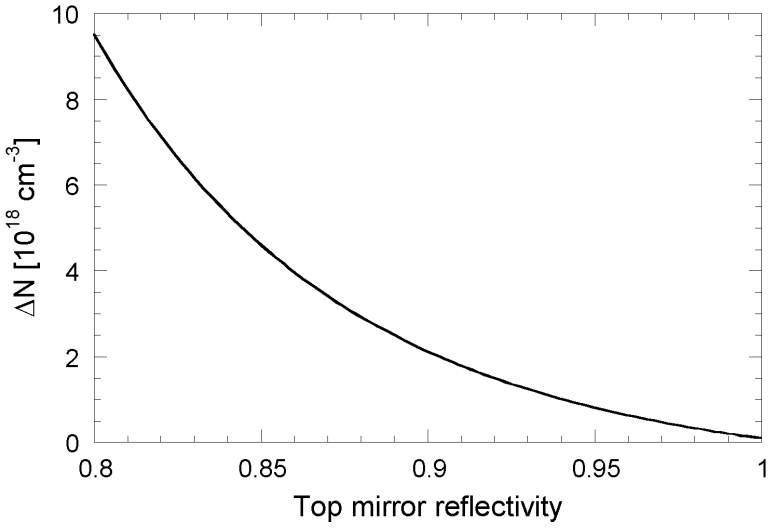


*Figure 5.4. Required change in carrier density between on and off states in a reflection mode VCSOA modulator.*

Small signal frequency response of the VCSOA was measured in order to determine the carrier lifetime. The drive current to the 980 nm pump laser was modulated, which modulated the gain of the amplifier and thereby the signal. Modulation response of the VCSOA is shown in Figure 5.5. For input signal powers of –30 dBm and –20 dBm a fiber-to-fiber gain of 10 dB was measured and the 3 dB roll-off occurred at 0.8 and 1.1 GHz, respectively. When the input signal power was increased to –10 dBm, the gain medium was saturated and the amplifier gain decreased to 5.5 dB. In the saturated regime a large fraction of the carriers go into stimulated recombination. This leads to

shorter carrier lifetime, which allows for faster modulation. In this regime the 3 dB roll-off in the modulation response was 1.8 GHz for $P_{in}$ = –10 dBm. The carrier lifetime can be calculated from the 3-dB modulation bandwidth using the relation $\tau = (2\pi f_{3dB})^{-1}$. The carrier lifetimes in the three cases here were determined to be 200 ps, 144 ps, and 90 ps.

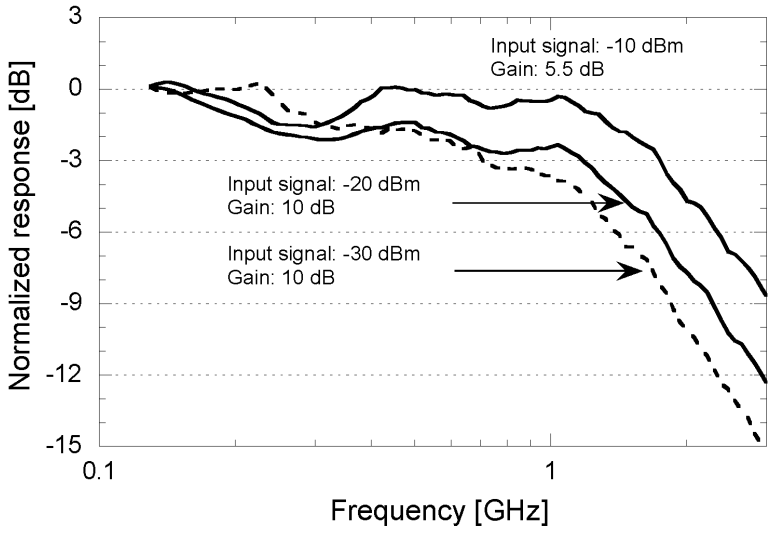


*Figure 5.5. Small signal frequency response of VCSOA for three different input signal powers.*

The curve fit in Figure 5.1 revealed that the carrier density in the on and off states were about $1.5 \times 10^{18}$ cm$^{-3}$ and $0.8 \times 10^{18}$ cm$^{-3}$, respectively. The fall-time can now be calculated from these carrier densities and the carrier lifetimes extracted from the modulation response. Assuming an exponential decay, the carrier density follows $N = N_0 \exp(-t/\tau)$. This calculation gives switching fall times of about 0.1 ns or lower for all cases. For $P_{in}$ = –10 dBm, the carrier lifetime of 90 ps yields a switching fall time of 48 ps.

For the use of VCSOAs as external modulators, the measured frequency response allows for 2.5-Gb/s modulation with 5.5 dB of fiber-to-fiber gain in the saturated regime. For applications like those proposed in Refs. [8,9], the SOA-

modulators are used to modulate the upstream signal from a single user. In those cases, bit rates lower than 1 Gb/s are used. This bandwidths measured for the VCSOAs in this thesis are clearly sufficient for such applications.

## 5.3 Optical preamplification

Optical preamplification is an attractive way to improve the receiver sensitivity of high-speed receivers. At high bit rates (10 Gb/s, 40 Gb/s, and higher) avalanche photo diodes (APDs) are limited by their gain-bandwidth product. Optical preamplification is a way to increase the sensitivity of a regular PIN-detector without compromising its high-speed performance. This has been demonstrated using both in-plane SOAs [17], and EDFAs [18]. EDFAs are naturally limited to operation around 1.5 μm, whereas SOAs can be designed to operate at any desired wavelength. Conventional in-plane SOAs are typically sensitive to polarization and show poor coupling efficiency to optical fiber. The good coupling efficiency, polarization independent gain, and favorable filtering properties of VCSOAs are advantages for this application.

The performance of our VCSOAs for optical preamplification was investigated. A Generation-1 VCSOA with top mirror reflectivity of 0.955 was used in these experiments. The experimental setup described in Chapter 4 was modified to allow modulation of the input signal and bit error rate (BER) measurements. The input signal was modulated using a $LiNbO_3$ Mach-Zehnder modulator before it was coupled into the VCSOA. The output signal was fed to a Nortel PP-10G PIN receiver, which was followed by an SHF broadband amplifier before the bit error rate tester (BERT). No optical filter was used between the VCSOA and the PIN detector. The experimental setup is shown in Figure 5.6.

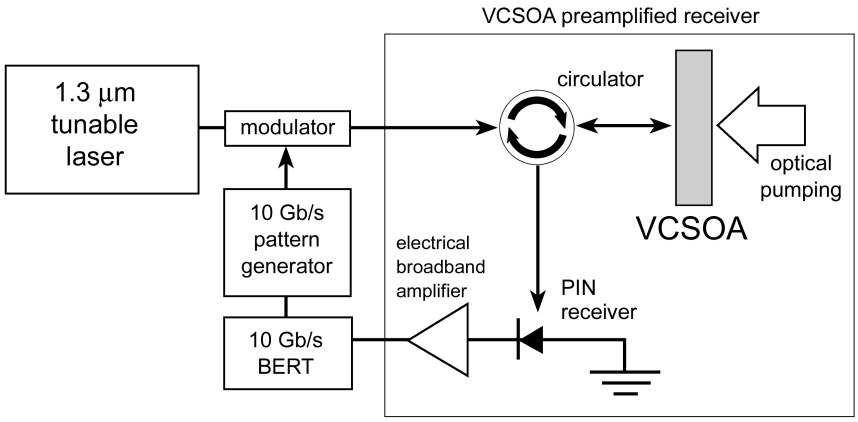


*Figure 5.6. Experimental setup for optical preamplification experiments.*

The receiver sensitivity was measured with and without the VCSOA preamplifier. The VCSOA was pumped at 80% of the pump power required to reach lasing threshold. The fiber-to-fiber gain at this pump level was measured to be 11 dB and the optical bandwidth was 37 GHz. The measured gain spectrum is shown in Figure 5.7. The population inversion was fairly low at this pump level; it was estimated that the noise figure was over 10 dB.

A 10 Gb/s non-return-to-zero $2^{31}$-1 pseudorandom bit sequence was transmitted to the receiver and the BER was measured. BER versus received power with and without preamplification is shown in Figure 5.8. The receiver sensitivity (corresponding to a BER of $10^{-9}$) without the VCSOA was –19.2 dBm. With the VCSOA operating at 11 dB fiber-to-fiber gain the receiver sensitivity was increased by 7 dB to –26.2 dBm. The 4 dB power penalty is caused by optical noise added by the amplifier. No error floor was observed. The eye pattern at a BER of $10^{-9}$ for preamplified signal is shown in Figure 5.9. Excess noise from the optical amplification is visible in the high level.

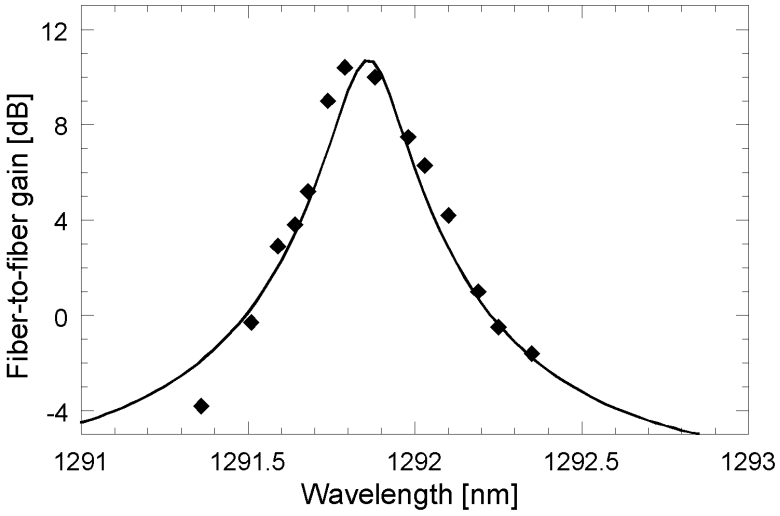


*Figure 5.7. Gain spectrum of VCSOA used for optical preamplification experiments. The optical bandwidth is 37 GHz.*

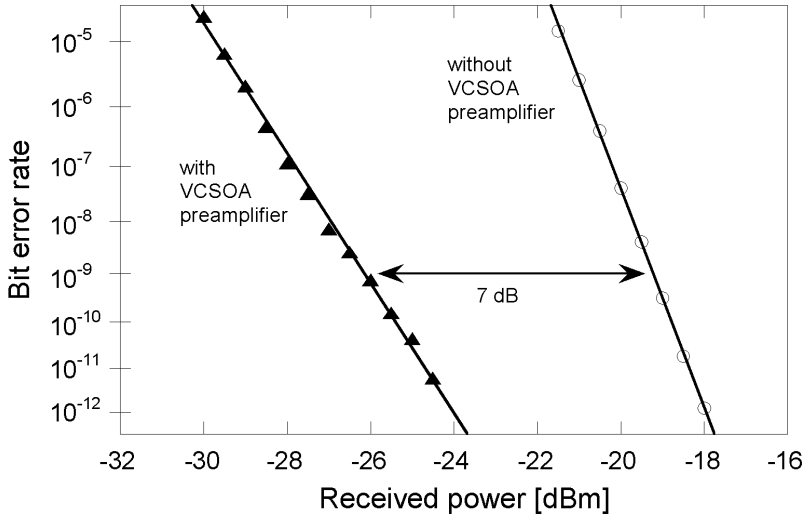


*Figure 5.8. Bit error rate versus received power. Operating the VCSOA at 11 dB of fiber-to-fiber gain produced a 7 dB improvement in receiver sensitivity.*

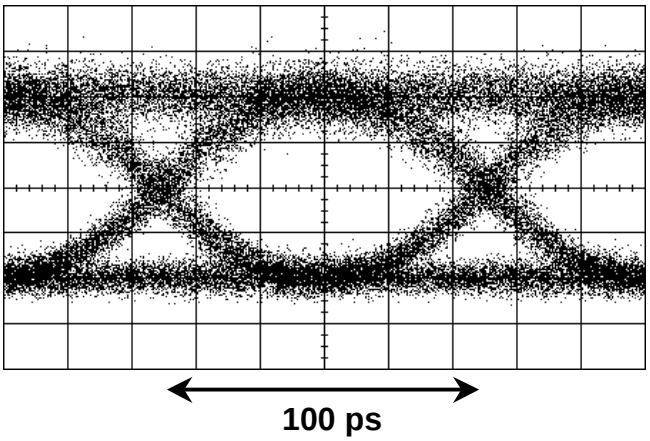


*Figure 5.9. Eye diagram. Optical noise from the preamplifier is visible in the high level.*

To analyze the BER curves and verify agreement between the power penalty and the noise figure of the VCSOA, the Q parameter can be calculated from the signal power and the noise currents. (The Q parameter is then related to the BER through the complementary error function, with Q = 6 corresponding to BER = $10^{-9}$ [19].) The Q of the receiver is given by the following expression [19].

$$Q = \frac{2R\overline{P}}{\sigma_0 + \sigma_1} \tag{5.1}$$

where R is the responsivity of the detector, $\overline{P}$ is the average received power, and $\sigma_0$ and $\sigma_1$ are the noise currents in the zeros and ones, respectively. Without the optical preamplification, the receiver is limited by thermal noise, which is the same for ones and zeros. In the case of any deviation from the ideal case a power penalty is introduced. Q is then given by

$$Q = \delta \cdot \frac{R\overline{P}}{\sigma_T} \tag{5.2}$$

where $\delta$ is the power penalty, which can be used as a fitting parameter. In our case, we attribute the power penalty to an imperfect extinction ratio. A power

penalty of 0.73 yields good agreement with the measurements. This corresponds to signal power in the zero bits that is 15% of the power in the ones. With optical preamplification, the noise currents are different in the ones and zeros. When no signal is present, the dominant noise is the thermal noise in the receiver. In the ones, the optical noise from the amplifier dominates. Q is in this case given by

$$Q = \delta \cdot \frac{2RG\overline{P}}{\sigma_T + \sigma_{Opt}} \tag{5.3}$$

The optical noise term is given by [20] $\sigma_{Opt} = 4 \cdot R^2 \cdot G^2 \cdot \overline{P} \cdot h\nu \cdot F \cdot B_e$, where G is the amplifier gain, hν is the energy per signal photon, F is the fiber-to-fiber noise factor of the preamplifier, and B is the electrical bandwidth of the receiver. In the regime where the receiver sensitivity is limited by the optical amplifier noise, the noise current increases with increased signal power. This results in a different slope of the BER curve, as compared to the case of constant noise. The 4-dB power penalty corresponds to a noise figure of 10.5 dB, which is in good agreement with the previously estimated value.

We can now use this model to calculate what can be achieved if the VCSOA performance is improved. For the same gain, 11 dB, and a more reasonable noise figure of 7 dB, the model yields a receiver sensitivity of –28.8 dBm. No transmission experiments were conducted using a Generation-2 device. However, the measured maximum gain and noise figure can be used to calculate a receiver sensitivity at 10 Gb/s of –31.3 dBm. For comparison, the highest sensitivity reported for an APD at 10 Gb/s is –28.0 dBm [21]

The maximum bit rate that the preamplifier can accommodate is limited by the gain bandwidth. The bandwidth can be tailored in the design of the VCSOA by varying the mirror reflectivity and the cavity length. The 37 GHz optical bandwidth of the device used in this experiment allows for transmission

at bit rates up to 33 Gb/s. Wider optical bandwidth, which would allow for transmission at higher bit rates, can be achieved by decreasing the pump level. This would result in decreased gain and a compromised receiver sensitivity. Figure 5.10 shows maximum obtainable fiber-to-fiber gain, limited by optical bandwidth, versus bit rate for the present device. Higher gain and wider gain bandwidth was measured for devices with lower top mirror reflectivity (Chapter 4).

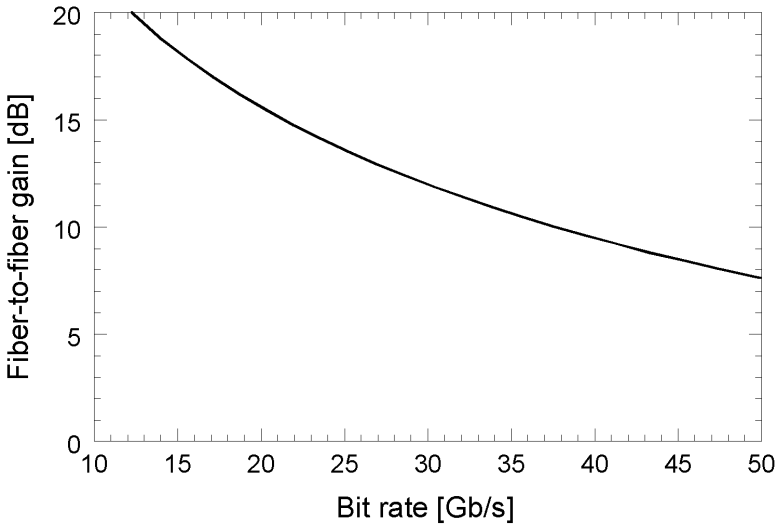


*Figure 5.10. Bandwidth limited fiber-to-fiber gain versus operating bit rate for a top mirror reflectivity of 0.955.*

If the VCSOA is to replace the optical filter in this application, it is of interest to be able to optimize the filter shape, *i.e.* the shape of the gain spectrum. The gain spectrum of the present device (Figure 5.6) is not ideal from a filter point of view. The isolation of adjacent channels can be determined from the curve fit, which is based on Equation 2.4. At 100 GHz and 50 GHz channel spacing, the suppression of adjacent channels is 14 dB and 8 dB, respectively. This is not sufficient for most systems applications. Better isolation is obtained for

transmission mode operation. It is certainly of interest to have a flatter passband. This can be obtained by using a coupled-cavity design [22]. A in-depth analysis of the optimum filter shape for preamplification is beyond the scope of this thesis.

## 5.4 Summary

In this chapter, possible applications for VCSOAs were outlined. The unique properties of VCSOAs suggest a few applications for which these devices appear ideal. The vertical-cavity geometry enables integration of VCSOAs in 2D array architectures, which makes them suitable for use in optical interconnects. They can serve as modulators in interconnects that use an external source, or as preamplifiers to ease the requirements on both transmitter and receivers. The fast gain dynamics of SOAs make them useful for switching and modulation. The amplifier gain enables precise control of the output power from the switch, and compensates for coupling loss and other losses. VCSOAs are ideal as preamplifiers in high-speed receivers. Their narrow gain bandwidth provides filtering, and their good coupling efficiency ensures low noise operation.

The feasibility of using VCSOAs for switching/modulation and optical preamplifaction were investigated experimentally. The switching speed and extinction ratio of a reflection mode VCSOA modulator was investigated. Small-signal modulation bandwidths up to 1.8 GHz were measured, indicating that switching times shorter than 1 ns should be possible. An output signal extinction ratio of 35 dB was measured. Preamplification at 10 GB/s was demonstrated. Using a VCSOA with 11 dB fiber-to-fiber gain, a 7-dB improvement in receiver sensitivity was obtained.

# References

[1] D. A. B. Miller, "Optical Interconnects to Silicon," *IEEE Journal of Selected Topics in Quantum Electronics*, vol. 6, no. 6, pp. 1312-1317, Nov./Dec. 2000.

[2] C. Fan, B. Mansoorian, D. A. Van Blerkom, M. W. Hansen, V. H. Ozguz, S. C. Esener, G. C. Marsden, "Digital free-space optical interconnections: a comparison of transmitter technologies," *Applied Optics*, vol. 34, pp. 3103-3115, 1995.

[3] P. Wen, M. Sanchez, O. Kibar, S. C. Esener, "Low-voltage, high contrast-ratio, low-noise VCSEL modulator," in *Proceedings to OSA Topical Meeting on Optical Amplifiers and Their Applications*, pp. 265-266, 2000.

[4] O. Kibar, P. J. Marchand, S. C. Esener, "Gain-bandwidth product of a VCSEL amplifier, " in *Proceedings to LEOS 11th annual meeting*, pp. 221-222, 1998.

[5] N. Suzuki, M. Ohashi, M. Nakamura, "A Proposed Vertical-Cavity Optical Repeater for Optical Inter-Board Connections", *IEEE Photonics Technology Letters*, vol. 9, no. 8, pp. 1149-1151, Aug. 1997.

[6] R. Ramaswami, K. N. Sivarajan, *Optical Networks*, San Diego, CA: Academic Press, 1998.

[7] M. D. Feuer, J. M. Wiesenfeld, J. S. Perino, C. A. Burrus, G. Raybon, S. C. Shunk, N. K. Dutta, "Single-Port Laser-Amplifier Modulator for Local

Access", *IEEE Photononics Technology Letters*, vol. 8, no. 9, pp. 1175-1177, Sept. 1996.

[8] N. Buldawoo, S. Mottet, F. Le Gall, D. Sigogne, D. Meichenin, S Chelles, "A semiconductor laser amplifier-reflector for the future FTTH applications", in *Proceedings of the 23rd European Conference on Optical Communication*, pp. 196-199, 1997.

[9] H. Takesue, F. Yamamoto, T. Sugie, "Novel Node Configuration for DWDM Photonic Access Ring Using CMLS", *IEEE Photonics Technology Letters*, vol. 12, no. 12, pp. 1698-1700, Dec. 2000.

[10] R. Lewén, K. Streubel, A. Karlsson, S. Rapp, "Experimental Demonstration of a Multifunctional Long-Wavelength Vertical-Cavity Laser Amplifier-Detector", *IEEE Photonics Technology Letters*, vol. 10, no. 8, pp. 1067-1069, Aug. 1998.

[11] M. Ikeda, "Switching Characteristics of Laser Diode Switch", *IEEE Journal of Quantum Electronics*, vol. QE-19, pp. 157-164, 1983.

[12] M. Gustavsson, B. Lagerström, L. Thylén, M. Janson, L. Lundgren, A-C. Mörner, M. Rask, B. Stolz "Monolithically integrated 4 x 4 InGaAsP/InP laser amplifier gate switch arrays", *Electron Letters*, vol. 28, pp. 2223-2225, 1992.

[13] E. Almström, C. P. Larsen, L. Gillner, W. H. van Berlo, M. Gustavsson, E. Berglind, "Experimental and Analytical Evaluation of Packaged 4 x 4 InGaAsP/InP Semiconductor Optical Amplifier Gate Switch Matrices for

Optical Networks", *IEEE Journal of Lightwave Technology*, vol. 14, no. 6. pp. 996-1004, June 1996.

[14] L. Gillner, "Modulation Properties of a near traveling-wave semiconductor laser amplifier," *IEE Proceedings*, vol.139, no. 5, pp. 331-338, Oct. 1992

[15] U. Koren, B. I. Miller, M. G. Young, T. L. Koch, R. M. Jopson, A. H. Gnauck, J. D. Evankow, M. Chien, "High frequency modulation of strained layer multiple quantum well optical amplifiers," *Electronics Letters*, vol. 27, no. 1, pp. 62-64, Jan. 1991.

[16] N. Bouché, B. corbett, R. Kuszelewicz, R. Ray, "Vertical-cavity Amplifying Photonic Switch at 1.5 μm," *IEEE Photonics Technology Letters*, vol. 8, no. 8, pp. 1035-1037, Aug. 1996.

[17] T. Ducellier, R. Basset, J. Y. Emery, F. Pommereau, R. N'Go, J. L. Lafragette, P. Aubert, P. Doussière, P. Laube, L. Goldstein, "Record low noise factor (5.2 dB) in 1.55 μm bulk SOA for high bit rate low-noise preamplification," *Proceedings of the 22nd European Conference on Optical Communication*, vol. 3, pp. 173-176, 1996.

[18] R. I. Laming, A. H. Gnauck, C. R. Giles, M. N. Zevas, D. N. Payne, "High-Sensitivity Two-Stage Erbium-Doped Fiber Preamplifier at 10Gb/s," *IEEE Photonics Technology Letters*, vol. 4, pp. 1348-1350, 1992.

[19] G. P. Agrawal, *Fiber-Optic Communication Systems*, New York, NY: Wiley, 1997.

[20] N. A. Olsson, "Lightwave Systems With Optical Amplifiers," *IEEE Journal of Lightwave Technology*, vol. 7, no. 7, pp. 1071-1082, July 1989.

[21] K. Sato, T. Hosoda, Y. Watanabe, s. Wada, Y. Iriguchi, K. Makita, A. Shono, J. Shimizu, K. Sakamoto, I. Watanabe, K. Mitamura, M. Yamaguchi, "Record highest sensitivity of –28.0dBm at 10 Gb/s achieved by newly developed extremely-compact superlattice-APD modulae with TIA-IC," *Technical Digest of 27th Optical Fiber Communication Conference (OFC '02), Postdeadline Papers*, pp. FB11-1-FB11-3, March 2002.

[22] S. F. Lim, C. J. Chang-Hasnian, "A Proposal of Broad-Bandwidth Vertical-Cavity Laser Amplifier," *IEEE Photonics Technology Letters*, vol. 7, no. 11, pp. 1240-1242, Nov. 1995.

# Chapter 6

# Summary and Future Directions

This thesis investigated a new class of optoelectronic devices: vertical-cavity semiconductor optical amplifiers (VCSOAs). This is the first VCSOA thesis at UCSB, and only very little VCSOA research had been done at other universities before this project. This thesis, therefore, had the goal of covering basic VCSOA properties as completely as possible. The main achievements of this thesis are, in summary: the development of a broad theoretical VCSOA model; the design, fabrication, and analysis of two generations long-wavelength VCSOAs; investigation of potential applications for these devices; demonstration of optical preamplification of a 10-Gb/s receiver using a VCSOA.

The theoretical model is based on previous work on in-plane Fabry-Perot SOA and initial theoretical studies of VCSOAs. The model covers amplifier gain, gain bandwidth, saturation power and noise figure. It was shown that the reflectivity of the mirrors affect all parameters of the VCSOA. If the reflectivity is too high, lasing threshold will impose a limit on the maximum carrier density that can be reached, and thereby also limit the maximum amplifier gain. The

active region gain in this case is not fully utilized. Operating the VCSOA at a carrier density below full inversion leads to poor noise performance. Furthermore, high mirror reflectivity leads to high photon density in the cavity, which results in low saturation power. Reduced reflectivity allows for stronger pumping/higher drive current, which produces higher amplifier gain, lower noise figure, and higher saturation power. If the mirror reflectivity is too low, there will not be enough feedback to reach good amplifier gain. The gain bandwidth is also affected by the mirror reflectivity. High reflectivity results in a narrow gain spectrum; reduced reflectivity results in a wider gain spectrum. The ideal reflectivity is high enough to reach as high amplifier gain as possible, but low enough so that lasing threshold is avoided.

There are, of course, a number of approximations in this theoretical model, and there is certainly room for improvement. For example, it was assumed that the dimensions of the cavity and the low mirror reflectivity make the diffraction loss small enough to be negligible. Optical guiding and diffraction loss should be included in future models. To best improve the model, theoretical work should be done in combination with well designed experiments. The materials need to be better characterized in order to establish some of the unknown parameters in the rate equation model.

Two generations of VCSOAs were presented in this thesis. The devices were fabricated using InP-GaAs wafer bonding. Both generations were optimized for reflection mode operation and optically pumped by a 980-nm diode laser. The objectives of the first generation were to demonstrate the first VCSOA at 1.3-μm wavelength, to investigate basic VCSOAs properties, and to develop a theoretical model for these devices. The structure of these devices was very simple. An InGaAsP/InP active region was wafer-bonded to two Al(Ga)As/GaAs DBRs, forming a planar chip without any structural definition of individual devices. The lateral dimensions of the active region were defined

by the spot size of the pump beam. The highest fiber-to-fiber gain measured on a Generation-1 VCSOAs was 13.5 dB. The reflectivity of the top and bottom mirror of that device was 0.955 and 0.999, respectively. Gain bandwidths between 0.12 nm (20 GHz) and 0.6 nm (100 GHz) were measured for Generation-1 devices with different top mirror reflectivites. The highest saturation output power was –3.5 dBm, measured for a device with top mirror reflectivity of 0.91. Noise figure was only measured on one device from Generation 1. That device had a top mirror reflectivity of 0.955, which was too high to achieve good population inversion. The fiber-to-fiber noise figure was 9 dB.

In the second generation of devices, a carrier confining structure was introduced. Pillars were etched through the active region, and the QWs were under-etched in order to keep the carriers in the active region and improve the efficiency of the devices. Higher gain was achieved with the second generation and the efficiency was improved by a factor of three. The best results of this generation were 17 dB of fiber-to-fiber gain, 6.1 dB noise figure, and -5 dBm saturation output power. The carrier confinement used in Generation 2 is definitely worth further investigation. The mesas had a step-like sidewall profile after the QW under-etch. The second bonding was performed at 575ºC, which is higher than the growth temperature for the QWs. At this temperature, InP from the cladding layers migrates to smoothen the steps in the sidewalls, thereby covering the edges of the QWs. The exact composition and crystalline structure of the material covering the QW edges was not established. However, it is likely that the re-flown InP that covers of the sidewalls significantly reduces the surface recombination. In-plane lasers fabricated by mass transport have been demonstrated [1]. The surface recombination in these laser was greatly reduced due to the buried heterostructure created by the mass transport. Wafer bonding provides an attractive way to fabricate buried heterostructure vertical cavity

lasers and amplifiers, as it gives the freedom to process the active region before the structure is completed.

The results in this thesis show that the top mirror reflectivity of reflection mode VCSOAs should be relatively low. For the active region material used here it was concluded that the reflectivity should be less than 0.9 in order to maximize the performance. This could be achieved without the use of wafer bonding, thereby reducing the number of wafer bonds from two to one. This would greatly simplify the fabrication of the devices.

The VCSOAs presented in this thesis had rather low efficiency, and the devices with the highest gain and lowest noise figure were polarization sensitive. It is not known exactly what the different losses are that lead to the poor efficiency. These are two obvious issues to deal with, but there are numerous others. For example, using an external optical pump and free-space optics is not a very practical way of pumping a device. There are ways to integrate the optical pump with the VCSOA. This has been done successfully in long-wavelength VCSELs [2]. Alternatively, it is of great interest to realize an electrically pumped device. Besides the pumping issue, the most important step for VCSOAs is to make these devices tunable to cover a wider wavelength range. The wavelength requirements on sources in low-cost CWDM systems are fairly loose, which has to be accommodated by the amplifiers in the system. DWDM sources, on the other hand, are temperature controlled, and the amplifier bandwidth does not have to cover wavelength deviations. However, it is of interest to take advantage of the filtering properties of VCSOAs and use them as channel selective elements. Tunability would be very attractive for such applications. Tunable VCSOAs could be realized by employing micro electromechanical systems (MEMS), similar to what is being used for tunable VCSELs [3].

## *CHAPTER 6: SUMMARY*

VCSOAs have a number of potential applications in fiberoptic communication systems. Applications investigated in this thesis were switching/modulation and optical preamplification. Small signal frequency response in the GHz range was measured, which indicates a switching time shorter than 1 ns. It was demonstrated that a 35 dB extinction ratio is possible to achieve for a switch/modulator based on the VCSOAs presented here. Optical preamplification at 10 Gb/s was demonstrated. The narrow gain bandwidth of VCSOAs makes them ideal for this application since it provides combined filtering and amplification. The modulated signal was coupled through the VCSOA to a regular PIN receiver without any additional optical filter after the VCSOA. The VCSOA was operated at 11 dB fiber-to-fiber gain. This produced a 7 dB sensitivity improvement, resulting in a receiver sensitivity of – 26.2 dBm.

A device that would be of great interest is a tunable VCSOA integrated monolithically with a photodetector. The integration would result in a footprint much smaller than for individually packaged discrete devices—preamplifier, filter, and receiver. There are, of course, a number of issues to be resolved before such a device can be realized. The pumping scheme, as mentioned above, is one issue. Another is back-reflections from the photodetector back into the VCSOA. If realized however, this device would be very attractive as a compact, highly sensitive, tunable receiver. 40-50 nm tuning range has been achieved for tunable VCSELs. A similar tuning range can be expected for VCSOAs. The sensitivity can be expected to be better than APDs at bitrates of 10 Gb/s and higher. A schematic of such a device is shown in Figure 6.1.

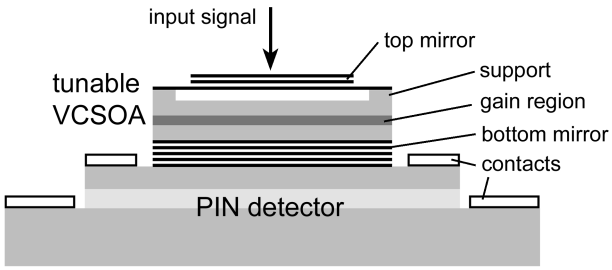


*Figure 6.1 Schematic of VCSOA integrated with photodetector. This type of structure could potentially provide very compact, highly sensitive, tunable receivers.*

# References

[1] Z.-L. Liau, J. N. Walpole, "Mass-Transported GaInAsP/InP Lasers," *Lincoln Laboratory Journal*, vol. 2, no.1, pp. 77-94, 1989.

[2] V. Jayaraman, T. J. Goodnough, T. L. Beam, F. M. Ahedo, R. A. Maurice, "Continuous-Wave Operation of Single-Transverse-Mode 1310-nm VCSELs up to 115°C," IEEE Photonics Technology Letters, vol. 12, no. 12, pp. 1595-1597, Dec. 2000.

[3] D. Vakhshoori, J.-H. Zhou, M. Jiang, M. Azimi, K. McCallion, C.-C. Lu, K. J. Knopp, J. Cai, P. D. Wang, P. Tayebati, H. Zhu, P. Chen, "C-band tunable 6 mW vertical-cavity surface-emitting lasers," *OFC 2000 Technical Digest Postconference Edition*, Paper PD13, pp. PD13-1-PD13-3, 2000.